1057

NEANDC (E) - 212 U Vol. V
INDC (Ger) - 22/L + Special

PROGRESS REPORT ON NUCLEAR DATA RESEARCH IN THE FEDERAL REPUBLIC OF GERMANY

for the Period April 1, 1979 to March 31, 1980

June 1980

Edited by
S.M. Qaim
Institut für Chemie (1): Nuklearchemie
Kernforschungsanlage Jülich GmbH

NEANDC (E) - 212 U Vol. V
INDC (Ger) - 22/L + Special

PROGRESS REPORT ON NUCLEAR DATA RESEARCH IN THE FEDERAL REPUBLIC OF GERMANY

for the Period April 1, 1979 to March 31, 1980

June 1980

Edited by
S.M. Qaim
Institut für Chemie (1): Nuklearchemie
Kernforschungsanlage Jülich GmbH

F O R E W O R D

This report has been prepared to promote exchange of nuclear data research information between the Federal Republic of Germany and the other member states of NEA and IAEA. It brings together progress reports from KFZ Karlsruhe, KFA Jülich, the Universities of Hamburg, Kiel, Köln, Darmstadt, Mainz, Marburg, Stuttgart und München, as well as from PTB Braunschweig and FIZ Karlsruhe. The emphasis in the works reported here has been on measurement, evaluation and compilation of application oriented nuclear data, such as those relevant to fission and fusion reactor technologies, development of intense spallation neutron sources, production of medically important short-lived radioisotopes, etc.

Each contribution is presented under the laboratory heading where the work was done. If the work is relevant to requests in the World Request List for Nuclear Data, WRENDA 79/8o (INDC(SEC)-73/URSF), the corresponding request identification numbers have been listed after the title and authors' names of the respective contribution.

Acknowledgement is made to the Board of Directors of KFA Jülich for a financial grant to publish this report. The CINDA type index has been prepared by Dr. H. Behrens and Mr. G. Schust of FIZ Karlsruhe.

Jülich, June 198o S.M. Qaim

C O N T E N T S

Page

INSTITUT FÜR ANGEWANDTE KERNPHYSIK

KERNFORSCHUNGSZENTRUM KARLSRUHE

Page

INSTITUT FÜR NEUTRONENPHYSIK UND REAKTORTECHNIK
KERNFORSCHUNGSZENTRUM KARLSRUHE

INSTITUT FÜR CHEMIE (1): NUKLEARCHEMIE
KERNFORSCHUNGSANLAGE JÜLICH

INSTITUT FÜR ANGEWANDTE KERNPHYSIK
KERNFORSCHUNGSZENTRUM KARLSRUHE

1. Isochronous Cyclotron

1.1 Determination of High-Precision Resonance Parameters for ^{12}C + n and ^{16}O + n in the Region 3 to 11 MeV*

S. Cierjacks[+], F. Hinterberger[++], G. Schmalz, D. Erbe, P. v. Rossen[++], B. Leugers

Narrow resonances in the ^{12}C + n and ^{16}O + n systems have been investigated from total neutron cross-section measurements performed at the Karlsruhe fast neutron facility with a spectrometer resolution of 5.5 ns · m^{-1}. Resonance energies and total and partical decay widths have been determined employing either a single- or multi-level Breit-Wigner formalism of non-interfering resonances. The results of the resonance analyses are listed in Tables I a and I b. Resonance energies and widths are given for the laboratory system as well as the cm system. Using neutron binding energies from Wapstra's data tables [1], the analyses also yielded very precise ^{13}C and ^{17}O excitation energies which are given in column 7. Spin and parity assignments in column 8 were taken from references 2 and 3. In cases of unknown J^{π} values a possible J^{π} value was derived from our analysis.

---

* Work published in Nucl.Instr.Methods 169 (1980) 185

+ Now at Institut für Kernphysik, Kernforschungszentrum und Universität Karlsruhe

++ Institut für Strahlen- und Kernphysik, Universität Bonn

Table I a. $^{16}O + n$ resonance parameters from the resonance analysis and recommended ^{17}O excitation energies

Lab. system			cm system				
E_R (keV)	Γ (keV)	Γ_{n_o} (keV)	E_R (keV)	Γ (keV)	Γ_{n_o} (keV)	E_x (keV)[a]	J^{π}[b]
3211.70 ± 0.17	1.45 ± 0.05	1.45 ± 0.05	3020.89 ± 0.16	1.38 ± 0.05	1.38 ± 0.05	7165.19 ± 0.8	$\frac{5}{2}$ −
3438.38 ± 0.19	0.68 ± 0.24	0.68 ± 0.24	3243.08 ± 0.19	0.64 ± 0.23	0.64 ± 0.23	7378.38 ± 0.8	$\frac{5}{2}$ +
3441.73 ± 0.14	1.02 ± 0.21	1.02 ± 0.21	3237.23 ± 0.14	0.96 ± 0.20	0.96 ± 0.20	7381.53 ± 0.8	$\frac{5}{2}$ −
3767.76 ± 0.22	15.4 ± 0.3	13.8 ± 0.6	3543.86 ± 0.21	14.4 ± 0.3	13.0 ± 0.6	7688.16 ± 0.8	$\frac{7}{2}$ −
4463.41 ± 0.26	12.1 ± 0.5	8.6 ± 0.3	4198.08 ± 0.24	11.4 ± 0.5	8.1 ± 0.3	8342.38 ± 0.8	$\frac{1}{2}$ +
4527.12 ± 0.07	6.56 ± 0.14	5.05 ± 0.12	4258.00 ± 0.07	6.17 ± 0.13	4.75 ± 0.11	8402.30 ± 0.8	$\frac{5}{2}$ +
4594.83 ± 0.09	2.26 ± 0.12	1.25 ± 0.04	4321.67 ± 0.09	2.13 ± 0.11	1.18 ± 0.04	8465.97 ± 0.8	$\frac{7}{2}$ +
4631.78 ± 0.12	7.33 ± 0.23	3.04 ± 0.09	4356.38 ± 0.11	6.89 ± 0.22	2.86 ± 0.08	8500.68 ± 0.8	$\frac{5}{2}$ −
4829.9 ± 0.4	58.8 ± 0.6	52.0 ± 1.2	4542.7 ± 0.4	55.3 ± 0.6	48.9 ± 1.1	8687.0 ± 0.9	$\frac{3}{2}$ −
5127.0 ± 1.6	28.0 ± 2.0	25.0 ± 2.0	4822.1 ± 1.5	26.3 ± 1.9	23.5 ± 1.9	8966.4 ± 1.7	$\frac{7}{2}$ −
5368.90 ± 0.09	3.75 ± 0.14	2.52 ± 0.08	5049.61 ± 0.08	3.53 ± 0.13	2.37 ± 0.08	9193.91 ± 0.8	$\frac{5}{2}$ +
5919.67 ± 0.14	24.6 ± 0.3	19.1 ± 0.6	5567.53 ± 0.13	23.1 ± 0.3	18.0 ± 0.6	9711.83 ± 0.8	$\frac{7}{2}$ +
5995.68 ± 0.15	12.4 ± 0.3	10.9 ± 0.3	5639.00 ± 0.14	11.7 ± 0.3	10.3 ± 0.3	9783.30 ± 0.8	$\frac{3}{2}$ +
6076.08 ± 0.15	4.26 ± 0.24	3.58 ± 0.21	5714.61 ± 0.14	4.01 ± 0.23	3.37 ± 0.20	9858.91 ± 0.8	$(\frac{5}{2}-)$[c]
6094.8 ± 1.0	17.8 ± 1,8	11.6 ± 1.3	5732.3 ± 0.9	16.7 ± 1.7	10.9 ± 1.2	9876.6 ± 1.2	$(\frac{1}{2}-)$[c]
6404.6 ± 0.5	52.2 ± 0.8	23.7 ± 0.6	6023.5 ± 0.5	49.1 ± 0.8	22.3 ± 0.6	10167.8 ± 0.9	$(\frac{7}{2}-)$[c]
6820.7 ± 0.6	45.2 ± 1.2	18.3 ± 0.7	6414.8 ± 0.6	42.5 ± 1.1	17.2 ± 0.7	10559.1 ± 1.0	$(\frac{7}{2}-)$[c]
7199.3 ± 1.3	44.4 ± 1.5	28.1 ± 1.0	6770.8 ± 1.2	41.7 ± 1.4	26.4 ± 0.9	10915.1 ± 1.4	$(\frac{5}{2}+)$[c]
7373.31 ± 0.18	2.5 ± 0.3	2.00 ± 0.13	6934.38 ± 0.17	2.4 ± 0.3	1.88 ± 0.12	11078.68 ± 0.8	$\frac{1}{2}$ −
8848.8 ± 0.6	7.3 ± 1.2	1.35 ± 0.15	8321.7 ± 0.6	6.9 ± 1.1	1.27 ± 0.14	12466.0 ± 1.1	$\frac{3}{2}$ −
9414.9 ± 0.6	2.7 ± 1.1	0.43 ± 0.06	8854.0 ± 0.6	2.5 ± 1.0	0.40 ± 0.06	12998.3 ± 1.0	$\frac{5}{2}$ −
10725.5 ± 1.5	21.8 ± 1.7	2.20 ± 0.17	10086.0 ± 1.4	20.5 ± 1.6	2.07 ± 0.16	14230.3 ± 1.6	$\frac{7}{2}$ −

[a] $^{16}O + n$ binding energy B = (4144.3 ± 0.8) keV from ref. [1].

[b] Ref. [2] unless otherwise noted. [c] Present work.

Table I b. $^{12}C + n$ resonance parameters from the resonance analysis and recommended ^{13}C excitation energies

Lab. system			cm system				
E_R (keV)	Γ (keV)	Γ_{n_o} (keV)	E_R (keV)	Γ (keV)	Γ_{n_o} (keV)	E_x (keV)[a]	J^{π} [b]
4937.12 ± 0.09	1.87 ± 0.08	1.72 ± 0.04	4553.45 ± 0.09	1.72 ± 0.08	1.60 ± 0.04	9499.84 ± 0.09	$(\frac{5}{2}-)$[c]
5365.21 ± 0.18	25.7 ± 0.4	22.3 ± 0.5	4948.19 ± 0.17	23.7 ± 0.4	20.6 ± 0.5	9894.58 ± 0.17	$\frac{3}{2}-$
6297.07 ± 0.32	55.2 ± 0.6	47.0 ± 1.0	5807.42 ± 0.30	50.9 ± 0.6	43.4 ± 0.9	10753.8 ± 0.3	$\frac{7}{2}-$
6361.1 ± 0.6	19.6 ± 1.1	5.1 ± 0.3	5866.5 ± 0.6	18.1 ± 1.0	4.7 ± 0.3	10813.0 ± 0.6	$(\frac{5}{2}-)$
6646.71 ± 0.20	4.3 ± 0.4	2.71 ± 0.17	6129.78 ± 0.19	4.0 ± 0.4	2.52 ± 0.16	11076.20 ± 0.19	$(\frac{1}{2}-)$
7726.8 ± 2.1	88.3 ± 3.6	74.8 ± 3.3	7125.6 ± 2.0	81.5 ± 3.3	69.0 ± 3.0	12072.0 ± 2.0	$(\frac{3}{2}-)$[c]

[a] $^{12}C + n$ binding energy B = (4946.392 ± 0.030)keV from ref. [1].

[b] Ref. [3] unless otherwise noted.

[c] Present work.

1.2 Experimental Investigation of $^{16}O + n \rightarrow {}^{17}O$ (T = 3/2) Resonances*

F. Hinterberger[+], S. Cierjacks[++], G. Schmalz, P. v. Rossen[+], D. Erbe, B. Leugers

Very sharp, isospin-forbidden, resonances have been studied by a measurement of the total neutron cross section of oxygen. Employing an improved neutron time-of-flight system, measurements were performed with a time-resolution of 1:2100 for 10 MeV neutrons. The absolute energy calibration allowed the determination of resonance energies with an accuracy between 10^{-5} and 10^{-4}. Besides the investigation of 10 known T = 3/2 states, a search for additional T = 3/2 resonances was undertaken. From resonance analyses of narrow cross section excursions, energies and total and partial decay widths (or upper limts of the last two quantities) were derived. In the neutron energy range from 11 - 15 MeV seventeen energy-sharp anomalies were found in the cross section at the predicted neutron energies of possible $^{16}O + n \rightarrow {}^{17}O$ (T = 3/2) resonances. The obtained results have been compared with shell-model predictions of isospin non-conserving particle decays.

References

[1] A.H. Wapstra, K. Bos, At.Data Nucl.Data Tables 19 (1977) 177

[2] F. Ajzenberg-Selove, Nucl.Phys. A 281 (1977) 1

[3] F. Ajzenberg-Selove, Nucl.Phys. A 268 (1976) 1

---

* Work to be submitted for publication in Nuclear Physics

+ Institut für Strahlen- und Kernphysik, Universität Bonn

++ Now at Institut für Kernphysik, Kernforschungszentrum und Universität Karlsruhe

2. 3MV Van de Graaff-Accelerator

2.1 Structural Materials

2.1.1 Determination of the Capture Width of the 27.7 keV s-Wave Resonance in ^{56}Fe *

K.Wisshak , F. Käppeler
(Relevant to request numbers: 692101, 692103, 692104, 714005, 741040, 741046, 753036, 792201)

The capture width of the 27.7 keV s-wave resonance in ^{56}Fe has been determined using a setup completely different from previous experiments. A pulsed 3 MV Van de Graaff accelerator and the $^{7}Li(p,n)$ reaction served as a neutron source. Capture gamma-rays were observed by a Moxon Rae detector and gold was used as a standard. The samples were positioned at a flight path of only 7.6 - 8.0 cm. This allowed the use of very thin samples avoiding large multiple scattering corrections. Three metallic discs enriched in ^{56}Fe were used with a thickness between 0.6 and 0.15 mm. Events due to capture of resonance scattered neutrons in the detector or surrounding material were completely eliminated by time-of-flight. The result for the capture width is $\Gamma_\gamma = 0.99$ with a statistical uncertainty of 1.3 % and a systematic uncertainty of $\sim$ 5%.

2.1.2 The Neutron Capture Cross Sections of Yb, ^{170}Yb, Lu, ^{175}Lu and ^{184}W

H. Beer, F. Käppeler, K. Wisshak
(Relevant to request numbers: 682037, 691204, 692309)

The neutron caputre cross sections of ^{170}Yb and ^{175}Lu in the keV range

---

* Submitted to Nucl.Sci.Eng. for publication

are of particular importance to s-process nucleosynthesis as they can provide information for the only s-process cosmochronometer ^{176}Lu [1,2]. The neutron caputre cross section of ^{184}W which is one of the main isotopes of natural tungsten is relevant for fast reactor design because tungsten is used as a structural material.

The measurements were carried out at a pulsed 3MV Van de Graaff accelerator. The experimental set-up was almost the same as reported previously [3,4]. Neutrons were generated via the ^{7}Li(p,n) and T(p,n) reactions with proton energies at 20 and 100 keV above threshold, respectively, to obtain a kinematically collimated neutron beam in the entire energy range from 5 to 200 keV. Neutron energies were determined by time-of-flight. Table I summarizes some important parameters of the experiment.

Table I . Experimental parameters

	RUN I	RUN II
Neutron producing reaction	^{7}Li(p,n)	T(p,n)
Average beam current	20 μA	10 μA
Repetition rate	2.5 MHz	2.5 MHz
Pulse width	700 ps	700 ps
Proton energy above reaction threshold	20 keV	100 keV
Time resolution	1.2-1.3ns	1.2-1.3ns
Flight path	67 mm	69 mm
Energy range	5-90 keV	50-200 keV

The prompt capture gamma rays were recorded with a Moxon-Rae detector. All cross sections were measured relative to the ^{197}Au standard cross section.

The results of the measurements are plotted in Figs. 1-4 together with cross sectionsfrom previous work. The present data are indicated in full black circles and squares for the measurements with ^{7}Li(p,n) (RUNI) and T(p,n) (RUN II), respectively. The solid line in Figs. 1- 3 represents a least squares fit of the present data by means of the statistical model.

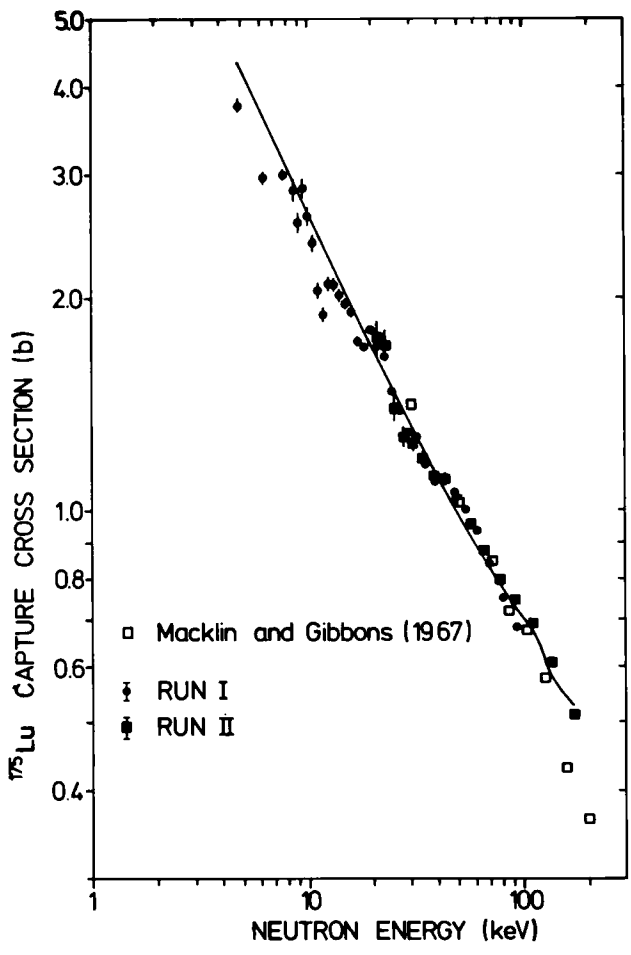

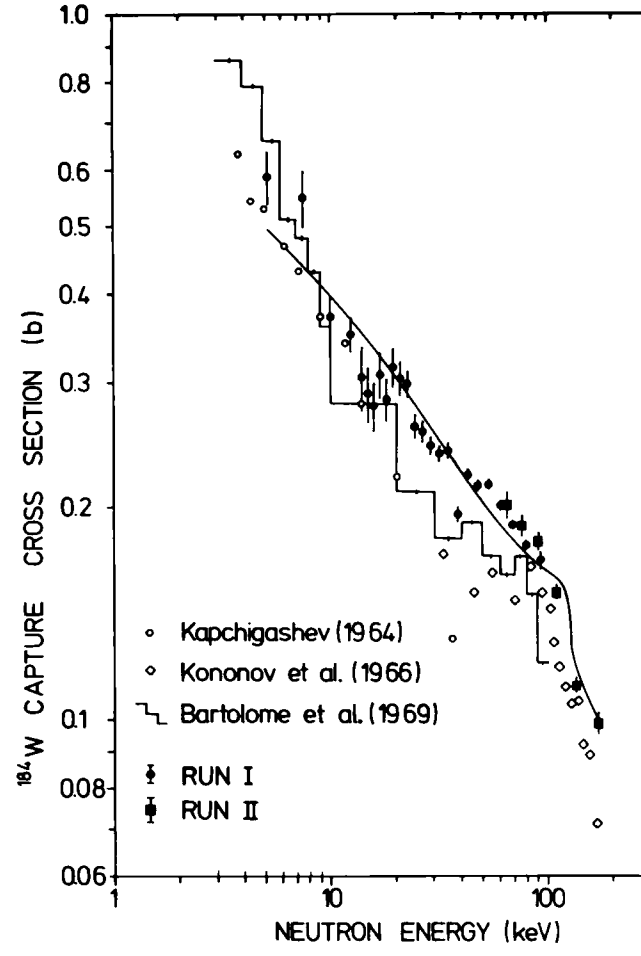

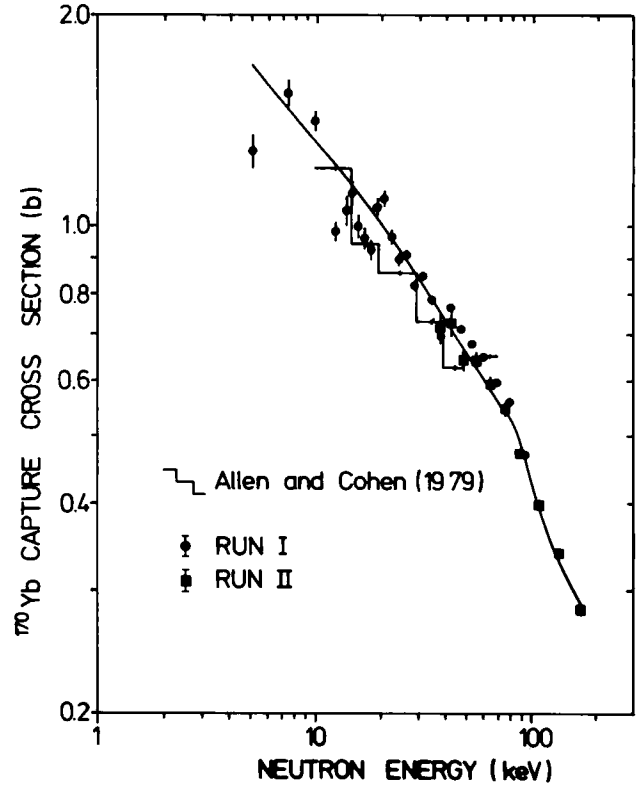

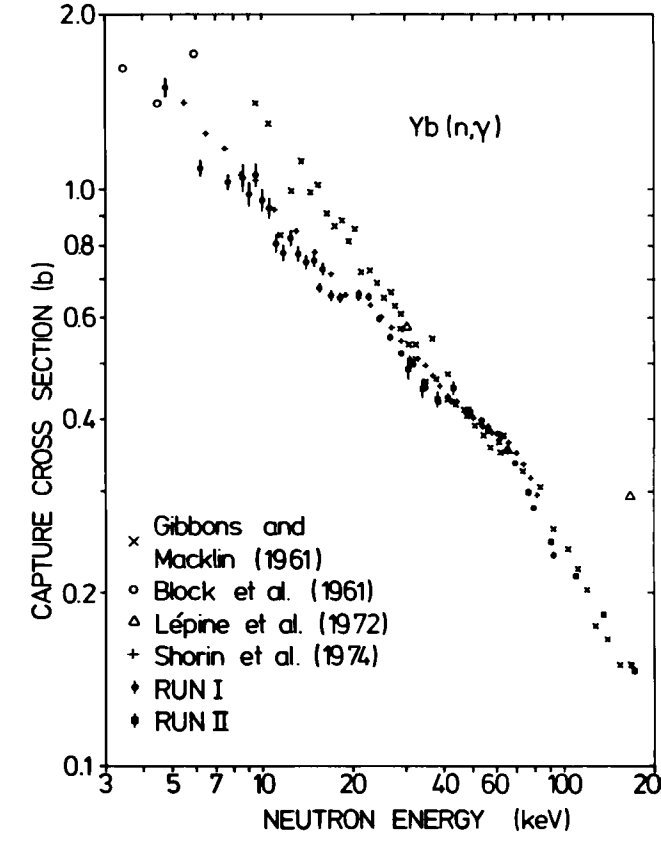

Figs. 1-4 Experimental results from the present capture cross section measurements in the energy range 5 to 200 keV (full black circles and squares) compared to previous work.

References

[1] H. Beer, F. Käppeler, Phys.Rev.C 21 (1980) 534

[2] H. Beer, F. Käppeler, K. Wisshak, Proc. of the Int.Conf. on Nuclear Cross Sections for Technology, Knoxville, Tenn., Oct. 1979, to be published

[3] K. Wisshak, F. Käppeler, Nucl.Sci.Eng. 66 (1978) 363; Nucl.Sci.Eng. 69 (1979) 39

[4] K. Wisshak, F. Käppeler, Proc. of the Int.Conf. on Nucl.Cross Sections for Technology, Knoxville, Tenn., Oct. 1979, to be published

[5] B.J. Allen, D.D. Cohen, Aust.J.Phys. 32 (1979) 447

[6] R.L. Macklin, J.H. Gibbons, Phys.Rev. 159 (1967) 1007

[7] Kapchigashev, Russian compilation 1964

[8] V.N. Kononov, Yu.Ya. Stavisskij, V.E. Kolesov, A.G. Dovbenko, V.S. Nesterenko, V.I. Soroka, Sov.J.Nucl.Phys. 4 (1965) 6708

[9] Z.M. Bartolome, R.W. Hockenbury, W.R. Moyer, J.R. Tatarczuk, R.C. Block, Nucl.Sci.Eng. 37 (1969) 137

[10] J.H. Gibbons, R.L. Macklin, Phys.Rev. 122 (1961) 182

[11] R.C. Block, G.G. Slaugther, L.W. Weston, F.C. Vonderlage, Proc.Symp. on Neutron Time-of-Flight Methods, Saclay, July 1961, Ed. J. Spaepen (Euratom Brussels 1961) p. 203

[12] J.R.D. Lêpine, R.A. Douglas, H.A. Maia, Nucl.Phys. A 196 (1972) 83

[13] V.S. Shorin, V.N. Kononov, E.D. Poletaev, Yad.Fiz. 20 (1974) 1092

[14] V.A. Konks, Yu.P. Popov, Yu.I. Femin, Yad.Fiz. 7 (1968) 493

2.2 Fission Products

2.2.1 Neutron Capture Cross Sections of ^{138}Ba, $^{140,142}Ce$, $^{175,176}Lu$, and ^{181}Ta at 30 keV: Prerequisite for Investigation of the ^{176}Lu Cosmic Clock*

H. Beer, F. Käppeler

(Relevant to request numbers: 682037, 691192)

The capture cross sections of ^{138}Ba, $^{140,142}Ce$, ^{176}Lu, ^{181}Ta and the capture cross section of ^{175}Lu to the 3.68 h isomeric state in ^{176}Lu have been determined at 30 keV neutron energy using the activation technique. Neutrons were generated via the $^{7}Li(p,n)$ reaction just above the reaction threshold at a 3 MV pulsed Van de Graaff accelerator. The capture cross sections are of importance to stellar nucleosynthesis. With the ^{138}Ba and ^{140}Ce cross sections the time integrated average neutron flux for the s-process was determined to be 0.22 mb^{-1}. This result, the capture cross section of ^{176}Lu and the ^{175}Lu cross section to the 3.68h isomeric state in ^{176}Lu were used to analyze the ^{176}Lu cosmic clock. The mean s-process age of solar matter before the solidification of the solar system was estimated to be 6×10^{9} yr. In addition the Hf/Lu abundance ratio was determined.

2.2.2 Capture Cross Sections of Noble Gases

B. Leugers, F. Käppeler

(Relevant to request numbers: 742040, 752014, 792069)

The experimental technique for capture cross section measurements on gaseous samples has been described in the previous progress report [1]. In the following some typical results are given. More complete information on data analysis and the evaluation of uncertainties is available in Ref. [2].

a) Total cross sections - Fig. 1 displays the total cross sections of ^{84}Kr and natural krypton. The error bars on the data points indicate the

---

* Phys. Rev. C 21 (1980) 534

statistical uncertainties. These are much smaller than the systematic uncertainties, which vary from about 20 % at 7 keV neutron energy to 7 % at 200 keV. Obviously, the resonance structure in the cross section for natural krypton is predominantly due to ^{84}Kr. The dashed line above 100 keV represents a recent optical model calculation by Prince [3] which describes existing measurements above 100 keV rather well.

b) Capture Cross Sections - The capture cross section of natural xenon is shown in Fig. 2. Again the error bars indicate only the statistical uncertainties. At present a systematic uncertainty of 15 % has to be quoted which is dominated by the uncertainty of the effective neutron binding energy for the isotopic mixture as it is required in the calculation of the cross section by the pulse height weighting technique.

In Fig. 3 the respective results for natural krypton and ^{84}Kr are given. Compared to natural xenon the cross sections are much smaller leading to rather large statistical uncertainties below 10-20 keV. Similar to the total cross sections the ^{84}Kr resonances clearly show up in the capture cross section of natural krypton, too. For ^{84}Kr a systematic uncertainty of less than 4 % was estimated. The cross section of natural krypton was calculated with an effective binding energy

$$B_n = \frac{\Sigma\, \sigma_i H_i B_i}{\Sigma\, \sigma_i H_i} \qquad (1)$$

where the index i denotes the various isotopes and H_i are the relative isotopic abundances. As averaged capture cross sections σ_i were used in eq. (1), the estimated systematic uncertainty of about 5 % is also only valid for the average capture cross section of natural krypton. Therefore, the cross section is overestimated by up to 15 % in those energy intervals which correspond to strong ^{84}Kr resonances. In Table I the capture cross sections of natural xenon and natural krypton are listed for energy bins of 10 and 20 keV.

Similar results were obtained for mixtures enriched in ^{83}Kr, ^{82}Kr and ^{80}Kr. These data together with the relative abundances and the isotopic cross sections define a system of linear equations. The solution of this system for the isotopic cross sections is complicated by the unexpected large values for ^{78}Kr, so that the systematic uncertainties for

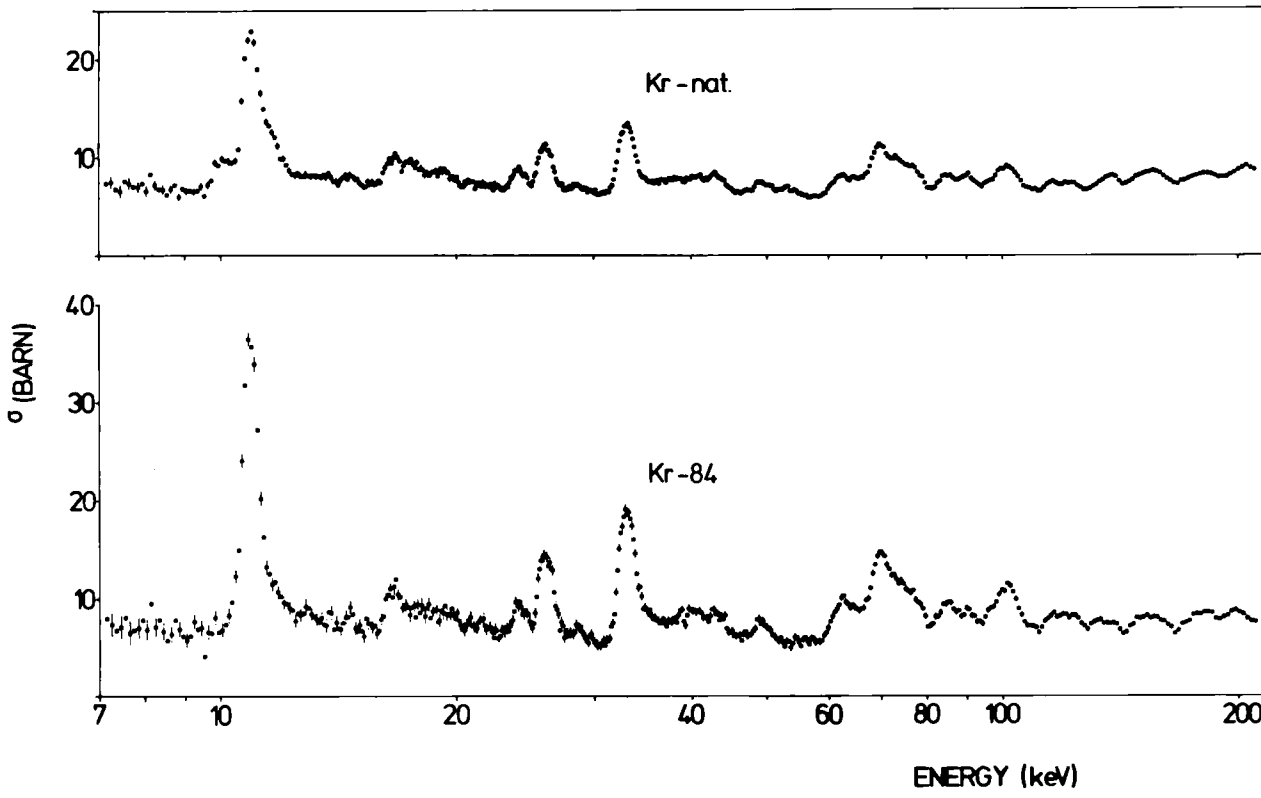

Fig. 1 The total neutron cross sections of natural krypton and ^{84}Kr between 7 and 200 keV. The error bars indicate the statistical uncertainty only.

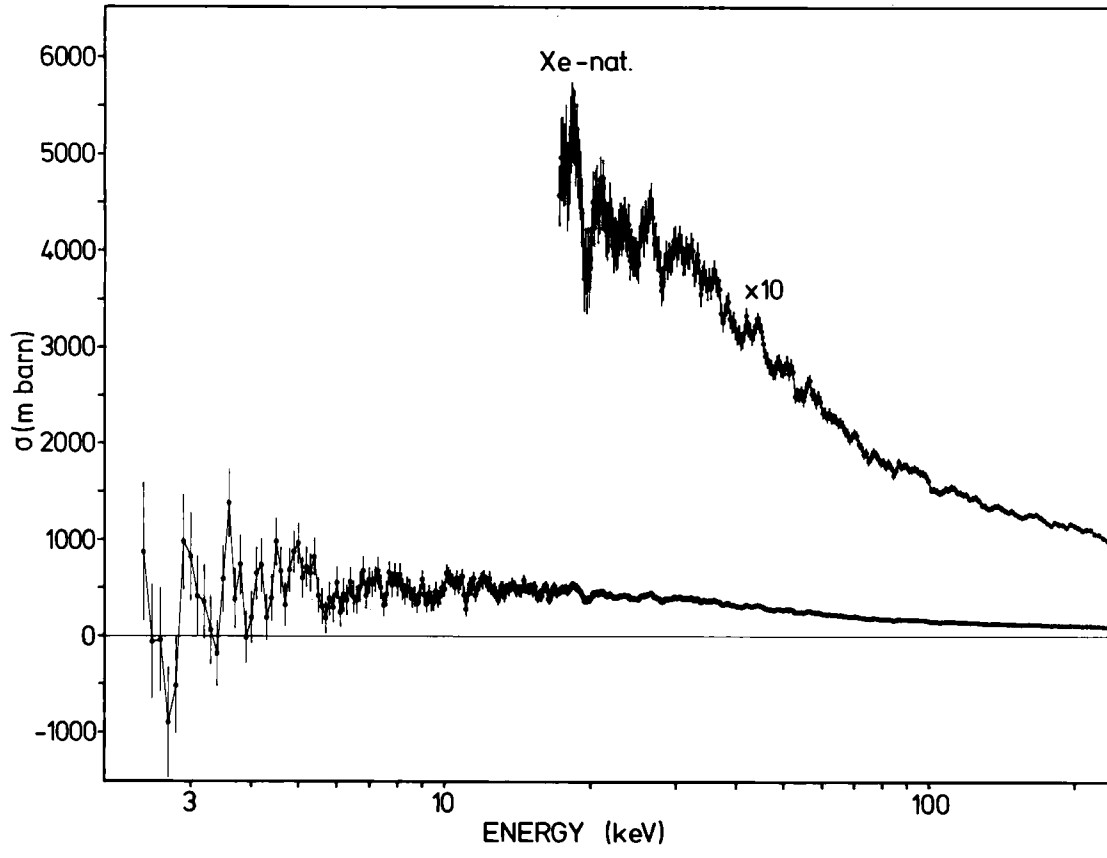

Fig. 2 The neutron capture cross section of natural xenon between 2.5 and 200 keV. The error bars indicate the statistical uncertainty only.

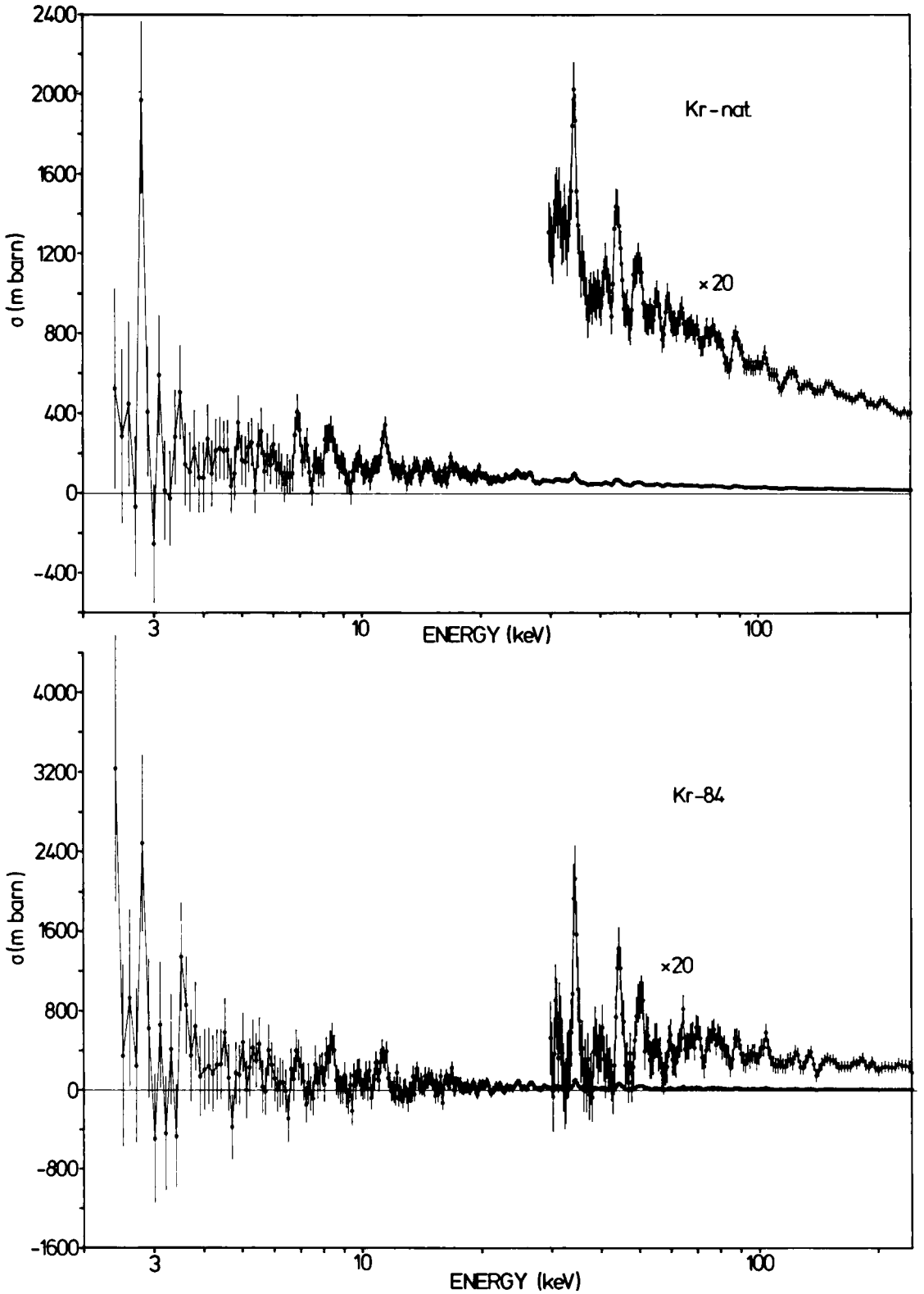

Fig. 3 The neutron capture cross sections of natural krypton and ^{84}Kr between 2.5 and 250 keV. The error bars indicate the statistical uncertainty only.

the cross sections of ^{80}Kr and ^{82}Kr are of the order of 15-20 %.

References

[1] B. Leugers, F. Käppeler, Report NEANDC(E)-202 U, Vol. V (1979) p.10

[2] B. Leugers, "Die Neutroneneinfangquerschnitte der Kryptonisotope und ihre Bedeutung für die Astrophysik", KfK-Report 2895, Kernforschungszentrum Karlsruhe, December 1979

[3] A. Prince, "ENDF/B-IV Neutron Cross Section Evaluation for the Krypton Isotopes", BNL-Report NCS-51028, Brookhaven National Laboratory, January 1979

Table I. Average capture cross sections of natural xenon and natural krypton including the statistical uncertainties. The systematic uncertainties are 5 % for natural krypton and 15 % for natural xenon

Neutron energy interval (keV)	Capture cross section (mb), natural Krypton		Statistical uncertainty (%) natural xenon	
10- 20	119.0	2.4	491	1.2
20- 30	77.5	2.0	416	0.7
30- 40	63.7	1.6	370	0.6
40- 50	52.3	1.6	302	0.6
50- 60	46.4	1.7	259	0.6
60- 80	41.1	1.3	207	0.5
80-100	34.4	1.5	173	0.5
100-120	30.0	1.6	150	0.6
120-140	27.7	1.7	137	0.7
140-160	26.4	1.7	128	0.7
160-180	24.3	1.9	122	0.7
180-200	23.2	2.3	116	0.9

2.3 Actinide Cross Sections

2.3.1 The Neutron Capture and Fission Cross Section of ^{241}Am in the Energy Range from 10 to 250 keV *

K. Wisshak, F. Käppeler

(Relevant to request numbers: 712108, 712109, 712110, 721099, 741127, 742108, 752033, 761098, 792228, 712103, 732115, 742018, 742107, 761099, 792227)

The neutron capture and subthreshold fission cross section of ^{241}Am was measured in the energy range from 10 to 250 keV, using ^{197}Au and ^{235}U as the respective standards. Neutrons were produced via the ^{7}Li(p,n) and the T(p,n) reaction at the Karlsruhe 3-MV pulsed Van de Graaff accelerator. Capture events were detected by a Moxon-Rae detector and fission events by a NE-213 liquid scintillator with pulse shape discriminator equipment. Flight paths as short as 50-66 mm were used to obtain optimum signal to background ratio. The capture cross section could be determined with a total statistical and systematic uncertainty of 4-10 % while the respective values are 13-20 % for the fission cross section. The results are compared with recent data of other authors which in some cases are severely discrepant.

2.3.2 Fission Cross-Section Measurement of ^{241}Am in the Energy Range from 10 to 1030 KeV *

W. Hage **, K. Wisshak , F. Käppeler

(Relevant to request numbers: 712103, 732115, 742018, 742107, 761099, 792227)

The neutron fission cross section of ^{241}Am was measured in the energy range from 10 to 1030 keV using ^{235}U as a standard. The measurements were carried out at the Karlsruhe 3 MV pulsed Van de Graaff accelerator with ^{7}Li targets for the generation of a continuous neutron spectrum below 120 keV and monoenergetic neutron spectra between 120 and 1030 keV. Fission events were detected by measuring the prompt fission neutrons with a NE 213 liquid scintillator with pulse shape discrimination. The

---

* accepted for publication in Nucl. Sci. Eng.

** CEC Joint Research Centre, Ispra

flight path was as short as 60 mm in measurements with continuous neutron spectra leading to a moderate energy resolution of 23 ns/m. The statistical uncertainty was between 0.8 % and 10 % and the systematic uncertainty between 3 % and 7.5 %. Discrepancies were found comparing our results with those of other experiments.

2.3.3 The Branching Ratio in ^{242}Am following Neutron Capture in ^{241}Am

K. Wisshak, J. Wickenhauser, F. Käppeler

(Relevant to request numbers: 671135, 671136, 681807, 741127, 752033, 762153, 762170, 792231)

Neutron capture in ^{241}Am populates not only the ground state, but also an isomeric state of ^{242}Am. While the ground state has a half life of only 16 h the life time of the isomeric state is 152 years. In the neutron flux of a reactor ^{242g}Am will decay predominantly to ^{242}Cm via β-decay, whereas ^{242m}Am may be transformed to ^{243}Am in a second capture event. The partial capture cross section to the ground state determines essentially the amount of ^{242}Cm produced in a reactor during burn up. This nucleus, however, is of interest because of its high specific neutron activity due to spontaneous fission.

The present experiment is the first attempt to determine the partial capture cross section to the ground state in ^{242}Am in a differential measurement [1,2] . A thin ^{241}Am sample (∿ 200μg weight, 7 mm diameter) is activated with monoenergetic neutrons for a period of ∿ 20 h. The ^{242g}Am nuclei produced are detected directly via the electrons emitted in beta decay. The beta spectrum was observed with a mini orange spectrometer [3,4] which offers the possibility of a selective detection of electrons in a high background of alpha-, gamma- and X-ray radiation. The measurements were performed relative to gold.

At thermal energies monoenergetic neutrons of 14.75 meV were provided from a triple axis spectrometer at the Karlsruhe FR2 reactor. The fast flux was obtained from our 3 MV Van de Graaff accelerator using the ^{7}Li(p,n) reaction. The proton energy was adjusted at 25 keV and in a second experiment 10 keV above the reaction threshold. The neutron spec-

trum produced is slightly asymmetric and has an energy of 30 $^{+35}_{-20}$ keV and 25 $^{+25}_{-15}$ keV, respectively. For the narrower distribution the neutron flux is a factor of three lower.

The preliminary results obtained until now are compiled in Table I. The ratio of the capture cross section to the ground state in ^{242}Am and gold could be determined with a total accuracy of ∿ 5 % at all energy points. The statistical accuracy of the measurement is ∿ 1 %. For the determination of the isomeric ratio IR from the experimental data the total capture cross sections of ^{241}Am and gold are required. The respective values are given in the second part of Table I. The data at 14.75 meV were calculated from the 2200 m/sec values of 625 b for ^{241}Am [5] and 98.8 b for gold [6] assuming a 1/v-dependence of the cross sections. For the fast energies a weighted cross section for the experimentally determined energy distribution was calculated from the data given in Ref. [7] and from the ENDF/B-IV gold cross section.
Preliminary results for the capture cross section to the ground state in ^{241}Am and the isomeric ratio are given in the third part of Table I.

Table I. Preliminary results for the capture cross section to the ground state and for the isomeric ratio IR

Neutron Energy	$\frac{\sigma_{\gamma},^{242g}Am}{\sigma_{\gamma},Au}$	Adopted cross sections for the determination of IR	$\sigma_{\gamma},^{242g}Am$	IR
30 $^{+35}_{-20}$ keV	2.86 ± 0.14	σ_{γ},Am=2.46 ± 0.12 b σ_{γ},Au=0.580 ± 0.015 b	1.66 ± 0.09 b	0.67 ± 0.05
25 $^{+25}_{-15}$ keV	3.06 ± 0.17	σ_{γ},Am=2.67 ± 0.13 b σ_{γ},Au=0.624 ± 0.015 b	1.91 ± 0.12 b	0.72 ± 0.06
14.74 meV	5.87 ± 0.3	σ_{γ},Am=818 ± 26 b σ_{γ},Au=129 ± 0.4 b	756 ± 39 b	0.92 ± 0.06

References

[1] K. Wisshak, J. Wickenhauser, F. Käppeler, Proc. of the Int.Conf. on Nuclear Cross Sections for Technology, Knoxville, Tennessee, October 1979, to be published

[2] K. Wisshak, F. Käppeler, J. Wickenhauser, W. Hage, Proc. of the 2nd Technical Meeting on the Nuclear Transmutation of Actinides Ispra, April 1980, to be published

[3] J. van Klinken, K. Wisshak,
Nucl. Instr. Methods 98 (1972) 1

[4] J. van Klinken, S. J. Feenstra, G. Dumont,
Nucl. Instr. Methods 151 (1978) 433

[5] B. Goel, Proc. of a Specialists' Meeting on Nuclear Data of Plutonium and Americium Isotopes for Reactor Applications, BNL 50991, NEANDC L-116 (1979) p. 177

[6] S.F. Mughabghab, D.J. Garber, BNL-325, 3rd ed., Brookhaven National Laboratory (1973)

[7] K. Wisshak, F. Käppeler, Nucl.Sci.Eng., in press

2.3.4 The Distribution of Fragment Mass, Fragment Kinetic Energy and the Number of Prompt Fission Neutrons from Fast Neutron Induced Fission of ^{237}Np

A. A. Naqvi, F. Käppeler, F. Dickmann, R. Müller*

Details of the 4-parameter spectrometer which was developed for the measurement of kinetic energies and velocities of correlated fragments from fast neutron induced fission were reported previously [1]. In the meantime, data analysis has been partly completed. Some typical results are given below.

a) Mass distribution

Fig. 1 shows the distribution of the primary fragment mass (before neutron evaporation) for incident neutron energies of 0.8 and 5.5 MeV. At the lower excitation energy the valley in the region of symmetric fission is very deep. We find peak to valley ratios between 450 and 650 dependent upon how wide we define the region of symmetric fission. This is in reasonable agreement with radiochemical values of 670 ± 70 [2].
At higher excitation the peak to valley ratio is reduced to 30 ± 5. For the lower neutron energy we observe also a fine structure in the mass distribution with a period of 2.5 - 3 amu. As pairing effects should not be significant for the odd-odd system ^{238}Np, this fine structure may be due to sub-shell effects in the fragments.

* Universität Tübingen

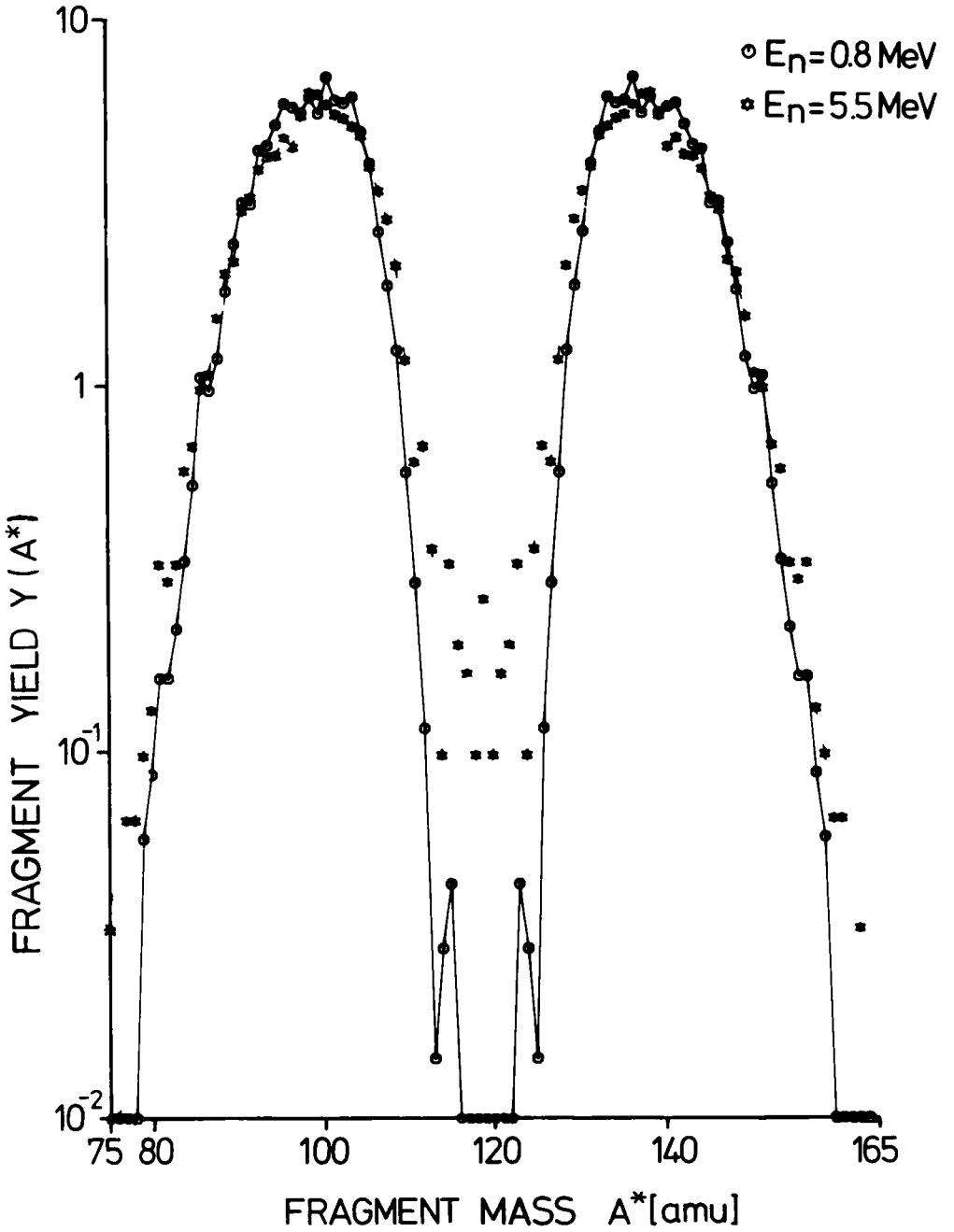

Fig. 1 Distribution of primary fragment masses for incident neutron energies of 0.8 and 5.5 MeV. For the points on the abscissa no events were recorded.

b) Kinetic energy distribution

The total kinetic energy distribution is given in Fig. 2 for both the excitation energies. One finds a pronounced maximum around A = 132 which reflects the spherical configuration of the doubly magic fragment with Z = 50 and N = 82. With increasing excitation energy the influence of shell effects is decreased.

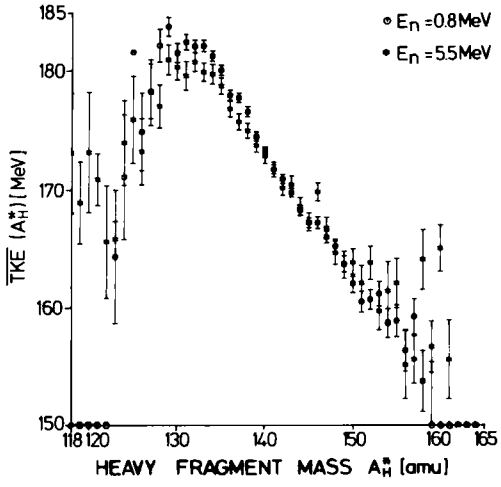

Fig. 2 The total kinetic fragment energy, as a function of fragment mass for incident neutron energies of 0.8 and 5.5 MeV.

c) Number of prompt fission neutrons

The number of evaporated prompt fission neutrons gives a measure for the excitation energy of the fragments. Fig. 3 shows the typical saw-tooth shape of these curves for incident neutron energies of 0.8 and 5.5 MeV. Again for A = 132 there is a minimum in fragment excitation as one would expect for this magic shell configuration. It is interesting to note that the number of prompt fission neutrons from the light fragments does not depend on the excitation energy of the fissioning system, whereas the heavy fragments exhibit a significant effect.

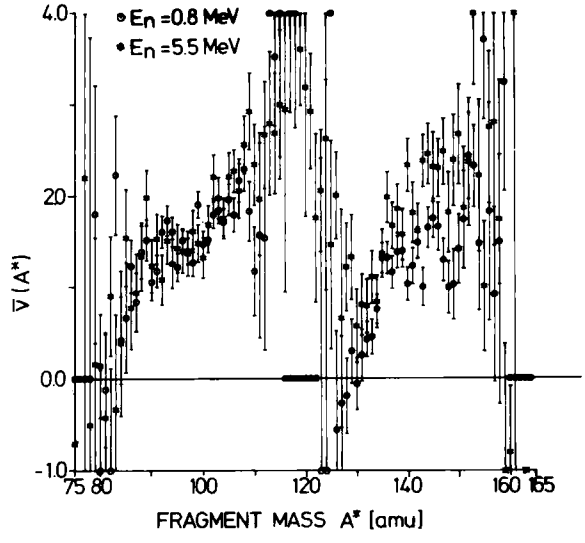

Fig. 3 The number of prompt fission neutrons as a function of fragment mass for incident neutron energies of 0.8 and 5.5 MeV.

References

[1] A.A. Naqvi, F. Käppeler, R. Müller, F. Gönnenwein, Report NEANDC (E) - 202 U, Vol V (1979) p. 18

[2] N.I. Borisova, V.I. Novgorodtseva, V.A. Pchelin, V.A. Shigin, Sov. J. Nucl. Phys. 2 (1966) 173

INSTITUT FÜR KERNPHYSIK
KERNFORSCHUNGSZENTRUM KARLSRUHE

1. SIN Cyclotron

1.1 Absolute Yields and Spectra of Neutrons and Secondary Protons from 590 MeV (p,x) Reactions on Lead Targets

S. Cierjacks, M.T. Rainbow, M.T. Swinhoe, L. Buth*

Time-of-flight measurements of neutrons and secondary charged particles produced by bombardment of thick lead targets with 590 MeV protons have been performed at the ring cyclotron of the Swiss Institute for Nuclear Research (SIN). Experimental data were taken at angles of 30°, 90° and 150° with respect to the incident proton beam for different penetration depths of protons in a 10 cm diam x 60 cm long target. The detector was an NE 213 liquid scintillator used for its pulse-shape (n/γ) discrimination properties. At present date evaluation has been completed for all neutrons and part of the secondary proton spectra observed at 90°. In Fig. 1 the 90° neutron spectrum integrated over the total target length is shown. It is a reasonable approximation to take this spectrum as representing the average spectrum for all angles of emission. On this 12.2 neutrons with a mean energy of 22.2 MeV are emitted from the whole target into all angles per incident protons. The spectrum of secondary protons emitted at 90° from the first 5 cm of 10 cm diam. lead targets is shown in Fig. 2. This figure indicates that elastic scattering of protons in lead is small. The bulk of the spectrum is the result of inelastic and nuclear reactions. Results obtained so far for lead and comparisons of these data with intranuclear-cascade-evaporation model predictions were presented at the 1980 Brookhaven Symposium [1].

Presently, data evaluation is proceeding on data already collected. In the near future similar measurements will be performed with a uranium target using the 590 MeV proton beam at SIN. Later this year the proton beam from SATURN (Saclay, France) will be used to measure neutron and proton yields from lead and uranium targets for an incident proton energy of 1.1 GeV.

1.2 Determination of Fast Neutron Spectra via Proton Recoil Detection Using Unfolding Techniques

M.T. Swinhoe, S. Cierjacks, M.T. Rainbow, L. Buth*

An important piece of information for the use of a spallation neutron source with moderated spectra concerns the fraction of fast neutrons escaping together

---

* Institut für Neutronenphysik und Reaktortechnik, Kernforschungszentrum Karlsruhe

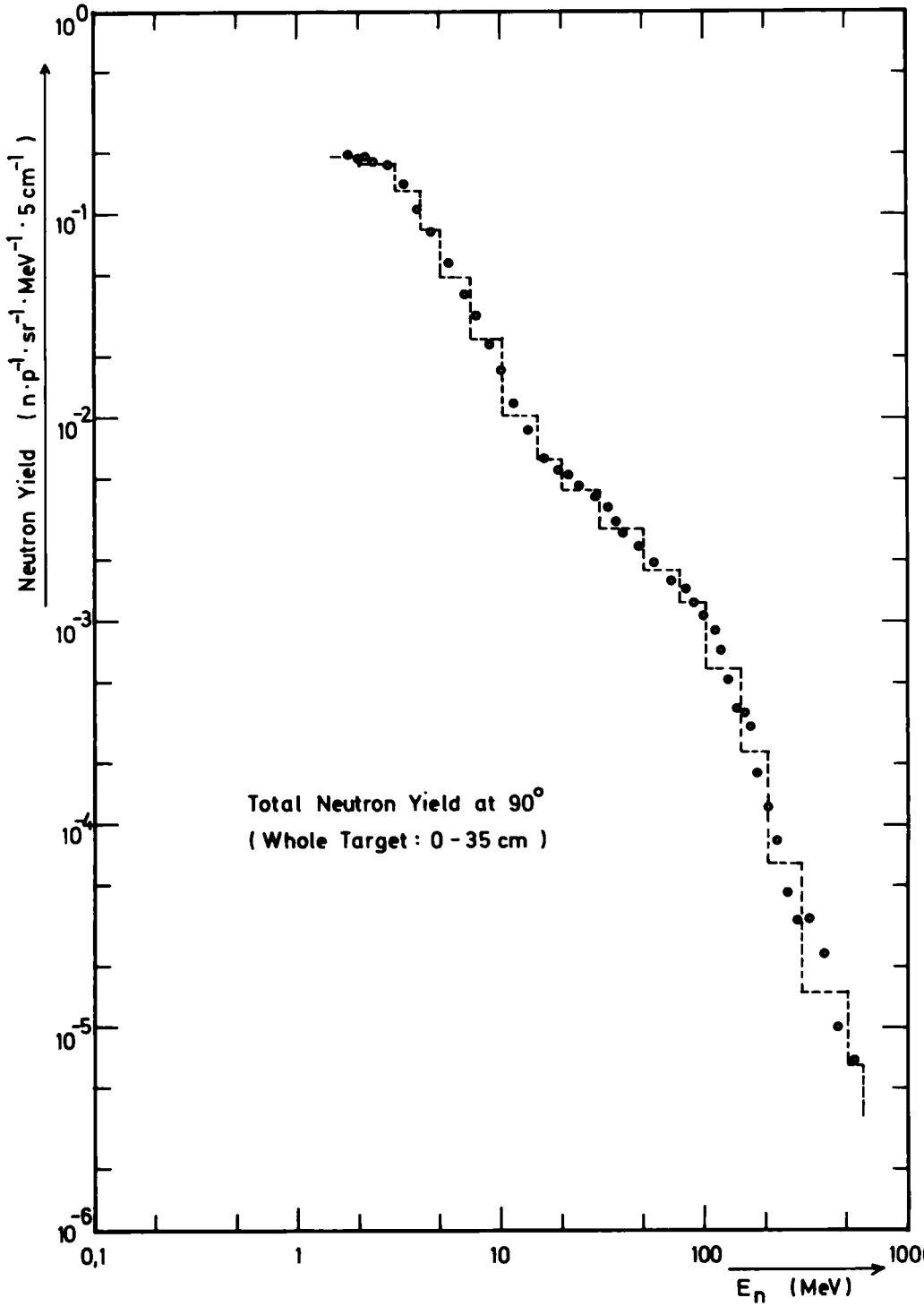

Fig. 1 Differential spectrum of neutrons emitted at 90° integrated over the first 30 cm of the 10 cm diam. lead target. The histogram is a possible energy grouping for numerical calculations.

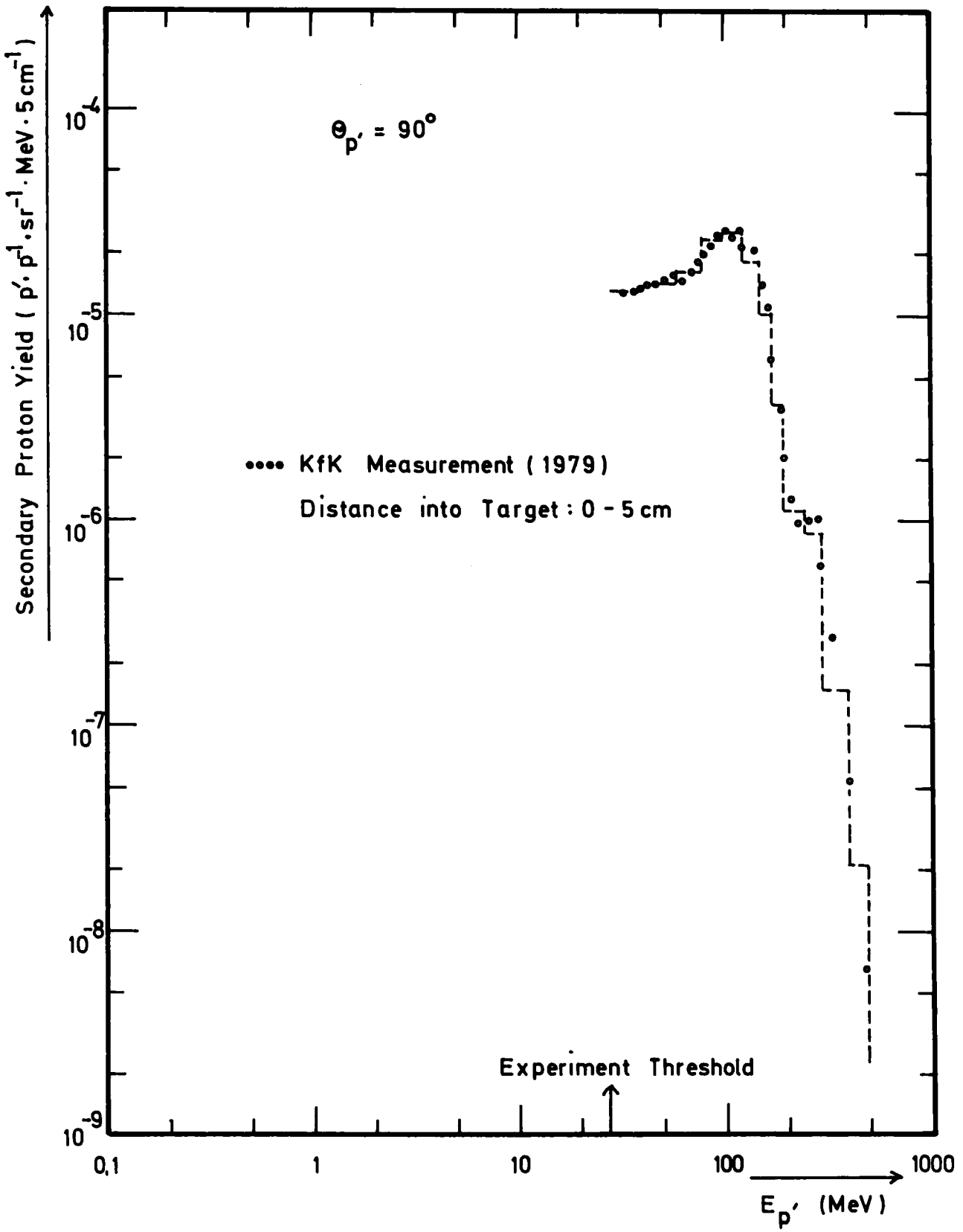

Fig. 2 Differential spectrum of secondary protons emitted at 90° from the first 5 cm of the 10 cm diameter lead target for an incident proton energy of 590 MeV.

with thermal neutrons through the beam tubes of a shielded target device. Even though time-of-flight measurements of fast neutron spectra would have been most desirable, this method was not applicable at the SIN cyclotron, where the only available pulse structure comes from the cyclotron microstructure providing proton bursts at 20 nsec intervals (or 60 nsec intervals at a particular operation mode). This time structure is much too narrow compared with the large time spread associated with the moderation process and so an unfolding method was necessary.

A measurement of the fast neutron spectrum in a moderated beam was made using an 8.9 cm thick NE 213 liquid scintillator with n/γ discrimination. A first result for light water moderated spectra from bombardment of 15 cm diameter Pb-Bi and U targets with 590 MeV protons is shown in Fig. 3. The resulting spectra were rectangularly unfolded. This gives an estimate for both the total number of neutrons and the shape of the spectrum from 5 to 140 MeV.

By simulating the experiment using charged particle spectra calculated by the Monte-Carlo programme of Cecil et al. [2] the error involved in the analysis was estimated. It turned out that the rectangular unfolding gives a very good estimate of the total number of neutrons, but underestimates the fraction of neutrons above about 30 MeV. The latter is to be expected as the response of the scintillator to monoenergetic neutrons above ∿ 30 MeV is far from rectangular due to charged particles produced from carbon. In addition, the finite size of the detector allows a significant fraction of high energy recoil protons to escape.

In order to achieve more reliable results for the high energy tails of the spectra, work is in progress on an iterated method of unfolding. Preliminary investigations indicate that this will allow a good determination of neutron spectra up to 100 MeV using an 8.9 MeV thick detector. For the current experimental programme an even higher energy limit is necessary, and it is planned to use a 30 cm thick NE 213 scintillator which should allow accurate spectra unfolding at least up to 200 MeV. The poorer energy resolution resulting from the larger detector size does not appear to be an important disadvantage for the intended application which deals with relatively smooth neutron spectra.

References

[1] S. Cierjacks, M.T. Rainbow, M.T. Swinhoe, L. Buth, Proc. Symposium on Neutron Cross Sections from 10 - 50 MeV, Brookhaven, May 1980, in press

[2] R.A. Cecil, B.D. Anderson, R. Madey, Nucl.Instr.Methods 161 (1979) 439

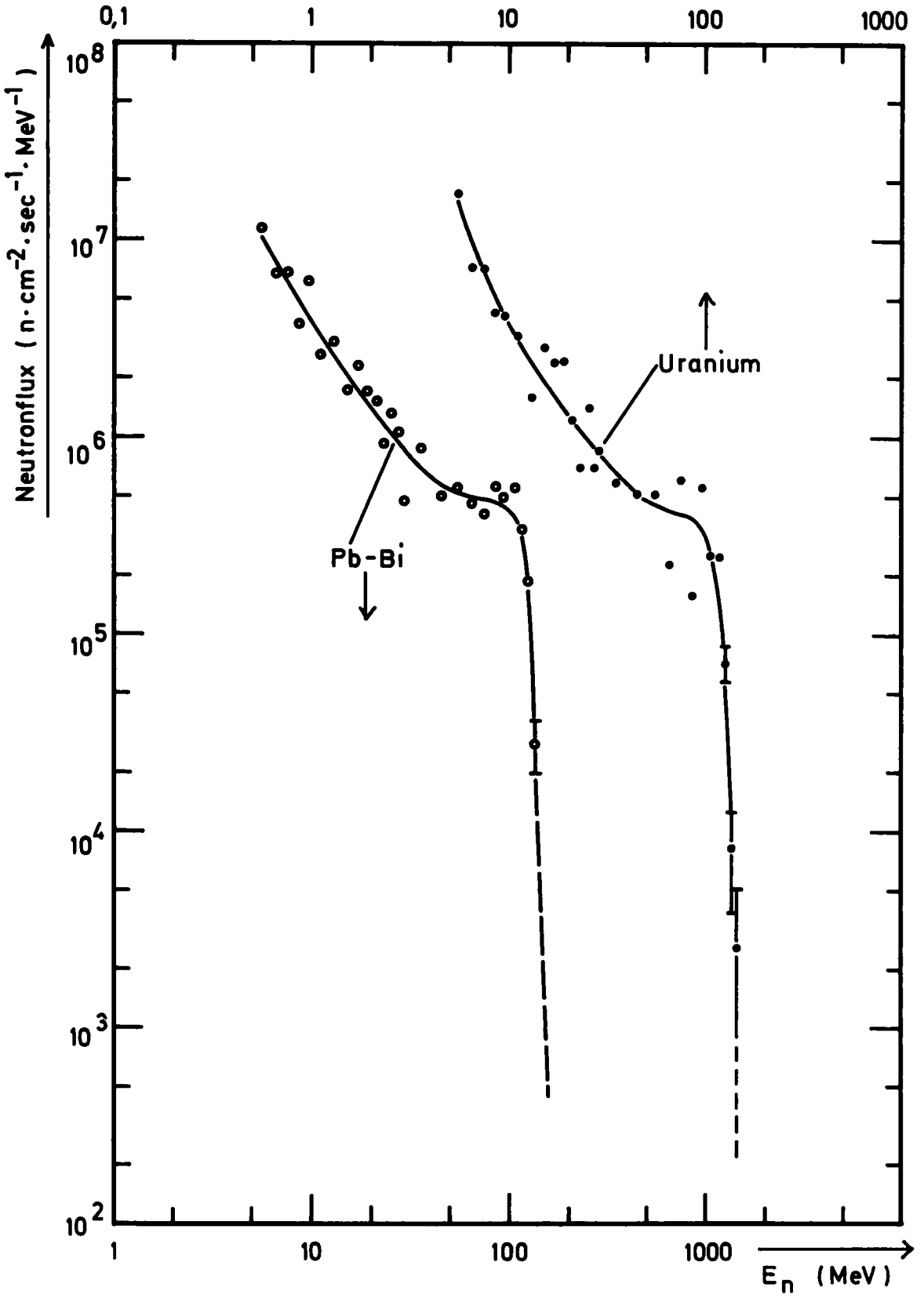

Fig. 3 Spectral distribution of fast neutrons in a light water moderated thermal neutron beam from 15 cm diameter Pb-Bi and U targets. Absolute neutron fluxes are given for a 10 mA proton current and a distance of 6 m from the target.

INSTITUT FÜR NEUTRONENPHYSIK UND REAKTORTECHNIK
KERFORSCHUNGSZENTRUM KARLSRUHE

1. Nuclear Data Evaluation

1.1 Neutron Cross Sections for Actinides

F.H. Fröhner, B. Goel

(Relevant to request numbers: 691262, 691263, 702025, 691286, 692385, 714016, 732113, 781193, 691336, 681805, 681806, 712106, 792169, 681807, 681808, 752032, 792230, 792229, 792257, 79271, 792258, 712113, 711806, 792236, 762174, 792259, 732109)

Thermal cross sections and resonance parameters were reevaluated for ^{235}U and ^{238}U and newly evaluated for ^{241}Am, ^{242m}Am, ^{243}Am and ^{244}Cm (see Table I). Bound levels were adjusted so as to reproduce the evaluated thermal cross sections correctly [1]. Other "distant" levels were accounted for by appropriate R-matrix contributions calculated from level-statistical parameters [2]. Missing fission widths for ^{241}Am were generated from their known distribution by Monte Carlo sampling. Point data were calculated from resolved resonance parameters with multi-level formulae where enough information existed, with single-level formulae otherwise (in case of capture and fission of fissile nuclides). Level-statistical parameters and Hauser-Feshbach formulae were used to generate further data points up to 100 keV.

Table I. New KEDAK evaluations in the resolved resonance region

Target nucleus	Energy range	Cross section formalism	Bound level
^{235}U	1meV - 100eV	MLBW/SLBW	2
^{238}U	1meV - 4keV	Reich-Moore	1
^{241}Am	1meV - 150eV	MLBW/SLBW	1
^{242}Am	1meV - 4eV	MLBW/SLBW	1
^{243}Am	1meV - 250eV	MLBW/SLBW	1
^{244}Cm	1meV - 1keV	MLBW/SLBW	1

Data above 100keV were obtained with the HAUSER+4 code. Calculations with optical model parameter extracted from the analysis of ^{238}U cross sections and angular distributions gave excellent agreement for ^{241}Am with the experimental data of

Phillips et al [3] for the total cross section. Agreement for capture and fission cross sections with the experimental data is also good.
The resonance parameters and point data will be part of the new version KEDAK-4 of the Karlsruhe evaluated file.

References

[1] F.H. Fröhner,
KfK 2669 (1978), p. 53

[2] ibid , p. 52

[3] T.W. Phillips et al, Nucl. Sci. Eng. 69 (1979) 375

1.2 Very Fast Calculation of Doppler-broadened Multi-level Cross Sections

F. H. Fröhner

Single-level formulae permit very fast calculation of Doppler-broadened cross sections via the well-known Voigt profiles ψ and χ, whereas no equally fast techniques were available for unitary multi-level formalisms of the Wigner-Eisenbud or Reich-Moore type (cf. e.g. [1]) . By combining Turing's method for Gaussian broadening of meromorphic functions [2] and a convenient prescription for conversion of real (Wigner-Eisenbud, Reich-Moore) to complex (Kapur-Peierls) R-matrix parameters [3] one can calculate Doppler-broadened multi-level cross sections practically as fast as single-level cross sections [4]. This removes the main computational obstacle which often prevented (rigorous) multi-level expressions to be used in resonance fitting and group constant preparation instead of (approximate) single-level expressions that can fail badly, especially near cross section minima and maxima [3].

References

[1] F.H. Fröhner, KfK 2669 (1978)

[2] A.M. Turing, Proc. London Math. Soc.,Ser. 2, 48, (1943) 180

[3] F.H. Fröhner, Proc. Int. Conf. on Neutron Physics and Nuclear Data for Reactors and Other Applied Purposes, Harwell (1978) p. 306

[4] F.H. Fröhner, Proc. Jahrestagung Kerntechnik 1980, Karlsruhe-Bonn (1980) p. 83

INSTITUT FÜR CHEMIE (1): NUKLEARCHEMIE
KERNFORSCHUNGSANLAGE JÜLICH

1. Neutron Data

1.1 Measurement of (n,t) and (n,^{3}He) Reaction Cross Sections

S. Khatun, S.M. Qaim, R. Wölfle

In continuation of earlier radiochemical and mass spectrometric studies on fast-neutron induced trinucleon emission reactions [1], the (n,t) and (n,^{3}He) cross sections were measured for isotopes of the elements Al, V, Cr, Mn, Fe, Co, Ni and Nb with neutrons produced via break-up of 30 MeV deuterons on a thick Be target. The data are appreciably higher than those at 14 MeV [2].

Work on the measurement of excitation functions of (n,t) reactions in the energy region 15 to 20 MeV was initiated in collaboration with the CBNM, Geel. Segments of Al were irradiated at various angles to the deuteron beam falling on a tritium target. These angles correspond to neutron energies of 16, 17, 18 and 19.5 MeV. The accumulated tritium was separated by vacuum extraction and counted in the gas phase. First results show that the (n,t) cross section increases sharply with the incident neutron energy.

1.2 Statistical Model Analysis of (n,t) and (n,^{3}He) Reactions

H.V. Klapdor*, S.M. Qaim, H. Reiss*

Total cross sections of 14.6 MeV neutron induced reactions (n,n'), (n,p), (n,d), (n,α), (n,t) and (n,^{3}He), on the target nuclei in the mass region A = 27 to 59, were calculated (for the first stage decay) by the Hauser-Feshbach method using a unified set of optical model parameters. The strong reaction channels are described well by the calculations. The data for the (n,t) and (n,^{3}He) reactions are given in Table I. The (n,t) reaction on target nuclei in the (2s,1d)-shell seems to proceed predominantly via statistical processes; for heavier nuclei non-statistical contributions become important. In the case of (n,^{3}He) reactions, the few experimentally measured cross sections are much higher than those obtained by theoretical calculations [3].

---

* MPI für Kernphysik, Heidelberg

Table I. Experimental and theoretical cross sections of (n,t) and (n,^{3}He) reactions induced by 14.6 MeV neutrons

Target nuclide	σ(n,t) μb		σ(n,^{3}He) μb	
	theor.	exp. or from [systematics]	theor.	exp.
Al-27	2860	3000 ±400	< 0.01	
Si-28	energetically not possible		0.7	
P-31	1400	[800 ±300]	< 0.01	≤ 13
S-32	9	7.2± 1.6	560	
K-39	500	184 ± 37	113	
K-41	380	[150 ± 60]	< 0.01	6 ± 3
Ca-40	6	27 ± 8	200	
Sc-45	90	[70 ± 20]	0.02	9 ± 4
		[800 ±200]		
Ti-46	< 0.1	115 ± 35	2.0	
Cr-50	< 0.1	66 ± 20	7.4	
Fe-54	< 0.1	105 ± 35	15.1	
Co-59	70	640 ±130	< 0.01	4.6±2.1

1.3 Cross-Section Measurements on Hydrogen and Helium Producing Reactions

S. Khatun, S.M. Qaim, R. Wölfle

(Relevant to request identification numbers: 762071, 762073, 762080, 762081, 762082, 762086, 762087, 781022, 781023, 781024, 781025, 781026, 781027, 781090, 781102, 781210, 781211, 781212, 781213, 781215, 781216, 781219, 781220, 792199, 792209, 792210)

Fission neutron spectrum averaged cross sections were measured for the relatively less known hydrogen and helium producing reactions ^{58}Ni(n,α)^{55}Fe, ^{62}Ni(n,α)^{59}Fe, ^{60}Ni(n,p)^{60}Co, ^{61}Ni(n,p)^{61}Co, ^{58}Ni[(n,n'p)+(n,pn)+(n,d)]^{57}Co and ^{50}Cr[(n,n'p)+(n,pn)+(n,d)]^{49}V by the activation technique using enriched isotopes as target materials, radiochemical separations and high-resolution γ- and X-ray spectroscopy [4].

In connection with the measurement of (n,x) reaction cross sections on FRT materials for radiation damage calculations [5], we recently constructed a 30 MeV d(Be) neutron source at the Jülich Isochronous Cyclotron (JULIC) and characterized the forward peaked neutron spectrum using the multiple foil activation technique. Integral cross sections were also measured [2] by the activation technique for some (n,2n), (n,p), [(n,n'p)+(n,d)] and (n,α) reactions on isotopes of the elements Al, Ti, V, Cr, Mn, Fe, Co, Ni, Cu, Nb and Mo. The data are given in Fig. 1 as a function of (N-Z)/A of the target nucleus. The trends are somewhat similar to those at 14 MeV. As is evident, in the light mass region the reactions involving the emission of charged particles compete strongly with the (n,2n) process. With increasing asymmetry, however, the cross section of the (n,2n) process increases and, as a general feature, those of processes involving the emission of charged particles decrease.

The measured integral cross-section data agree within 20% with the spectrum averaged cross-section values deduced from the known excitation functions of a few reactions.

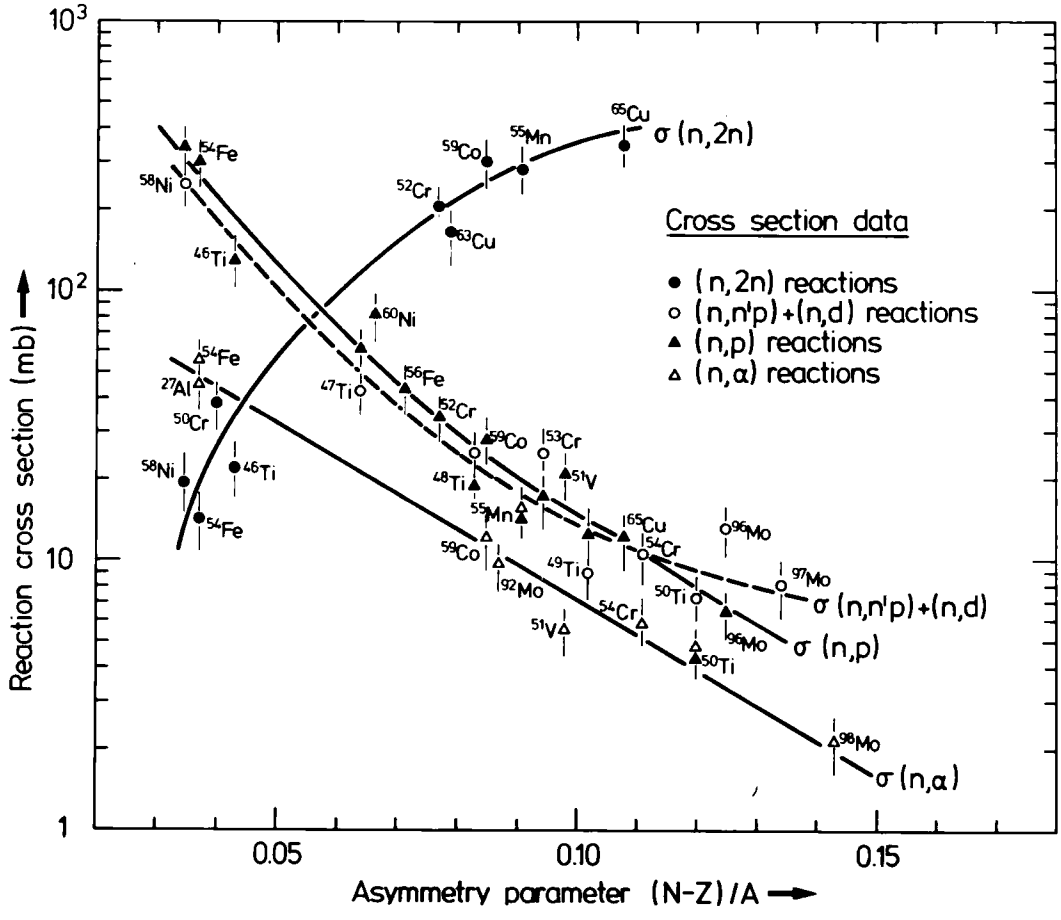

Fig. 1 Systematic trends in cross sections of (n,2n), (n,p), [(n,n'p)+(n,d)] and (n,α) reactions induced by 30 MeV d(Be) neutrons on some structural materials.

1.4 Review of Cross-Section Data

S.M. Qaim

A survey of the recent developments in the study of (n,charged particle) reactions was carried out and presented at the Gaussig Symposium [6]. Similarly the field of fast neutron induced reactions involving the emission of complex particles was covered at the IAEA-Winter College on Nuclear Theory for Applications held in February 1980 at Trieste [7].

2. Charged Particle Data for Radioisotope Production

2.1 Excitation Functions for the Production of "Organic" Radioisotopes

H. Backhausen, S.M. Qaim, G. Stöcklin, R. Weinreich

In view of the increasing importance of positron tomography in nuclear medical in-vivo diagnostics, emphasis has been on the development of newer methods of production of short-lived β^+ emitters. Thus, measurement of the excitation functions for the formation of ^{18}F ($T_{1/2}$ = 110 min) via the reactions $^{20}Ne(^3He,\alpha p)^{18}F$ and $^{20}Ne(^3He,\alpha n)^{18}Ne(\beta^+)^{18}F$ was started with the aim to separate the directly produced ^{18}F from that formed via ^{18}Ne. Similarly for the formation of ^{30}P ($T_{1/2}$ = 2.5 min) three further reactions, $^{28}Si(^3He,p)^{30}P$, $^{28}Si(\alpha,d)^{30}P$ and $^{32}S(d,\alpha)^{30}P$, were investigated. Of all the reactions investigated for the production of ^{30}P, the reaction $^{27}Al(\alpha,n)^{30}P$ was found to be the most suitable. In continuation of the cross-section data measurements for the production of ^{75}Br ($T_{1/2}$ = 1.6 h) [8], investigation of the $^{75}As(^3He,xn)^{74m-76}Br$ reactions was completed and the results are given in Fig. 2. Furthermore, the high-energy process $^{79}Br(d,6n)^{75}Kr(\beta^+)^{75}Br$ was investigated over the deuteron energy range of 60 to 88 MeV. The yields are rather low. The reaction $^{75}As(^3He,3n)^{75}Br$ therefore is the most suitable for the production of ^{75}Br at medical compact cyclotrons.

2.2 Cross-Section Data for the Production of "Inorganic" Radioisotopes

G. Comparetto, S.M. Qaim, G. Stöcklin, R. Weinreich

In continuation of earlier cross-section measurements [9] for the production of some specific inorganic radionuclides, excitation functions were measured for the formation of $^{94,95,97}Ru$ in α- and ^3He-particle induced nuclear

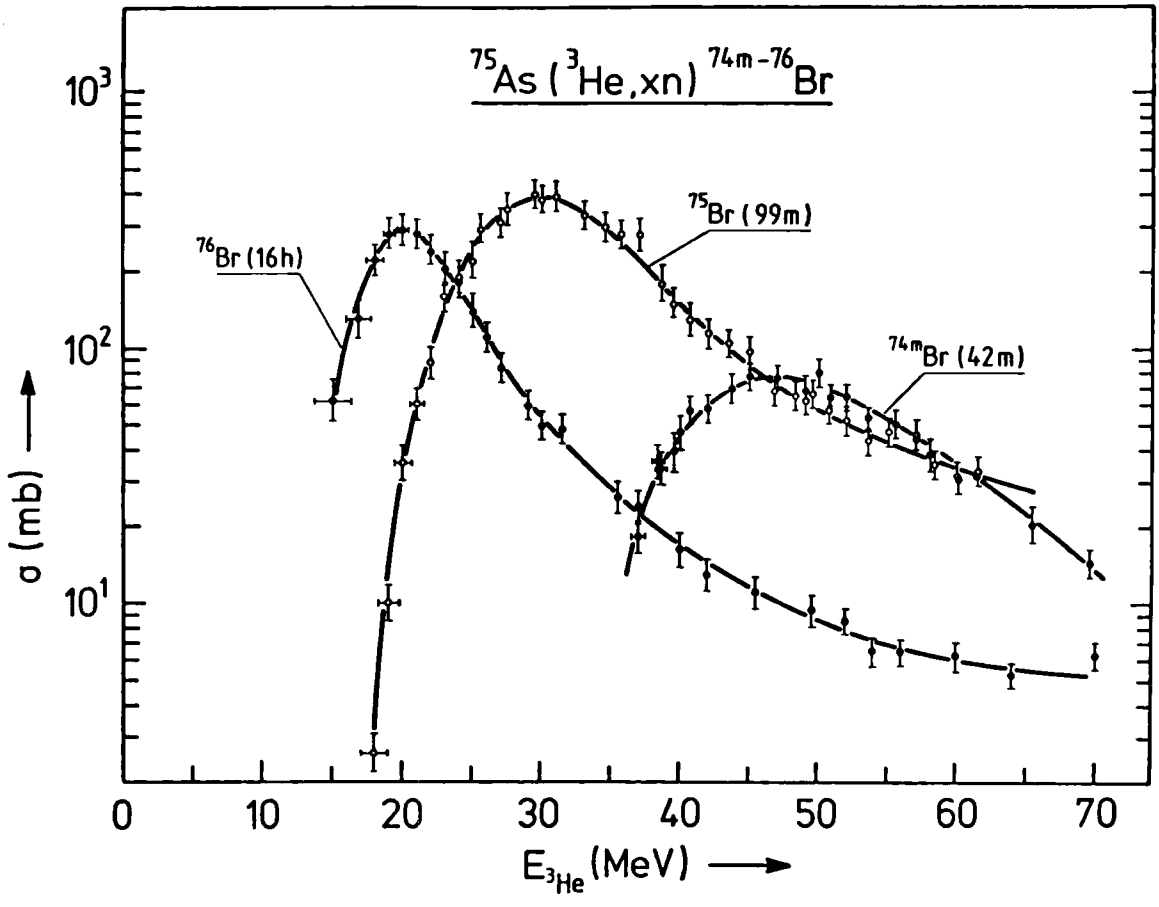

Fig. 2 Excitation functions for the formation of $^{74m,75,76}Br$ in ^{3}He-particle induced nuclear reactions on arsenic.

reactions on molybdenum [10]. The results on the ^{3}He-induced reactions are shown in Fig. 3. The three short-lived neutron deficient isotopes of ruthenium, ^{94}Ru ($T_{1/2}$ = 52 min), ^{95}Ru ($T_{1/2}$ = 1.6 h) and ^{97}Ru ($T_{1/2}$ = 2.9 d), can be produced in good yields using the ^{3}He-induced reactions at compact cyclotrons.

2.3 Radiation Dose Calculations

R. Weinreich

The whole body radiation doses caused by the medically useful neutron deficient radioisotopes of bromine were calculated by means of the classical

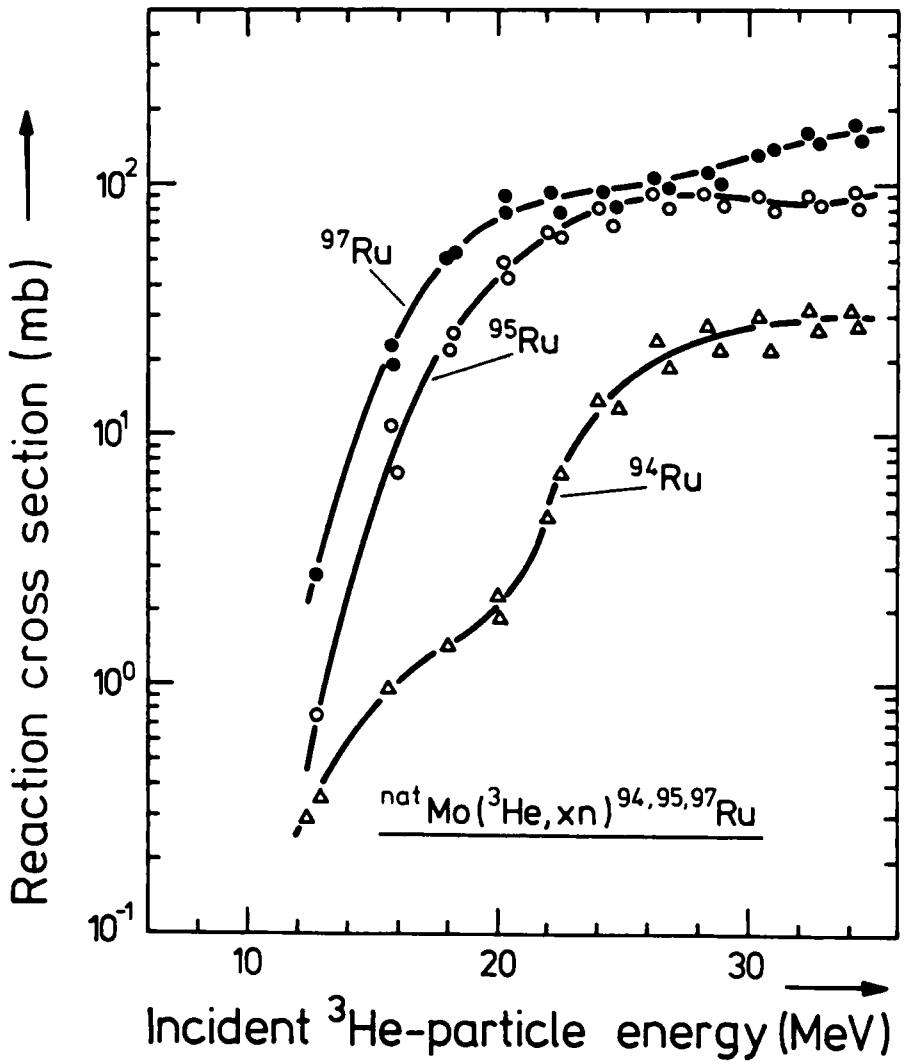

Fig. 3 Excitation functions for the formation of ^{94,95,97}Ru in ^{3}He-particle induced nuclear reactions on molybdenum.

MIRD-model using the recently reported decay data on those radioisotopes. The results are given in Table II. The high dose rate for ^{76}Br is due to its longer half-life. ^{77}Br is the isotope which can be used with conventional Anger cameras, but it is useless in positron emission tomography. Because of its physical properties ^{75}Br appears to be the best bromine isotope for positron emission tomography.

Table II. Whole-body radiation doses by medically useful neutron deficient isotopes of bromine

Nuclide	$T_{1/2}$	Decay mode	$\bar{D}(\frac{mR}{mCi})$
Br-74m	41.5 min	β^+(92.6%) E.C.(7.4%)	81
Br-75	98 min	β^+(73.0%) E.C.(27.0%)	78
Br-76	16.2 h	β^+(57.1%) E.C.(42.9%)	1080
Br-77	56.0 h	E.C.(99.2%) β^+(0.8%)	281

References

[1] C.H. Wu, R. Wölfle, S.M. Qaim, Activation and mass spectrometric study of ^{3}He particle emission in the interactions of fast neutrons with medium mass nuclei, Nucl.Phys. A329 (1979) 63

[2] S.M. Qaim, S. Khatun, R. Wölfle, Integral cross-section measurements on (n,x) reactions induced by 30 MeV d(Be) break-up neutrons on FRT wall and structural materials, Proc.Symp. on Neutron Cross Sections from 10 to 50 MeV, Brookhaven (May 1980), in press

[3] S.M. Qaim, H.V. Klapdor, H. Reiss, Statistical model analysis of cross sections of (n,t) and (n,^{3}He) reactions induced by 14.6 MeV neutrons on target nuclei with A = 27 to 59, Phys.Rev.C, in press

[4] R. Wölfle, S.M. Qaim, Measurement of fission neutron spectrum averaged cross sections of some (n,p), (n,n'p) and (n,α) reactions on nickel and chromium, Radiochimica Acta 27 (1980) 65

[5] S.M. Qaim, Nuclear data needs for radiation damage studies relevant to fusion reactor technology, Proc. Advisory Group Meeting on Nuclear Data for Fusion Reactor Technology, Vienna, IAEA-TECDOC-223 (1979) p. 75

[6] S.M. Qaim, Recent developments in the study of (n,charged particle) reactions, Proc. IX Symposium on Interaction of Fast Neutrons with Nuclei, Gaussig/Dresden (November 1979), in press

[7] S.M. Qaim, Integral cross sections for the emission of complex particles in neutron induced reactions, IAEA-Winter College on Nuclear Theory for Applications, Trieste (February 1980), Lecture Notes to be published

[8] R. Weinreich, Z.B. Alfassi, G. Blessing, G. Stöcklin, Short-lived neutron deficient bromine isotopes for applications in nuclear medicine, Proc. 17th Intern.Annual Meeting, Soc.Nucl.Med., Innsbruck (September 1979), in press

[9] R. Weinreich, H.J. Probst, S.M. Qaim, Production of ^{48}Cr for applications in life sciences, Int.J.appl.Radiat.Isotopes 31 (1980) 223

[10] G. Comparetto, S.M. Qaim, A comparative study of the production of short-lived neutron deficient isotopes $^{94,95,97}Ru$ in α- and ^{3}He-particle induced nuclear reactions on natural molybdenum, Radiochim.Acta, in press

INSTITUT FÜR KERNPHYSIK: EXPERIMENTELLE KERNPHYSIK II
KERNFORSCHUNGSANLAGE JÜLICH

Studies at the Fission Product Separator JOSEF

G. Battistuzzi, K. Kawade[+], B.D. Kern[++], T.A. Khan[+++], W.D. Lauppe*,
H. Lawin, H.A. Selič**, K. Sistemich, A. Wolf***

The separator JOSEF at the research reactor FRJ-2 "DIDO" of the Kernforschungsanlage Jülich is used for nuclear spectroscopic investigations on fission products. Presently the main aims are the study of the onset of nuclear deformations around A=100 and of the nuclear shell structure near ^{132}Sn. In ^{98}Zr [1], ^{99}Zr [2], ^{100}Zr [3-5], ^{99}Nb [2], ^{132}Sn [6,7], ^{134}Te [8] and ^{136}Xe [8] the properties of special levels (like spin, parity and life-time) have been studied through γ,γ angular correlation and through delayed β,γ coincidence measurements. For ^{104}Mo [9,10] a detailed level scheme has been established (Fig. 1) which indicates a permanent deformation of this nucleus. The properties of new levels in ^{132}Te [11] support the interpretation that ^{132}Sn is a good closed shell nucleus.

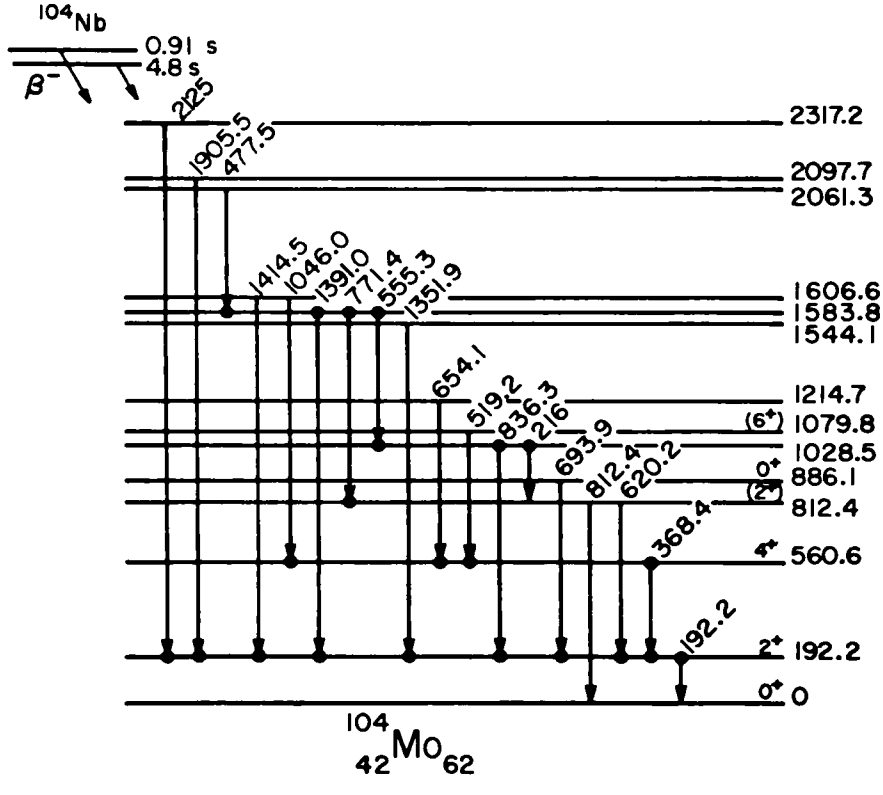

Fig. 1 Partial energy level diagram of ^{104}Mo. The energies are in keV. The dots indicate observed (γ,γ) coincidences.

+ On leave from Nagoya University, Japan

++ Permanent address: Dept. of Phys. and Astron., University of Kentucky, USA

+++ Now at the Tandem Laboratory, McMaster University, Hamilton, Canada

* Now at the Programmgruppe Kernenergie und Umwelt, KFA Jülich

** Presently at the Weizmann Institute of Science, Rehovot, Israel

*** Permanent address: Negev Nuclear Research Centre, Beer Sheva, Israel

References

[1] K. Kawade, G. Battistuzzi, H. Lawin, K. Sistemich, F. Schussler, Institut für Kernphysik der KFA Jülich, Annual Report 1979, p. 62

[2] H.A. Selič, G. Sadler, T.A. Khan, W.D. Lauppe, H. Lawin, K. Sistemich, E. Monnand, J. Blachot, J.P. Bocquet, F. Schussler, Z.Physik A 289 (1979) 197

[3] T.A. Khan, W.D. Lauppe, K. Sistemich, H. Lawin, H.A. Selič, Z.Physik A 284 (1978) 313

[4] H.A. Selič, W. Borgs, W.D. Lauppe, H. Lawin, K. Sistemich, Z.Physik A 286 (1978) 123

[5] A. Wolf, G. Battistuzzi, K. Kawade, H. Lawin, K. Sistemich, Institut für Kernphysik der KFA Jülich, Annual Report 1979, p. 63

[6] K. Sistemich, W.D. Lauppe, M. Iyer, K. Kawade, H. Lawin, O.W.B. Schult, Proc.Int. Winter Meeting on Nuclear Physics, Bormio/Italy, ed. I. Jori (1979) p. 224

[7] K. Kawade, G. Battistuzzi, H. Lawin, K. Sistemich, J. Speth, Institut für Kernphysik der KFA Jülich, Annual Report 1979, p. 65

[8] K. Kawade, G. Battistuzzi, H. Lawin, K. Sistemich, J. Blomqvist, Institut für Kernphysik der KFA Jülich, Annual Report 1979, p. 67

[9] B.D. Kern, W.D. Lauppe, H. Lawin, K. Sistemich, Institut für Kernphysik der KFA Jülich, Annual Report 1978, p. 42

[10] K. Sistemich, W.D. Lauppe, H. Lawin, H. Seyfarth, B.D. Kern, Z.Physik A 289 (1979) 225

[11] K. Sistemich, W.D. Lauppe, H. Lawin, F. Schussler, J.P. Bocquet, E. Monnand, J. Blomqvist, Z.Physik A 292 (1979) 145

I. INSTITUT FÜR EXPERIMENTALPHYSIK
UNIVERSITÄT HAMBURG

1. Postfission Neutrons from Proton Induced Fission of $^{235,236,238}U$

P. Plischke, R. Langkau, W. Scobel, R. Wien

A system of time-of-flight detectors for the measurement of fast ($E_n^{lab} \geq 0.7$ MeV) neutrons in coincidence with fission fragments has been presented recently [1]. Neutrons can be measured at 0° and 90° with respect to the fission fragment direction, and pre- and postfission neutron spectra are separated by means of an iterative procedure [2] that assumes isotropic emission in the c.m.s. system of the emitting compound nucleus or fragment, respectively. The masses of the initial fragments are calculated from their velocities with the techniques reported in [3]. The mass resolution obtained in our experiment varied between 2 and 5 mass units (fwhm), depending on the fragmentation.

Measurements were performed in 1979 with targets ^{238}U, ^{236}U and ^{235}U for projectile energies 12.7, 15.2, 18.3, 22.4 and 25.6 MeV (^{236}U: not for 25.6 MeV; ^{235}U: only for 12.7, 15.2 MeV). Targets had a thickness of typically 150 $\mu g/cm^2$ on 50 $\mu g/cm^2$ carbon backing.

Off-line analysis of the list mode data showed that for all systems under investigation the number of prefission neutrons is as least a factor of 5 smaller than that of the postfission neutrons for both fragments. The mass dependence of the number of neutrons emitted per fragment presented in Fig. 1 shows the well-known sawtooth dependence. The minimum at $A = 132$ is seen for ^{235}U as well as for ^{238}U. It is, however, washed out rapidly with increasing projectile energy.

Postfission neutrons are predominantly detected from the fragment flying towards the neutron TOF detector; therefore, the low energy threshold prevents neutron detection only for a few low energy neutrons, and the average neutron energies $\langle\varepsilon_n^{cm}\rangle$ shown in Fig. 2 are scarcely affected by this low energy cutoff. It is interesting to note that the differences between $p + {}^{235,236,238}U$ at the same projectile energy are concentrated on the heavy fragments. The same applies for the comparison of $p + {}^{238}U$ at different excitation energies, indicating that most of the increased excitation energy seems to be transferred to the heavy fragment.

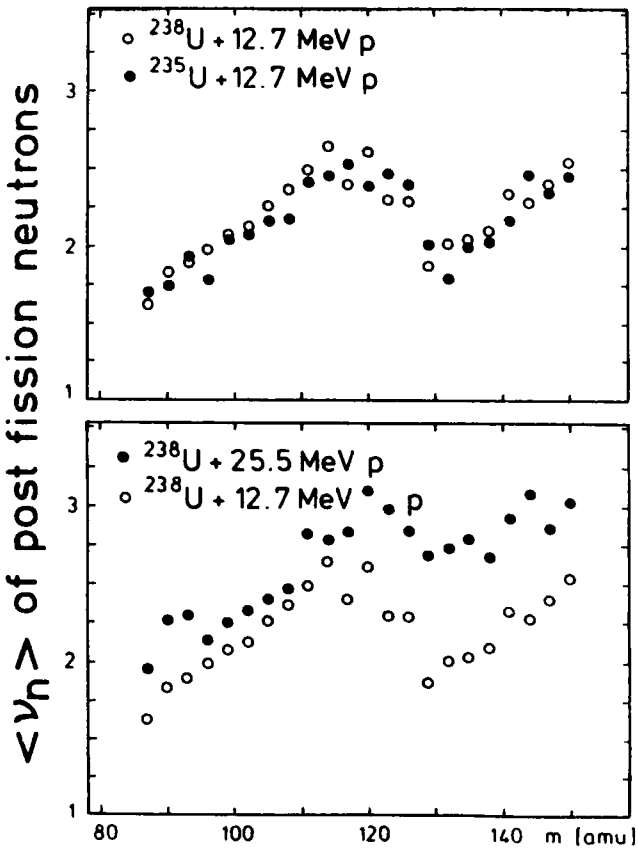

Fig. 1 Number of postfission neutrons per fragment vs. fragment mass m.

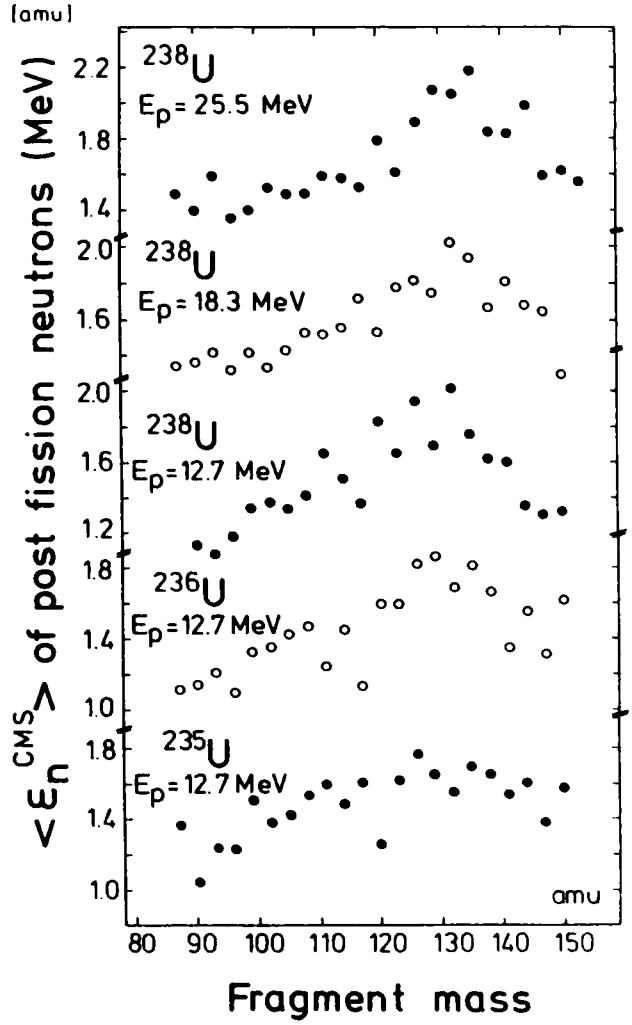

Fig. 2 Average energy of postfission neutrons vs. fragment mass.

2. Spin Depletion by Preequilibrium Neutron Emission

H.H. Bissem, Md.A. Rahman, W. Scobel

Preequilibrium emission (PE) influences the energy and spin population of the residual nuclei. If they are radioactive and have a spin isomer, information on the amount of PE contributions and the resulting spin distribution may be obtained from the excitation functions $\sigma_g(E)$ and $\sigma_m(E)$ for the population of ground and isomeric state, respectively, and from the isomeric ratio σ_g/σ_m. We analyze data of the $^{93}Nb(^3He,xn)^{96-x}Tc$ reactions [4] this way. Hauser-Feshbach calculations, including γ-deexcitation with multipolarities $L \leq 3$, indicate too strong a population of the ground (i.e. high spin) state in all cases, where PE dominates in the excitation function $\sigma_g + \sigma_m$, cf. Fig. 3.

If we assume that (i) the PE depletion as given by the Hybrid Model is equally distributed over all partial waves of the entrance channel and (ii) the relative spin distribution after PE of a neutron of energy ε is identical with that following neutron evaporation with energy ε, the discrepancies between experimental and calculated isomeric ratios are reduced (Fig. 3). Replacement of (ii) by the assumption (iii), that due to the forward peaked angular distribution in PE, the angular momentum carried away by the neutron is parallel to that of the reaction system $^{96}Tc^*$, we obtain a spin population (Fig. 4) that results in a very good prediction of the isomeric ratios, in particular if the spin cutoff parameter σ is reduced to 70% of the rigid body value $\sigma_{Rig.}$. Assumption (iii) also is in agreement with conclusions drawn from $(\alpha,xn\gamma)$ reaction data [5].

References

[1] P. Plischke, H. Krause, R. Langkau, W. Scobel, NEANDC(E)-202U Vol. V (1979) p. 65

[2] Z. Fraenkel, I. Mayk, J.P. Unik, A.J. Gorski, W.D. Loveland, Phys. Rev. C12 (1975) 1809

[3] Y. Patin, S. Cierjacks, J. Lachkar, J. Sigand, G. Haouat, F. Cocu Nucl. Instr. & Meth. 160 (1979) 471

[4] H.H. Bissem, R. Georgi, W. Scobel, J. Ernst, M. Kaba, J. Rama Rao, H. Strohe, Phys. Rev. C, in press

[5] H. Sakai, H. Ejiri, T. Shibata, Y. Nagai, K. Okada, Phys. Rev. C20 (1979) 464

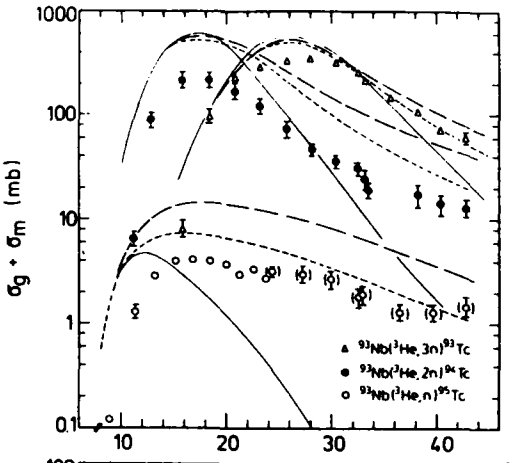

Fig. 3 Excitation functions and isomeric ratios for ^{93}Nb(^{3}He,xn). Data are from [4]. Calculations: Hauser-Feshbach with $\sigma/\sigma_{Rig} = 1$ (thin solid line), 0.7 (solid), 0.5 (dash dotted); PE competition included with $\sigma/\sigma_{Rig} = 1$ and assumption (ii) (dashed) and (iii) (short dashed), respectively.

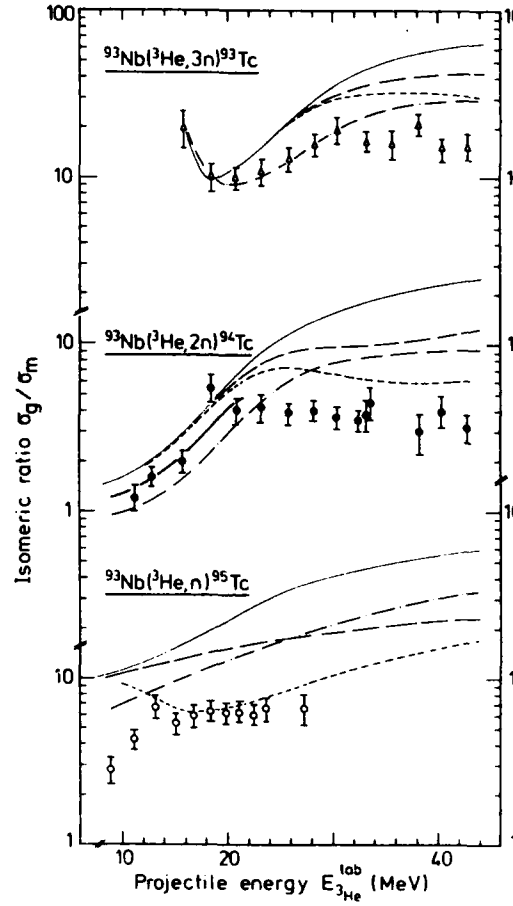

Fig. 4 Population of ^{95}Tc* following neutron emission for (from left to right) pure Hauser-Feshbach calculation, inclusion of PE with assumption (ii), and with assumption (iii). Population drops by $\sqrt{10}$ between two lines.

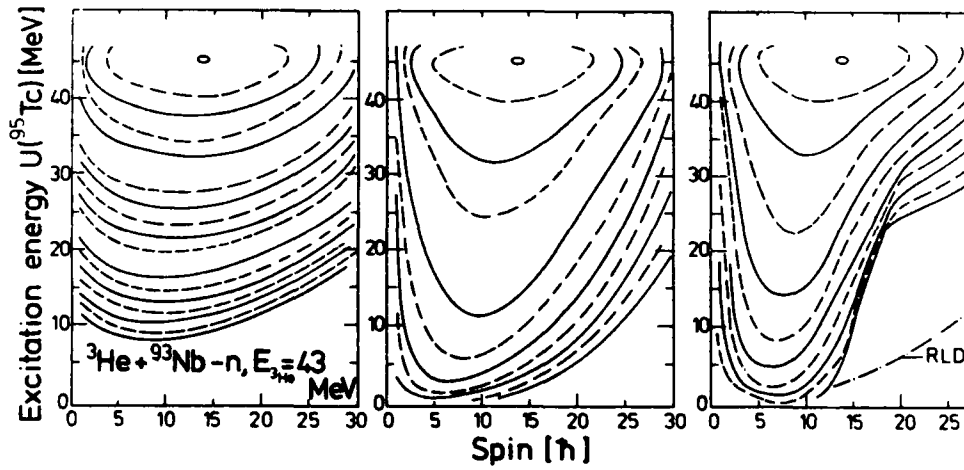

INSTITUT FÜR REINE UND ANGEWANDTE KERNPHYSIK
UNIVERSITÄT KIEL, FORSCHUNGSREAKTOR GEESTHACHT

Fast-Chopper Time-of-Flight Spectrometer

H.G. Priesmeyer, U. Harz, P. Fischer

1. Improvements Concerning the Experiment

The shut down period of research reactor FRG-1 was used to improve the Fast-Chopper Spectrometer in several aspects: both hardware and software of the data acquisition system have been modernized; the storage capacity for time-of-flight spectra was doubled; an integrated rotor speed control has been developed and remote adjustment of the neutron beam collimators was installed. A cryostat for LN_2 or LHe investigations and a device for measurements on gaseous samples have been built. As a result of the FRG-1 backfitting the neutron intensity increased.

2. Recalibration of the Flight Distance

It was considered necessary to redetermine the flight path length by a calibrating transmission experiment. Reference neutron energies were those of the low-lying ^{238}U resonances recommended by James. [NBS SP 493 (1977), 319]. The result is a flight path length of 42.93 ± 0.01 m.

3. Transmission of ^{99}Tc below 30 eV

The experiment is completed and the final results of the resonance shape analysis are given below. The exceptionally high values of Γ_γ for the first two resonances - found in a slowing-down-time experiment - were the reason for a reinvestigation by time-of-flight. Contaminations in the slowing-down-time samples are thought to have caused the high capture width values. Consistency with values derived from Russian measurements at higher energies is achieved. The contribution of the first two resonances to the resonance capture integral is 258 b.

The following data were determined:

E_o [eV]	Γ [meV]	$2g\ \Gamma_n^o$
5.59 ± 0.01	171.5 ± 4.5	1.45 ± 0.07
20.32 ± 0.01	176.0 ± 3.9	1.49 ± 0.015

4. Cs-Fission Product Mixture

The sample was investigated in 1969. Two resonances were seen, but no isotopic identification could be given. After 10 years 21 % of the ^{137}Cs originally present in the sample have decayed: this is adequate to allow for an isotopic identification of the resonances. The 1979 measurement with better resolution and statistics shows a third resonance at about 380 eV. Resonance analysis is in progress. The resonance at 42.08 eV can be assigned to longlived ^{135}Cs ($T_{1/2} = 2.3 \cdot 10^6$ y). SHAPE analysis gives the following preliminary results: Γ = 214 meV and $2g\ \Gamma_n$ = 33.4 meV. The contribution to the capture resonance integral is calculated to be ≈ 33 b.

Figs. 1 and 2 show the transmission spectra of the Cs Fission Product Mixture. The four resonances belonging to the either radioactive isotope are marked with an arrow. Co and Mn contaminations from the steel sample canning can also be seen.

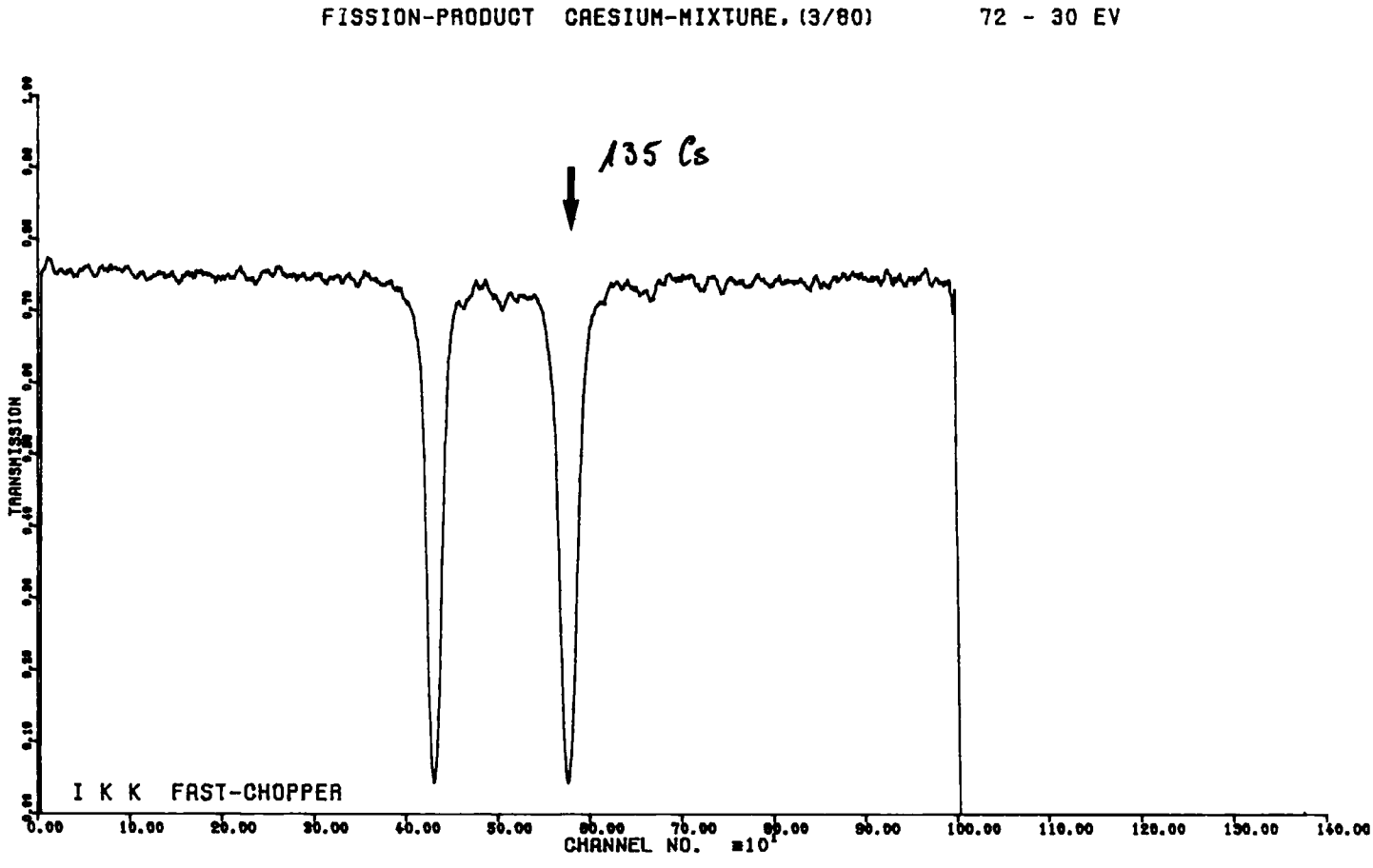

Fig. 1 Transmission spectrum of the Cs fission product mixture (72-30 eV).

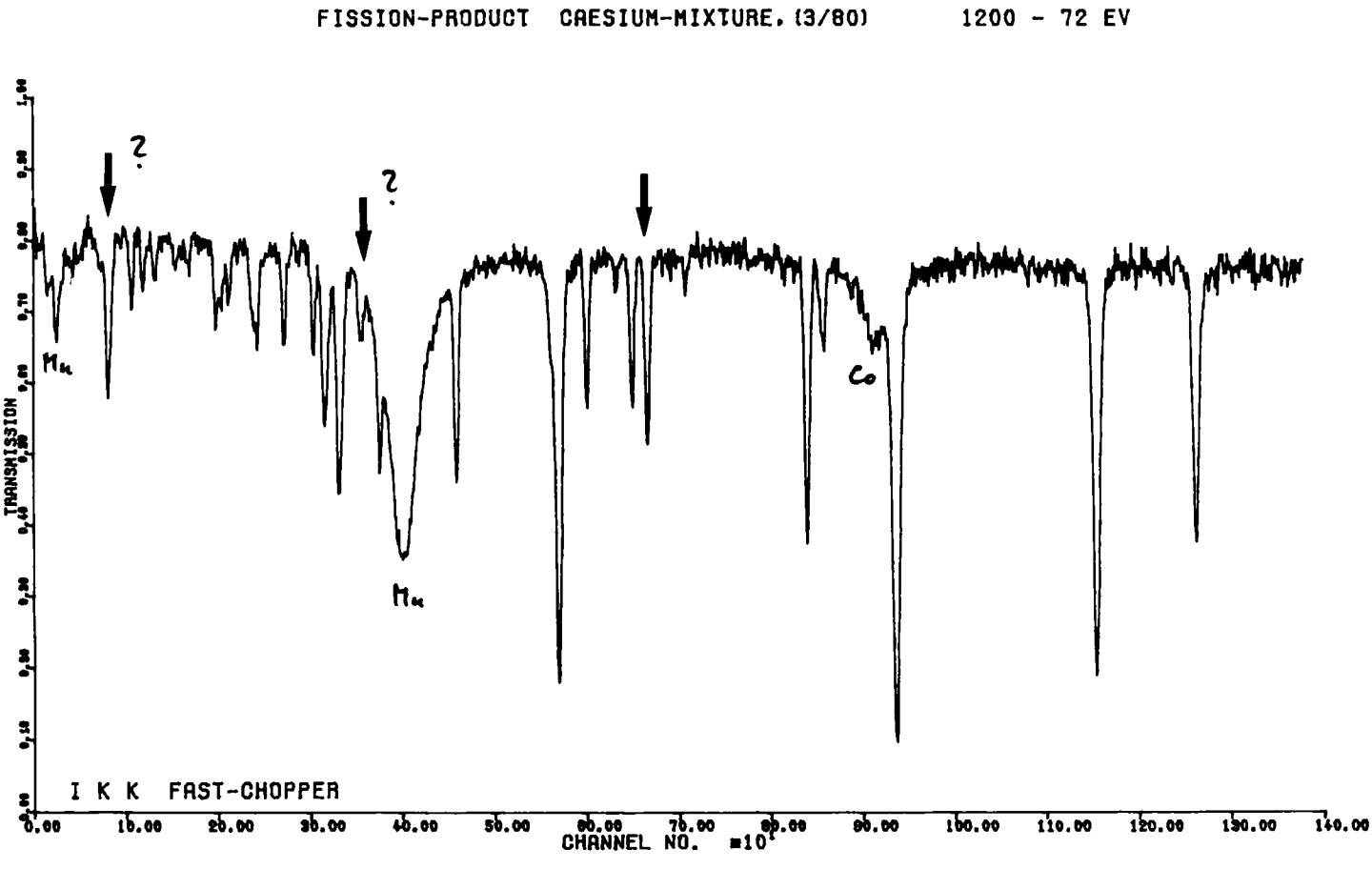

Fig. 2 Transmission spectrum of the Cs fission product mixture (1200-72 eV).

5. ^{129}I Transmission Experiment

An experiment on ^{129}I using the sample in its original canning showed 5 known resonance levels below 160 eV. The neutron intensity had to be considerably reduced. The measurements will be continued after repacking the material into another geometry.

Publications

P. Fischer, U. Harz, ASTA - a FORTRAN program for transmission calculations from time-of-flight spectra (in German), GKSS 78/E/47

P. Fischer, U. Harz, H.G. Priesmeyer, The total cross section of ^{99}Tc from 4.5 eV to 44 eV, Proc.Int.Conf. on Neutron Physics and Nuclear Data for Reactors and other Applied Purposes, Harwell (September 1978), NEA-Paris (1979) p. 718

H.G. Priesmeyer, Nuclear physics aspects of radiation damage in materials (in German), GKSS 79/E/16

H.G. Priesmeyer, Low energy neutron cross-section measurements of radioactive FP nuclides, Proc.Fission Products Nuclear Data - Specialist Meeting, Bologna 1979, NEANDC, in press

INSTITUT FÜR KERNCHEMIE
UNIVERSITÄT ZU KÖLN

1. Integral Excitation Functions of Nuclear Reactions Relevant to Cosmochemistry

R.Michel, G.Brinkmann, W.Herr

Extending our studies of p-induced reactions with target-elements $22 \leq Z \leq 28$ [1-4], we investigated α-induced reactions for the same elements in the energy region from 25 to 172.5 MeV. Both p- and α-induced reactions have to be considered for the interpretation of the various cosmic ray produced radionuclides observed in extraterrestrial matter. For specific cosmochemical applications, e.g. the determination of exposure ages, high precision σ-measurements are needed, but unless the respective experimental data are easily available, reliable theoretical predictions are necessary.

1.1 α-Induced Production of ^{24}Na and ^{22}Na from Aluminium

In order to check the absolute magnitude of our cross sections as well as the quality of the energy determination, we first measured excitation functions for the well-known reactions ^{27}Al(α,4p3n)^{24}Na and ^{27}Al(α,4p5n)^{22}Na using the 100 μm stopping foils in our stacks. A detailed description of the experimental procedure is given elsewhere [1-3,5].The cross-section results are presented in Table I and as an example our data for ^{24}Na are given in Fig.1 together with those from other authors.

The data for both radionuclides are in excellent agreement with earlier determinations, with the exception of the works of Bowman et al [13] and Lindner et al [6]. The excitation functions of the latter authors are evidently too low.

In the case of ^{24}Na the production from Al by secondary neutrons was corrected for as described by Martens and Schweimer [12]. The neutron contribution which was measured in Al-foils below 25 MeV was ~ 10 µb.

Thus the results for ^{24}Na and ^{22}Na in the stopping aluminium foils allow for a continuous quality control of the measurement of excitation functions of α-induced reactions on other target elements.

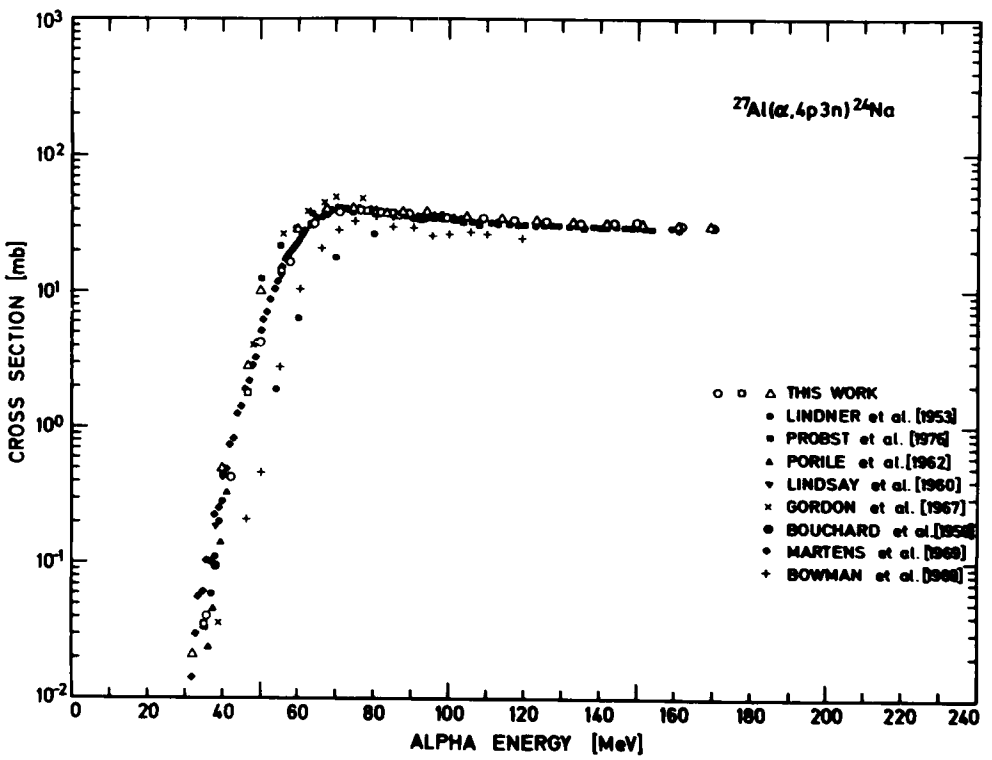

Fig.1 Excitation function for the reaction ^{27}Al(α,4p3n)^{24}Na. The data from other authors [6-14] are also shown. Three different symbols are used for our experimental data in order to distinguish between different experiments.

Table I. Experimental cross sections for the reactions $^{27}Al(\alpha,4p3n)^{24}Na$ and $^{27}Al(\alpha,4p5n)^{22}Na$

$E_\alpha \pm \Delta E_\alpha$ [MeV]	Cross-Section [mb] ^{24}Na	Cross-Section [mb] ^{22}Na	$E_\alpha \pm \Delta E_\alpha$ [MeV]	Cross-Section [mb] ^{24}Na	Cross-Section [mb] ^{22}Na	$E_\alpha \pm \Delta E_\alpha$ [MeV]	Cross-Section [mb] ^{24}Na
170.78 ± 0.28	30.07 ± 3.00	43.50 ± 3.92	170.38 ± 0.41	29.99 ± 2.74	42.24 ± 2.95		
161.68 ± 0.44	30.78 ± 3.10	43.60 ± 4.36	160.97 ± 0.58	30.84 ± 2.82	45.27 ± 3.17		
152.39 ± 0.55	32.04 ± 3.20	43.52 ± 3.92	151.27 ± 0.70	30.99 ± 2.83	43.70 ± 3.06		
144.04 ± 0.62	32.03 ± 3.52	42.94 ± 4.73	142.39 ± 0.77	32.14 ± 2.93	43.47 ± 3.04		
135.28 ± 0.68	32.82 ± 3.28	42.25 ± 3.80	133.00 ± 0.85	32.94 ± 3.00	44.78 ± 3.13		
126.07 ± 0.75	33.17 ± 2.99	40.96 ± 4.10	123.11 ± 0.92	33.79 ± 3.08	43.61 ± 3.05		
117.69 ± 0.80	34.47 ± 3.10	40.66 ± 3.66	114.08 ± 0.98	34.99 ± 3.19	40.32 ± 2.83		
108.79 ± 0.86	35.99 ± 3.96	40.19 ± 3.62	104.46 ± 1.05	35.99 ± 3.28	39.24 ± 2.75		
99.29 ± 0.90	36.43 ± 3.28	36.06 ± 3.25	94.13 ± 1.12	37.59 ± 3.42	34.20 ± 2.39		
89.02 ± 0.96	38.47 ± 3.84	30.38 ± 2.43	86.66 ± 0.60	37.76 ± 3.02	33.34 ± 2.66		
86.96 ± 0.39	37.82 ± 3.03	33.57 ± 2.35	82.85 ± 1.20	39.79 ± 3.62	30.92 ± 2.48	84.37 ± 0.64	38.77 ± 3.88
81.76 ± 0.47	39.20 ± 3.53	31.11 ± 2.18	80.73 ± 0.70	39.18 ± 3.13	30.69 ± 2.46	77.98 ± 0.74	40.77 ± 4.08
76.29 ± 0.54	40.09 ± 3.61	30.20 ± 2.12	74.42 ± /.79	42.31 ± 3.38	30.33 ± 2.43	71.11 ± 0.83	40.77 ± 3.92
70.50 ± 0.60	38.99 ± 3.12	33.73 ± 2.36	67.70 ± 0.87	40.84 ± 3.27	33.62 ± 2.69	63.69 ± 0.93	32.87 ± 3.13
64.31 ± 0.66	32.53 ± 2.60	40.61 ± 3.65	60.40 ± 0.96	29.53 ± 2.36	44.87 ± 3.59	55.45 ± 1.03	13.97 ± 1.12
57.63 ± 0.72	16.76 ± 1.34	53.58 ± 3.75	52.30 ± 1.07	10.53 ± 0.87	55.66 ± 4.45	46.15 ± 1.16	1.85 ± 0.17
50.26 ± 0.81	4.10 ± 0.33	50.69 ± 3.55	46.38 ± 1.16	2.84 ± 0.23	45.54 ± 3.64	35.12 ± 1.38	0.033 ± 0.003
41.95 ± 0.89	0.423 ± 0.038	10.35 ± 0.73	39.47 ± 1.28	0.488 ± 0.039	12.96 ± 1.04		
35.69 ± 0.97	0.040 ± 0.003		31.87 ± 1.47	0.021 ± 0.002			

1.2 Measurement and Hybrid Model Analysis of α-induced Reactions on Cobalt

20 individual excitation functions were measured for the production of ^{61}Cu, ^{57}Ni, $^{60m+g}Co$, $^{58m+g}Co$, ^{57}Co, ^{56}Co, ^{55}Co, ^{59}Fe, ^{52}Fe, ^{56}Mn, ^{54}Mn, $^{52m+g}Mn$, ^{51}Cr, ^{48}V, ^{47}Sc, $^{46m+g}Sc$, ^{44m}Sc, ^{44g}Sc, ^{43}K and ^{42}K from cobalt for α-particle energies from 25 to 172.5 MeV. The experimental data and a detailed discussion are given elsewhere [5]. Although the target element Co is of secondary importance for cosmochemical applications due to its rather low abundances in extraterrestrial matter, it is well suited for comparing excitation functions with theoretical predictions, since it has just one stable isotope. In our case, the experimental data were compared with calculations based on the hybrid model of Blann [15]. The excitation functions of nearly half the product nuclides are dominated by preequilibrium effects over wide energy ranges. From the reaction $^{59}Co(\alpha,2n)^{61}Cu$ an initial exciton number between $n_o = 4$ (2n-2p-0h) and $n_o = 5$ (2n-3p-0h) or (3n-2p-0h) is deduced. The theoretical predictions, however, which for p-induced reactions were very successful, show severe shortcomings for α-induced reactions. The excitation functions for $^{60m+g}Co$ (Fig.2) and for $^{58m+g}Co$ and ^{59}Fe (Fig.3) are underestimated by up to two orders of magnitude. For $^{60m+g}Co$ the discrepancy between theory and experiment can be attributed to break-up reactions of α-particles, whereas for the two other product nuclides even more complex reaction mechanisms have to be assumed. Moreover, the strong contribution of preequilibrium emission of α-particles observed for (α,2pxn) and (α,4pxn) reactions, which are not accounted for by the program OVERLAID ALICE[16], indicate that the initial reaction phase of α-induced reactions is more differentiated than is assumed by the hybrid model in its present form [17].

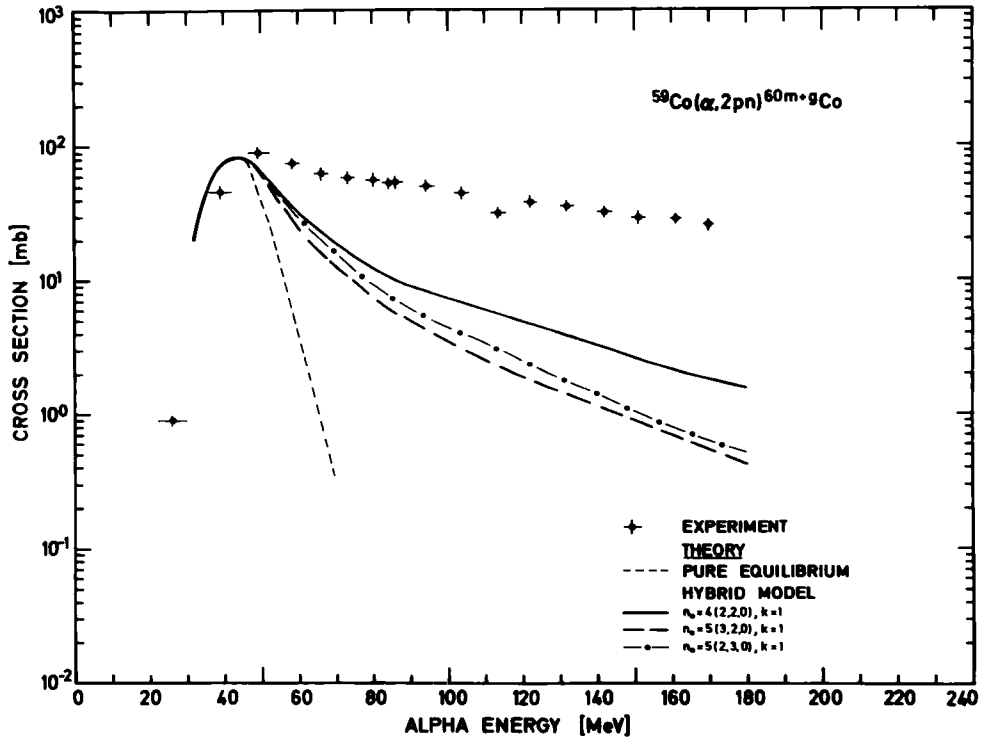

Fig.2 Comparison of the experimental excitation function for the reaction ^{59}Co(α,2pn)$^{60m+g}$Co with theoretical predictions.

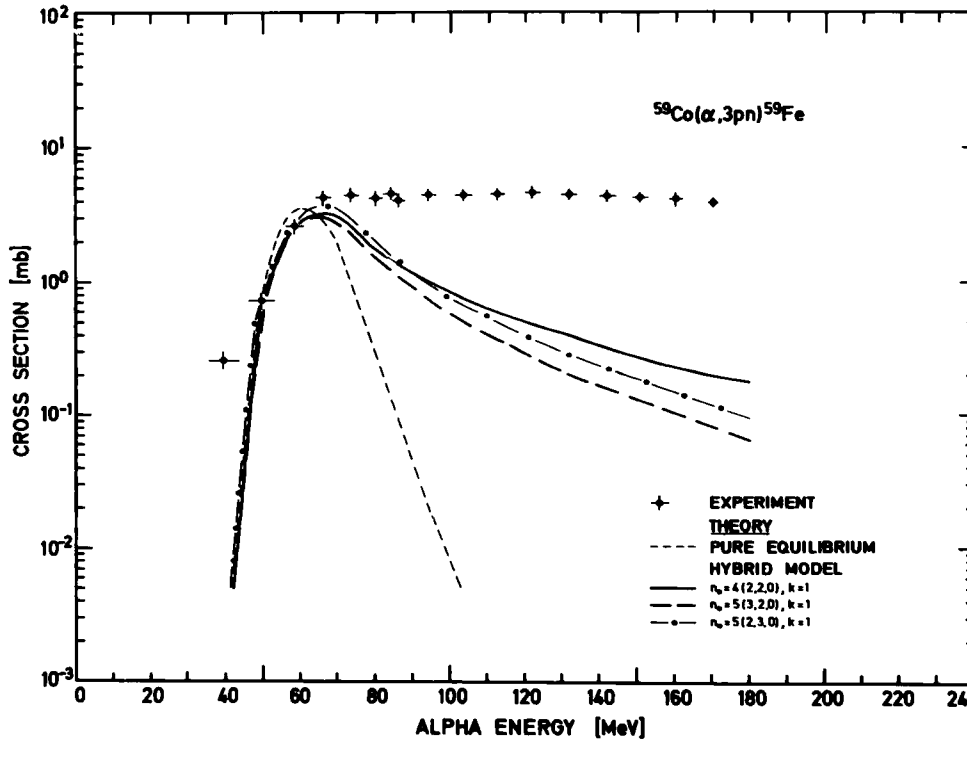

Fig.3 Comparison of the experimental excitation function for the reaction ^{59}Co(α,3pn)^{59}Fe with theoretical predictions.

1.3 Revision of Cross-Section Data for the Reaction $Ti(p,xn)^{48}V$

A typographical error occurred in our last year's progress report [4] in Table I (p.69) with respect to the cross section data for the production of ^{48}V from titanium.
The corrected data are:

$\sigma = 213 \pm 26$ mb at $E_p = 16.42 \pm 0.19$ MeV
$\sigma = 324 \pm 39$ mb at $E_p = 14.77 \pm 0.26$ MeV
$\sigma = 395 \pm 47$ mb at $E_p = 12.97 \pm 0.35$ MeV
$\sigma = 379 \pm 45$ mb at $E_p = 10.93 \pm 0.38$ MeV
$\sigma = 358 \pm 31$ mb at $E_p = 8.02 \pm 0.48$ MeV

2. Experimental Excitation Functions of p-Induced Reactions on Ba and Comparison with Theory

K.Prescher, G.Brinkmann, W.Herr

The cosmochemical interpretation of solar cosmic ray produced stable Xe-isotopes in meteorites and lunar samples is impeded by the lack of production cross-section data for these nuclides at proton energies < 100 MeV. In extraterrestrial matter, spallation-Xe is predominantly produced by proton reactions on Ba and most Xe-isotopes receive their main contributions from radioactive precursors.

Therefore, we have measured excitation functions for the production of ^{135}La, ^{133}La, ^{132}La, ^{135m}Ba, ^{133m}Ba, ^{133}Ba, ^{131}Ba, ^{129}Ba, ^{136}Cs, ^{134}Cs, ^{132}Cs, ^{129}Cs and ^{127}Xe from Ba in the proton energy range of 12 to 45 MeV. The cross sections also allow a test of the applicability of the hybrid model predictions to specific cosmochemical problems.

Ba-glass targets of natural isotopic composition were irradiated at the Jülich isochronous cyclotron JULIC. The excitation functions were determined using the stacked foil technique. In order to check the accuracy of the determina-

tion of the proton beam current as well as of the energy determination throughout the stack, we used vanadium-foils and the respective excitation functions for ^{51}Cr and ^{47}Sc as monitors. The cross-section data are shown in Table II.

Table II. Experimental cross sections for the production of ^{51}Cr and ^{47}Sc in the p-induced reactions on V

$E_p \pm \Delta E_p$ [MeV]	Cross Section [mb]		$E_p \pm \Delta E_p$ [MeV]	Cross Section [mb]	
	^{51}Cr	^{47}Sc		^{51}Cr	^{47}Sc
44.95 ± 0.11	22.8 ± 2.5	6.24 ± 0.62	33.06 ± 0.38	37.1 ± 3.7	11.8 ± 1.2
43.56 ± 0.18	25.3 ± 2.3	6.92 ± 0.69	31.03 ± 0.40	40.2 ± 4.0	9.45 ± 1.04
43.43 ± 0.10	24.4 ± 1.9	7.20 ± 0.50	29.26 ± 0.42	45.1 ± 4.5	7.41 ± 0.81
41.58 ± 0.25	28.3 ± 3.1	8.43 ± 0.84	28.99 ± 0.28	46.8 ± 3.3	9.06 ± 0.63
39.49 ± 0.28	29.0 ± 2.6	9.69 ± 0.87	27.39 ± 0.44	51.4 ± 5.1	5.06 ± 0.55
37.49 ± 0.31	31.5 ± 3.2	11.4 ± 1.0	25.35 ± 0.46	59.5 ± 6.0	2.85 ± 0.28
35.33 ± 0.34	34.4 ± 3.1	12.7 ± 1.2	23.09 ± 0.36	72.4 ± 5.8	1.81 ± 0.13
34.48 ± 0.11	33.8 ± 2.7	13.4 ± 0.94	22.51 ± 0.14	81.1 ± 6.5	1.55 ± 0.12

In Fig.4 the overall concordance with the data from the literature [3, 18, 19] is demonstrated.

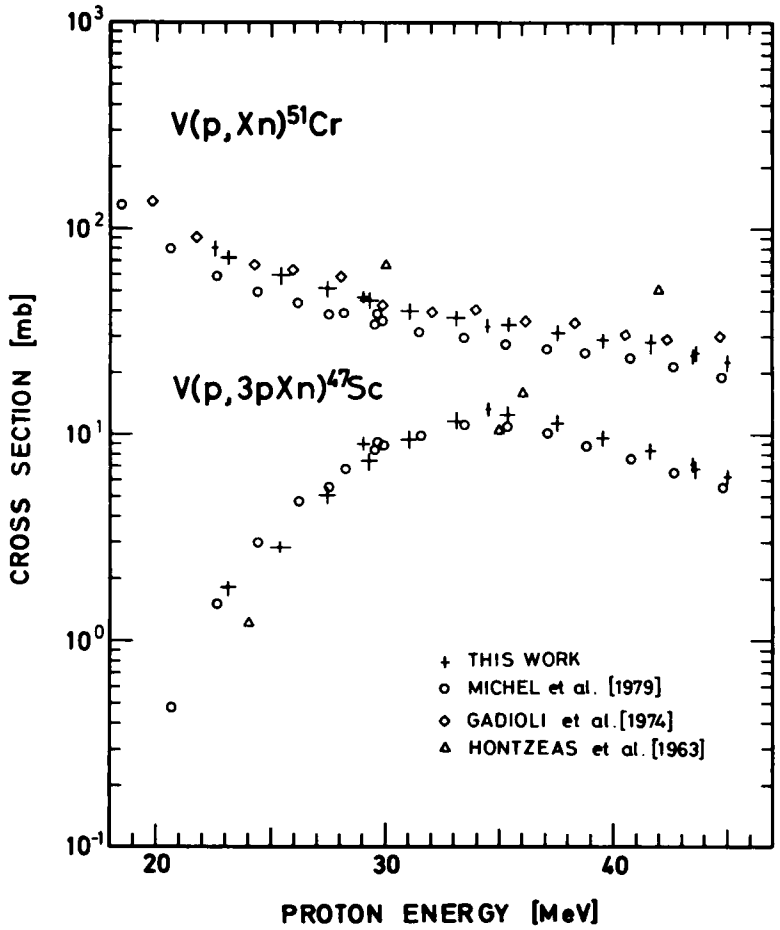

Fig 4 Experimental cross sections of the reactions $V(p,xn)^{51}Cr$ and $V(p,3pxn)^{47}Sc$.

Our new experimental excitation functions for Ba were compared with calculations using the computer code OVERLAID ALICE [16], which combines the concept of the compound nucleus in statistical equilibrium with that of preequilibrium reactions.

The general good agreement between theory and experiment is shown as an example in Fig.5. The shape of the ^{132}La excitation function is well reproduced; the theoretical curve, however, is shifted by ~ 4 MeV to lower energies. The reason may be the application of the rather crude mass formula from Meyers and Swiatecki [20]. There is also a discrepancy in the

low energy part of the ^{132}Cs-excitation function which results from the emission of α-particles.Similar deviations have already been observed for p-induced reactions on Ti [1] and on Ni [2]. They were explained by preequilibrium emission of α-particles, which is not considered in the hybrid model.

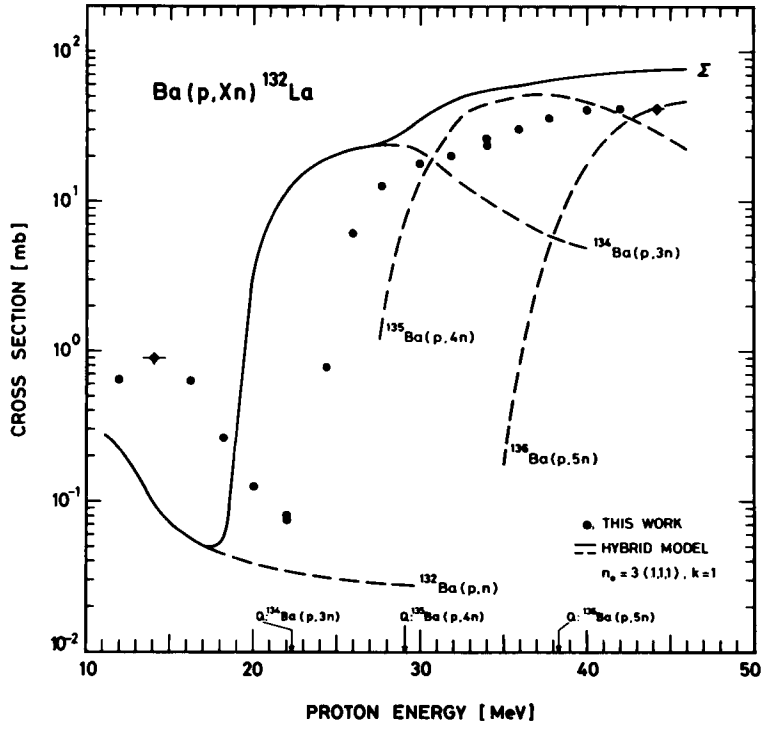

Fig.5 Experimental excitation function and hybrid model calculations of the reaction Ba(p,xn)^{132}La.

References

[1] R.Michel, G.Brinkmann, H.Weigel, W. Herr, J.Inorg.Nucl.Chem.40 (1978) 1845

[2] R.Michel, H.Weigel, W.Herr, Z.Phys.A 286 (1978) 393

[3] R.Michel, G.Brinkmann, H.Weigel, W. Herr, Nucl.Phys.A 322 (1979) 40

[4] R.Michel, G.Brinkmann, W.Herr, in NEANDC (E)-202 U Vol.V/ INDC(Ger)-21/L + Special (1979)

[5] R.Michel, G.Brinkmann, Nucl.Phys.A 338(1980) 167

[6] M.Lindner, R.N.Osborne, Phys.Rev.91 (1953) 342

[7] H.J.Probst, S.M.Qaim, R.Weinreich, Int.J.Appl.Rad.and Isot. 27 (1976) 431

[8] N.T.Porile, Phys.Rev.127 (1962) 224

[9] R.H.Lindsay, R.J.Carr, Phys.Rev.120 (1960) 2168; idem 118 (1960) 1293

[10] B.Gordon, BNL-50082 (1967) 82

[11] G.H.Bouchard, A.W.Fairhall, Phys.Rev.116 (1959) 160

[12] U.Martens, G.W.Schweimer, KFK-1083 (1969); Z.Physik 233 (1970) 170

[13] W.W.Bowman, M.Blann, Nucl.Phys. A 131 (1969) 513

[14] A.Karpeles, Radiochim.Acta 12 (1969) 115

[15] M.Blann, Phys.Rev.Lett.27 (1971) 337

[16] M.Blann, UR-NSRL-181 (1978)

[17] M.Blann, A.Mignerey, W.Scobel, Nukleonika 21 (1976) 335

[18] E.Gadioli, A.M.Grassi Strini, G.Lo Bianco, G.Strini, G.Ragliaferri, Nuovo Cim. 22 A (1974) 547

[19] S.Hontzeas, L.Yaffe, Can.J.Chem.41 (1963) 2194

[20] W.D.Meyers, W.J.Swiatecki, Nucl.Phys.81 (1966) 1

FACHBEREICH ANORG. CHEMIE UND KERNCHEMIE
TECHNISCHE HOCHSCHULE DARMSTADT

(p,t..), (d,t..) and (α,t..)-Cross Sections for Al, V, Nb and Au*

M. Merkel, H. Münzel

Our previous studies about the cross sections for (p,t..), (d,t..) and (α,t..)-reactions were extended to higher projectile energies. Stacks of Al, V, Nb and Au foils were irradiated at the Karlsruhe Isochronous Cyclotron and the Jülich Isochronous Cyclotron (JULIC). Thick target yields for triton formation have been measured for proton induced reactions up to 45 MeV, deuteron induced up to 70 MeV and α-induced up to 104 MeV. After the irradiations the foils were heated in a hydrogen-atmosphere and the activity of the extracted tritium was determined in a proportional counter using methane as counting gas [1]. The thick target yields are given in Table I. From those thick target yields cross sections were calculated. As an example the corresponding cross sections for the (α,t..)-reactions versus the energy ΔE^* are shown in Fig. 1. ΔE^* is the difference $E_{CM} - E_{TH}$ between the projectile-energy in the center of mass system and the reaction threshold energy [1]. The excitation functions for different target materials show a similar behaviour. The cross sections increase up to a maximum which is located at about 70 MeV. It should be pointed out here that cross sections of 100 mb for triton emission are surprisingly high.

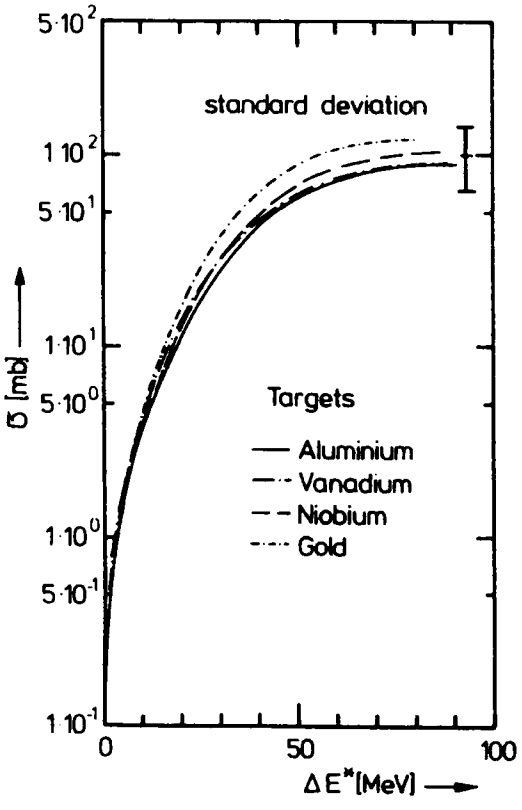

Fig.1 Measured cross sections for (α,t..)-reactions

* Supported by the Bundesministerium für Forschung und Technologie, Federal Republic of Germany and the Nuclear Research Centers in Karlsruhe and Jülich

Table I. Thick target yields for (x,t..)-reactions

Projectile	Incident projectile energy (MeV)	Thick target yields *			
		Aluminium	Vanadium	Niobium	Gold
p	16.0	-	1.20E-7	-	8.64E-8
p	20.0	-	2.84-6	4.05E-6	-
p	21.0	-	-	-	4.49E-6
p	25.0	1.53E-5	1.51E-5	1.35E-5	1.53E-5
p	35.0	8.24E-5	6.02E-5	4.12E-5	4.88E-5
p	45.0	2.36E-4	1.72E-4	1.06E-4	1.26E-4
d	12.0	2.05E-6	2.05E-6	2.37E-6	6.80E-7
d	18.0	2.03E-5	1.51E-5	1.85E-5	1.97E-5
d	24.0	7.27E-5	5.19E-5	5.14E-5	5.08E-5
d	38.0	2.91E-4	1.99E-4	1.60E-4	1.46E-4
d	50.5	-	4.61E-4	-	-
d	50.8	7.53E-4	-	3.42E-4	2.69E-4
d	60.0	1.31E-3	8.96E-4	5.45E-4	4.79E-4
d	70.0	1.77E-3	1.23E-3	7.26E-4	5.98E-3
α	20.0	1.02E-6	3.36E-7	1.88E-8	-
α	25.0	3.14E-6	-	-	7.55E-8
α	30.0	8.60E-6	4.93E-6	1.54E-6	4.50E-7
α	40.0	3.10E-5	1.70E-5	9.71E-6	4.79E-6
α	48.0	7.05E-5	-	-	-
α	50.0	-	5.75E-5	2.99E-5	1.49E-5
α	60.0	2.33E-4	1.48E-4	7.60E-5	3.96E-5
α	70.0	3.65E-4	2.82E-4	1.33E-4	8.00E-5
α	80.0	5.39E-4	3.76E-4	2.23E-4	1.58E-4
α	90.0	9.24E-4	6.28E-4	3.40E-4	2.32E-4
α	102,0	1.19E-3	7.95E-4	5.01E-4	3.45E-4

* The yields are given as the number of tritons per incident projectile

Reference

[1] M. Merkel, H. Münzel, Formation of tritium in nuclear reactions induced by deuterons and α-particles, Nucl.Phys. A333 (1980) 173

INSTITUT FÜR KERNCHEMIE
UNIVERSITÄT MAINZ

Influence of Prompt Neutron Emission and Scission Shape on the Product Yield Distribution in $^{235}U(n_{th},f)$

H.O. Denschlag, H. Braun, W. Faubel, G. Fischbach, H. Meixler, G. Paffrath, W. Pörsch, R. Sehr, B. Sohnius, M. Weis, H. Schrader[1)], G. Siegert[1)], J. Blachot[2)], Z.B. Alfassi[3)+], H.N. Erten[4)+], T. Izak-Biran[5)+], T. Tamai[6)+], A.C. Wahl[7)+], K. Wolfsberg[8)+]

Fission products were separated according to mass, ionic charge state, and kinetic energy [1,2] using the mass separator LOHENGRIN. The yields of single members of the mass chains were obtained by measuring the γ-rays emitted following their β-decay. Absolute γ-ray line intensities and branching ratios - when not known - were determined by separate radiochemical experiments [3].

---

1) Institut Laue-Langevin, Grenoble, France
2) Centre d'Etudes Nucleaires, Grenoble, France
3) Ben Gurion University, Beer Sheva, Israel
4) Middle East Technical University, Ankara, Turkey
5) Soreq Nuclear Research Centre, Yavne, Israel
6) Kyoto University Research Reactor Institute, Japan
7) Washington University, St. Louis, Missouri, USA
8) Los Alamos Scientific Laboratory, Los Alamos, New Mexico, USA
+ Guest Scientist at Universität Mainz

Since the kinetic energy of a given fission product is related to the shape of the compound nucleus at scission and is inversely correlated to the internal excitation energy (i.e. mainly prompt neutron emission) of both complementary fragments, the results may be discussed with respect to these parameters.

The discussion presented in [1] may be summarized in four points.

(1) A preferential formation of neutron rich (low Z) chain members is found at high kinetic energies of the fragments and is presumably accounted for by the decreasing prompt neutron emission with increasing excitation energy.

(2) The persistence of an even-odd pairing effect in the yields throughout the range of kinetic energies studied leads to the conclusion that the high internal excitation energy of the fragments is appearing in the form of collective energy (e.g. deformation energy) at scission rather than in the form of single particle excitation.

(3) Generally, the yield distribution at constant kinetic energy is invariant with respect to the ionic charge state of the isotopes separated. However, a converted isomeric transition of a ns-isomer decaying in the vacuum of the separator before entering the magnetic field will produce a higher than average ionic charge state due to Auger events. In consequence, this nuclide is observed preferentially at high ionic charge states and the other chain members will be relatively depleted. The effect was observed in chains 99, 102, 133, 136 [1] and 139 [2].

(4) A particularly interesting aspect of the results obtained is the variation of the independent formation ratio of single isomeric states with the kinetic energy of the fragments. All the isomeric pairs observed (Nb-99, Nb-102, Sb-132, Te-133, I-134, and I-136) show a more or less pronounced decrease in the yield of the high spin isomer with increasing kinetic energy. The results can be interpreted in terms of the angular momentum produced at the scission point and its dependence on fragment deformation.

References

[1] H.O. Denschlag, H. Braun, W. Faubel, G. Fischbach, H. Meixler, G. Paffrath, W. Pörsch, M. Weis, H. Schrader, G. Siegert, J. Blachot, Z.B. Alfassi, H.N. Erten, T. Izak-Biran, T. Tamai, A.C. Wahl, K. Wolfsberg, in Physics and Chemistry of Fission (Proceedings Symp. Jülich, 1979), IAEA, Vienna (1980), in press

[2] H. Braun, H.O. Denschlag, W. Faubel, W. Pörsch, R. Sehr, B. Sohnius, H. Schrader, ILL-Annex to the Annual Report (1979) und H. Braun, H.O. Denschlag, H. Erten, W. Faubel, H. Meixler, W. Pörsch, R. Sehr, B. Sohnius und H. Schrader, Jahresbericht 1979, Institut für Kernchemie, Universität Mainz

[3] Progress Report on Nuclear Data Research in the Federal Republic of Germany (1979), Report NEA NDC (E)-202 U Vol V and INDC (Ger)-21/L + Special

INSTITUT FÜR STRAHLENPHYSIK
UNIVERSITÄT STUTTGART

Analyzing Power of Uranium-238 and Lanthanum for 7.6 MeV Neutrons

J.W. Hammer, D. Kollewe, W. Kratschmer, G. Schleußner, E. Speller

With a scattering experiment using 50 % polarized neutrons of the $^{9}Be(\alpha,n)^{12}C$ reaction the analyzing power of Uranium-238 and natural lanthanum has been determined. The α-beam of 2.8 MeV was delivered by the high current Dynamitron accelerator of the Institut für Strahlenphysik at Stuttgart. The used DC-beam currents were in the range of 300 μA to 1 mA. The resulting neutron energy was 7.6 MeV at a reaction angle of 60°.

The Stuttgart scattering facility consists of a shielded source, a spin flip magnet between source and scattering sample and 4 neutron detectors which are properly shielded too. The reaction angle can be varied between 0 and 70 degrees, the angle of the detectors between 0 and 125 degrees. Fig. 1 shows a schematic top view of the neutron scattering experiment.

Neutron spectroscopy has been performed by unfolding the proton recoil spectra,obtaining a resolution of about 8 - 10 %. Gamma events have been nearly totally removed by n-γ-discrimination. Background has been measured and subtracted separately. Measuring left-right asymmetries with symmetrically arranged detectors and with spin up and down we could eliminate apparative asymmetries and evaluate the analyzing power. Fig. 2 shows a plot of the analyzing power of uranium-238 and Fig. 3 of lanthanum.

We have made an optical model analysis using a coupled channels code for both the elements. The results are shown as solid lines in Figs. 2 and 3. The agreement of the coupled channels calculations with the experiments are not yet satisfactory and will have to be improved.

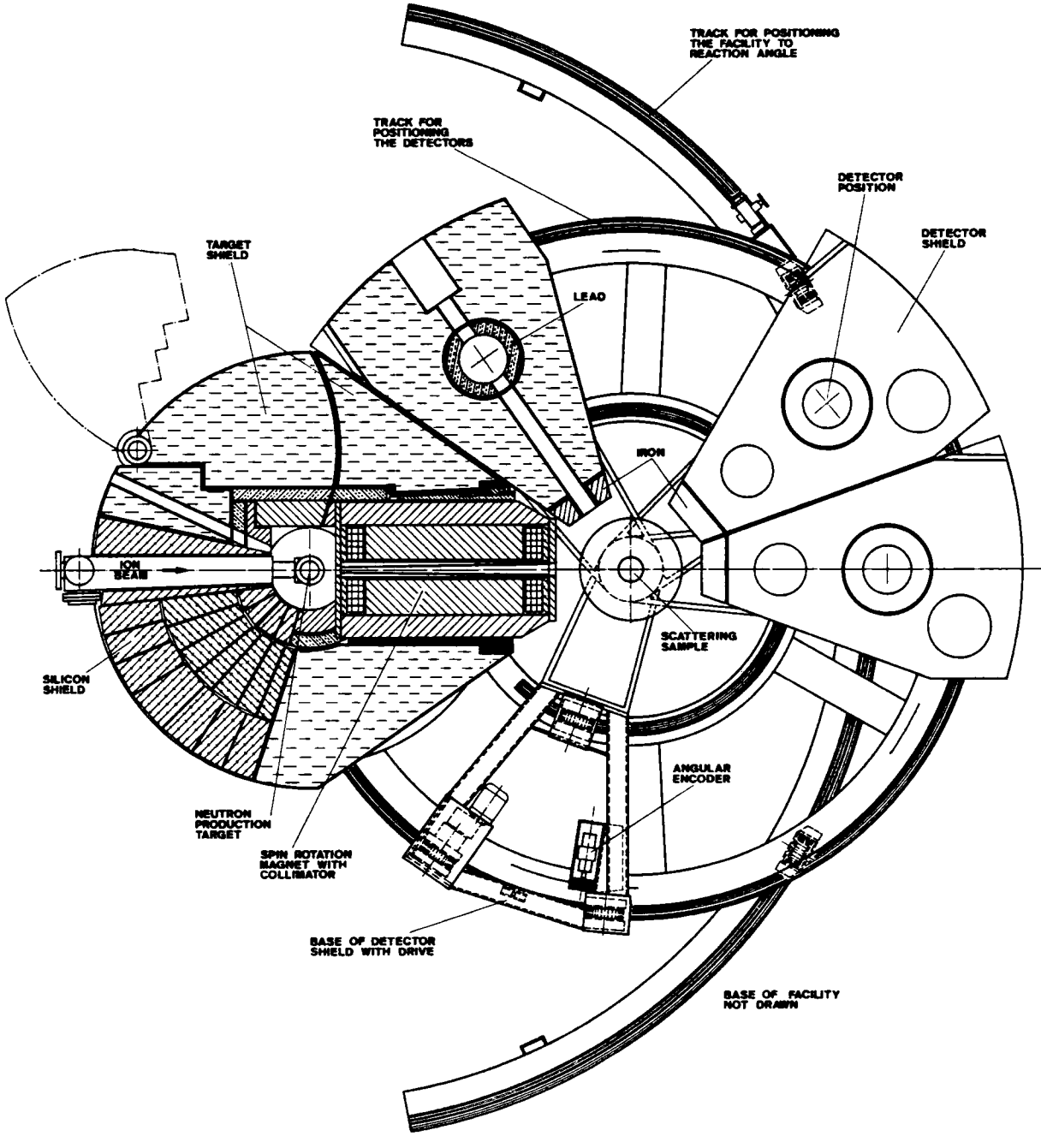

Fig. 1 Schematic top view of the Stuttgart neutron diffraction experiment.

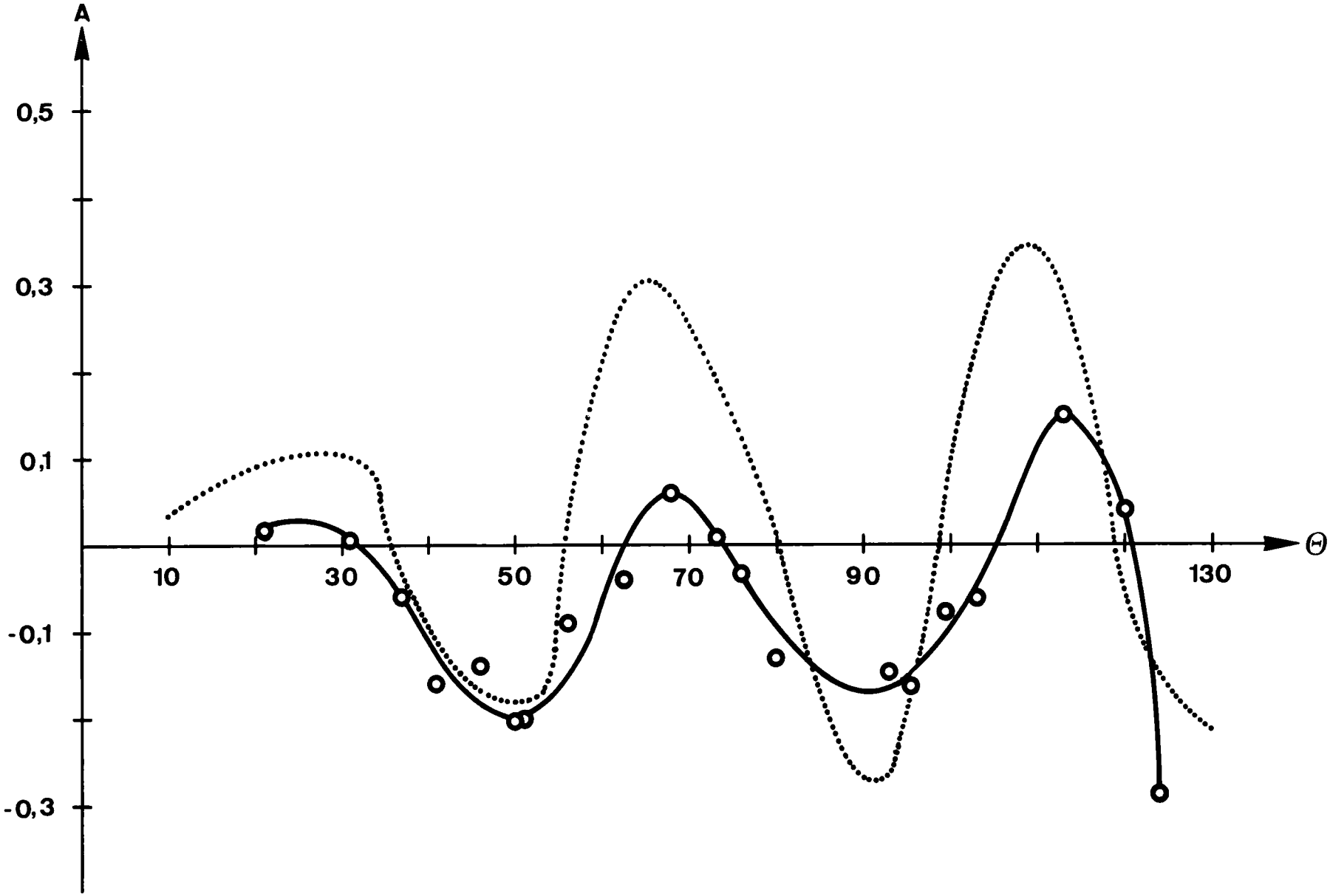

Fig. 2 Analyzing power of uranium-238 (solid line) and optical model calculations (dashed line).

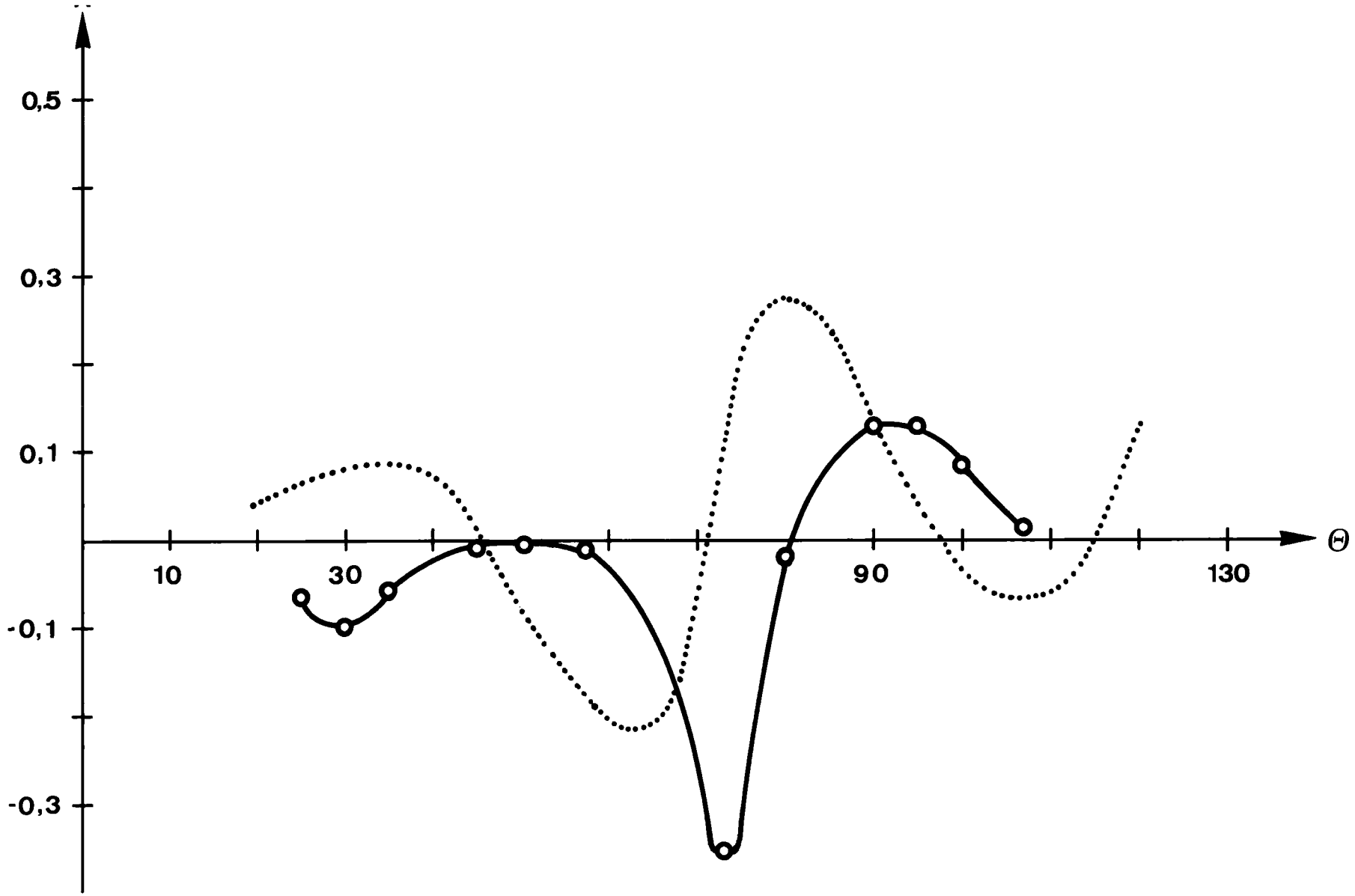

Fig. 3 Analyzing power of lanthanum (solid line) and optical model calculations (dashed line).

REAKTORSTATION GARCHING, FACHBEREICH PHYSIK
TECHNISCHE UNIVERSITÄT MÜNCHEN

1. Coherent Neutron Scattering Lengths

L. Koester, K. Knopf, J. Meier

In continuation of the work for the determination of the fundamental spin state scattering lengths we applied the Christiansen filter technique to measure the bound coherent scattering lengths in particular for separated isotopes of the elements arsenic, selenium, bromine, strontium, yttrium, zirconium, silver and indium.
Some results are available at present.
We found for As and Se the following values:

As: $b = 6.58 \pm 0.01$ fm and
$b_+ = 6.04 \pm 0.05$ fm, $b_- = 7.47 \pm 0.08$ fm

Se: $b = 7.970 \pm 0.009$ fm and
$b(76) = 12.2 \pm 0.1$ fm; $b(77) = 8.25 \pm 0.08$ fm
$b(78) = 8.24 \pm 0.09$ fm; $b(80) = 7.48 \pm 0.03$ fm and
$b(82) = 6.34 \pm 0.08$ fm

These results were compared with the resonance parameters of the nuclei and with different sets of potential scattering radii. We found that there is no evidence for a bound level of ^{76}As, but clear indications for strong bound levels of ^{77}Se and ^{78}Se.

Measurements on silver and indium isotopes resulted in values for the bound scattering lengths as follows:

Ag: $b = 5.97 \pm 0.01$ fm
$b(107) = 7.64 \pm 0.04$ fm and
$b_+ = 8.22 \pm 0.09$ fm, $b_- = 5.9 \pm 0.2$ fm
$b(109) = 4.19 \pm 0.03$ fm and
$b_+ = 3.27 \pm 0.08$ fm, $b_- = 7.0 \pm 0.2$ fm

In: $b = 4.065 \pm 0.020$ fm
$b(113) = 5.39 \pm 0.06$ fm
$b(115) = 4.00 \pm 0.03$ fm and
$b_+ = 2.1 \pm 0.1$ fm, $b_- = 6.4 \pm 0.1$ fm

These values are consistent with the resonance data listed in BNL 325, Vol. I, 3rd ed. (1973), if bound levels of silver isotopes are assumed.

Experiments on Christiansen filters filled with gases at various pressures and with powder as reference led to preliminary data for the coherent scattering lengths of the bound atoms as listed in the following:

argon	: b = 1.85 ± 0.10 fm
neon	: b = 4.547 ± 0.011 fm
krypton	: b = 7.80 ± 0.10 fm
deuterium	: b = 6.65 ± 0.05 fm

These values are only in fair agreement with data obtained recently by interferometer experiments [1].

2. Neutron Cross Sections

L.Koester, W. Waschkowski

Exact values for scattering cross sections at "zero-energy" σ_0 and coherent scattering lengths are needed for the determination of the fundamental spin state scattering lengths, which describe completely the scattering of slow neutrons by nuclei.

Zero-energy scattering cross sections are derived from total cross sections measured in the eV-region of the neutron energy. Transmission measurements were carried out on powdered samples of compounds of ordinary elements or separated isotopes with neutrons of 1.2 eV and 5.2 eV energy detected by means of rotating resonance detectors. From the measured total cross section the value of the scattering cross section at zero energy was obtained by taking into account the absorption, solid state effects and resonance contributions.

Measurements were performed on samples of the ordinary elements Zr, Mo and Se and on compounds containing the elements Y, As, Ca and Br.

The results for As and Se are:

σ_0(As) = 5.43 ± 0.02 b and σ_0(Se) = 8.22 ± 0.10 b.

These values contain incoherent parts of

σ_{inc}(As) = 0.06 ± 0.01 b [2] and σ_{inc}(Se) = 0.34 ± 0.10 b.

References

[1] H. Kaiser et al., Z.Physik A291 (1979) 231

[2] H. Glättli et al., J. de Physique 40 (1979) 629

PHYSIKALISCH-TECHNISCHE BUNDESANSTALT
BRAUNSCHWEIG

1. Radionuclide Data

Gamma- and X-Ray Emission Probabilities

K. Debertin, U. Schötzig

Gamma- and X-ray emission probabilities of several radionuclides were determined by using activity-calibrated sources and germanium spectrometers. Particular emphasis was given to measurements with nuclides emitting gamma- or X-rays in the energy range from 30 to 400 keV. Most of the results which are quoted in Table I have already been published [1,2]. The given uncertainties correspond to one standard deviation and include systematic uncertainties.

2. Neutron Cross Sections

Evaluation of a "Best" Set of Californium-252 Spectrum-Averaged Cross Sections

W. Mannhart

In continuation of earlier published work [3], the data of six different experiments [3-9] were reanalyzed to generate the specific covariance matrices containing the complete uncertainty information of each experiment. Based on this data, the experiments were combined by a non-diagonal weighted least-squares fit to generate a "best" set of recommended cross-section data. The procedure used [9] in combining the various data allows in a purely mechanical (i.e., independent of any arbitrary weighting) way the evaluation of data as soon as the covariances of the data are determined. Additionaly, each new data set with a covariance matrix can simply be added to the present evaluation without the need of starting the whole evaluation from the very beginning. The results are given in Tables II and III. With the exception of a few measurements with standard deviations evident larger than 2%, representing data only measured in a single experiment, one recognizes from Table III that there are strong correlations between all non-fission reactions and between all fission reactions. However, one recognizes also relatively small correlations between the fission and non-fission reactions. This fact indicates the need of performing an additional experiment which connects closer the fission and non-fission data to improve the consistency of the total data set.

Table I. Gamma- and X-ray emission probabilities p per decay

Nuclide	Energy in keV	p
^{51}Cr	320.1	0.0985(9)
^{57}Co	136.5	0.1058(8)
^{133}Ba	30.8(K_α)	0.971(16)
	35.1(K_β)	0.232(5)
	53.1	0.0220(4)
	79.6	0.0261(7)
	81.0	0.340(8)
	356.0	0.623(7)
^{141}Ce	145.4	0.489(4)
^{152}Eu	39.9(Sm-K_α)	0.591(12)
	45.7(Sm-K_β)	0.149(3)
	42.8(Gd-K_α)	0.00648(22)
	48.9(Gd-K_β)	0.00176(18)
	121.8	0.2837(24)
^{182}Ta	31.7	0.00892(21)
	42.7	0.00266(8)
	58.o/59.3(K_α)	0.2802(52)
	65.7...69.1($K_\beta+\gamma$)	0.571(13)
	84.7	0.0263(10)
	100.1	0.1423(42)
	113.7	0.0187(6)
	116.4	0.00445(15)
	152.4	0.0695(9)
	156.4	0.0263(5)
	179.4	0.0309(4)
	198.3	0.0144(2)
	222.1	0.0750(10)
	229.3	0.0364(5)
	264.1	0.0362(6)
	1121.3	0.3530(32)
	1189.0	0.1644(15)
	1221.4	0.2717(25)
	1231.0	0.1158(11)
	1257.5	0.0150(2)
	1289.2	0.0136(2)

Table II. Evaluated set of californium-252 spectrum-averaged cross sections

Reaction	$\langle\sigma\rangle$ (mb)	Std. dev. %
Mg-24(n,p)	1.918	4.90
Al-27(n,p)	4.862	3.55
Al-27(n,α)	1.014	2.00
S-32(n,p)	71.78	4.50
Ti-46(n,p)	14.11	2.20
Ti-47(n,p)	19.26	2.12
Ti-48(n,p)	0.4240	2.41
V-51(n,p)	0.7156	8.94
Fe-54(n,p)	86.55	2.12
Fe-56(n,p)	1.459	2.36
Ni-58(n,p)	115.4	1.67
Co-59(n,α)	0.2186	7.41
Zn-64(n,p)	40.14	2.46
In-113(n,n')	162.2	2.27
In-115(n,γ)	125.7	2.96
In-115(n,n')	197.9	2.19
Au-197(n,γ)	76.83	2.27
Au-197(n,2n)	5.512	2.51
U-235(n,f)	1204	1.61
Np-237(n,f)	1339	2.14
U-238(n,f)	319.1	2.08
Pu-239(n,f)	1798	1.83

Table III. Correlation matrix (x 100) of the evaluated data

Mg-24(n,p)	100									
Al-27(n,p)	21	100								
Al-27(n,α)	36	48	100							
S-32(n,p)	22	26	38	100						
Ti-46(n,p)	28	38	69	30	100					
Ti-47(n,p)	30	40	72	32	74	100				
Ti-48(n,p)	27	36	63	28	73	67	100			
V-51(n,p)	5	15	18	6	15	16	14	100		
Fe-54(n,p)	31	41	71	33	63	66	58	15	100	
Fe-56(n,p)	30	38	67	31	58	62	55	14	65	100
Ni-58(n,p)	33	46	82	36	77	81	70	17	83	68
Co-59(n,α)	9	19	23	12	18	19	17	9	19	18
Zn-64(n,p)	27	39	64	29	55	59	51	15	57	54
In-113(n,n')	33	43	70	31	61	64	61	18	63	60
In-115(n,γ)	25	32	53	23	46	49	47	14	48	46
In-115(n,n')	35	44	71	32	63	66	66	18	66	62
Au-197(n,γ)	31	43	69	30	61	63	59	18	63	59
Au-197(n,2n)	28	42	64	27	55	58	54	19	58	54
U-235(n,f)	8	11	19	9	17	18	16	4	19	16
Np-237(n,f)	6	8	14	6	13	13	12	3	14	12
U-238(n,f)	5	7	12	6	11	12	10	3	12	10
Pu-239(n,f)	7	10	17	8	15	16	14	4	16	14

100											
21	100										
64	19	100									
70	20	56	100								
53	15	43	68	100							
73	20	58	85	65	100						
70	20	56	83	65	84	100					
64	21	52	75	57	74	81	100				
27	5	15	16	13	17	16	15	100			
20	4	11	12	9	13	12	11	73	100		
17	3	10	10	8	11	11	10	89	75	100	
24	5	13	15	11	15	15	13	73	61	70	100

3. Variable Energy Cyclotron

High-Precision Fast Neutron Scattering Experiments

H.J. Brede, H. Klein, H. Schölermann, B.R.L. Siebert

Recently some details of the multi-angle TOF-spectrometer have been published regarding the properties of the cyclotron [10], the multiparameter data acquisition system [11], the multichannel collimator [12] and the design of liquid scintillation detectors [13].

In addition, details of the experimental setup for high precision neutron scattering experiments in the energy range of 6 MeV to 14 MeV have been studied with regard to:

(a) $D(d,n)^3He$ neutron source

This reaction is often used because of the simple handling of deuterium gas targets. Assumming that the material and thickness of the entrance foil as well as the beam stop of the deuterium gas cell are optimized the applicability of this neutron source is limited due to the energy and angular resolution and to background neutrons [14]. The large amount of neutrons from d-breakup reactions, which rapidly increases with the projectile energy, finally restricts inelastic scattering experiments.

(b) Sample size corrections

The corrections due to the neutron flux attenuation and the multiple scattering within the sample and the influence of the geometrical setup of the gas cell, the scatterer and the detector on the evaluation of the angular distribution have been studied. For various samples of carbon, polyethylene or iron the time-of-flight (TOF) spectra have been simulated by means of Monte-Carlo technique because often used analytical approaches fail in correcting the scattering on light nuclei where kinematical effects become important. Calculations on the basis of averaged cross sections (ΔE = 0.5 MeV) for carbon (Fig. 1a) and polyethylene (Fig. 1b) samples of the same size demonstrated the need to fully simulate the TOF-spectra. The contributions of multiple scattered neutrons in the region of elastic and inelastic scattering on carbon are quite different and therefore require quite different evaluations.

This program is used to optimize the shape, size and geometrical setup of scattering samples [15]. An improved version based on point cross sections will allow to determine all corrections with sufficient accuracy.

(c) Detector efficiency

The efficiency of our various liquid TOF-scintillators for neutrons in the energy range of 1 MeV up to 20 MeV will be calibrated with reference to a proton recoil telescope. A Monte-Carlo program [16] has been developed which simulates the geometry of the neutron source, the telescope and various detectors and computes appropriate correction factors. In addition the well known differential cross sections of the D(d,n)-reaction [17] and n-p-scattering in a polyethylene reference scatterer are considered. This calibration will be compared to extensive MC-calculations of response functions [18]. The analysis of recent experiments is in progress.

References

[1] K. Debertin, Nucl.Instr.Methods 165 (1979) 279

[2] U. Schötzig, K. Debertin, K.F. Walz, Nucl.Instr.Methods 169 (1980) 43

[3] W. Mannhart, NEANDC(E)-202 U, Vol. V (1979) p. 86

[4] V. Spiegel et al., NUREG/CP-0004, Vol. 2 (1978) p. 959

[5] M.C. Davies, G.F. Knoll, Annals Nucl.Energy 5 (1978) 583

[6] V.M. Adamov et al., NBS Spec.Publ. No. 493 (1977) p. 313

[7] J.J. Wagschal, R.E. Maerker, D.M. Gilliam, Proc. Third ASTM-Euratom Symposium on Reactor Dosimetry, Ispra, Italy (Oct. 1979), in press

[8] K. Kobayashi, I. Kimura, ibid.

[9] W. Mannhart, F.G. Perey, ibid.

[10] H.J. Brede, M. Cosack, G. Dietze, H. Gumpert, S. Guldbakke, R. Jahr, M. Kutscha, D. Schlegel-Bickmann, H. Schölermann, Nucl.Instr.Methods 169, (1980) 349

[11] H. Klein, H.J. Barrenscheen, G. Dietze, B.R.L. Siebert, Nucl.Instr.Methods 169 (1980) 359

[12] D. Schlegel-Bickmann, G. Dietze, H. Schölermann, Nucl.Instr.Methods 169 (1980) 517

[13] H. Schölermann, H. Klein, Nucl.Instr.Methods 169 (1980) 25

[14] H. Klein, H.J. Brede, Contribution to the IAEA Consultants Meeting on Neutron Source Properties, Debrecen (March 1980), in press

[15] B.R.L. Siebert, H.J. Brede, H. Klein, H. Schölermann, Contribution to the Neutron Interlab Seminar, Paris (June 1979), to be published

[16] B.R.L. Siebert, H.J. Brede, H. Lesiecki, to be published

[17] M. Drosg, Nucl.Sci.Engineering 67 (1978) 190

[18] G. Dietze, to be published

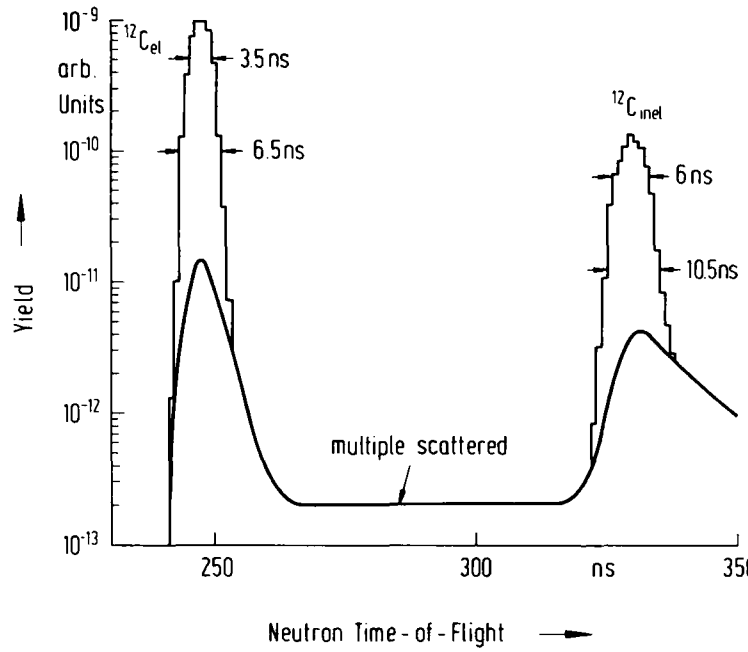

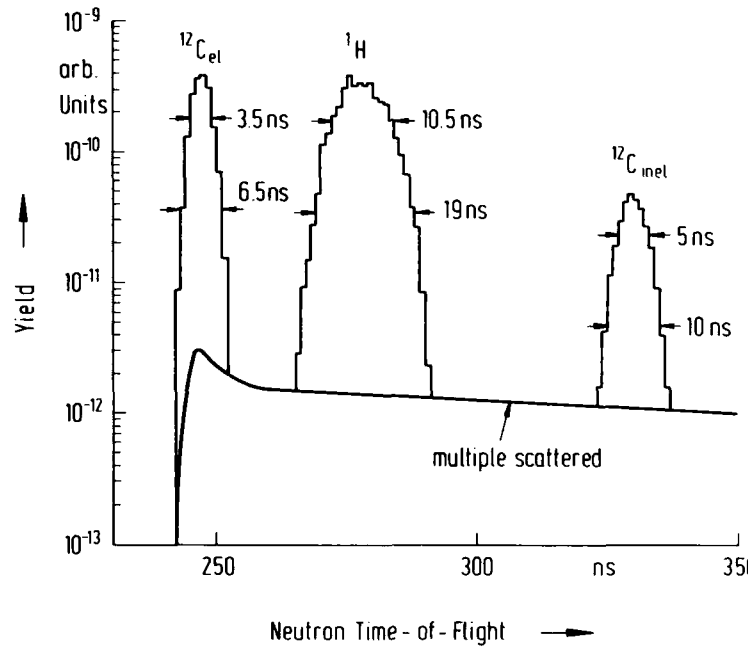

Fig. 1 Monte-Carlo simulation of TOF-spectra to be expected at 28.75 degree for the scattering of 10 MeV neutrons on carbon (a) and polyethylene (b) samples of the same size (2.55 cm in diameter, 3.15 cm in height). A deuterium gas target (10^5 Pa, 3 cm in length) at a distance of 17.5 cm and a liquid scintillator (25.4 cm in diameter, 5 cm in length) at a distance of 1050 cm are considered.

INSTITUT FÜR KERNCHEMIE

PHILIPPS-UNIVERSITAET MARBURG

1. Gamma-Ray Catalog

U. Reus, W. Westmeier, I. Warnecke[+]

The catalog has been described in the last Progress Report NEANDC (E) - 202 U Vol. V p. 98, and we refer to this description for details. A total of 250 copies of the catalog were printed under the sponsorship of GSI[+]. The demand has been such that in the beginning of 1980, no more copies were left. We therefore regret not to be able (at the moment) to fulfil further requests.

A second, updated edition of the catalog is in preparation. It will include references to the literature through January 1980, and also some minor modifications will be made, e.g. the inclusion of the most important X-ray data. Discussions are being carried out at the moment with regard to publishing the catalog in an appropriate journal, in order to make it generally available.

The appearance of this second edition is scheduled for the end of 1980.

2. Alpha-Energy Table

W. Westmeier, R.A. Esterlund

A compilation covering data on alpha energies, intensities and abundances for all known alpha emitters is updated from the literature informations in two month intervals. At present, the table covers data on 516 alpha emitters with a total of 1579 alpha energies.

A computer printout of the table, ordered by increasing energy, is available on request from the authors.

[+]Gesellschaft für Schwerionenforschung mbH, Darmstadt

FACHINFORMATIONSZENTRUM ENERGIE PHYSIK MATHEMATIK

Status Report

H. Behrens, J.W. Tepel

1. Information System for Physics Data in the Federal Republic of Germany

This project has been described earlier in the Progress Reports NEANDC (E) - 172 U Vol. V, NEANDC (E) - 182 U Vol. V and NEANDC (E) - 192 U Vol. V. No details are therefore given here.

2. New Data Compilations

The following new issues in the series Physics Data were published in the meantime:

3-4 (1979):	Datensammlungen in der Physik. Data Compilations in Physics. H. Behrens and G. Ebel. 86 pages. Supplement to No. 3-1, 3-2 and 3-3 containing about 42o further references to tables and compilations.
5-5 (1979):	Gases and Carbon in Metals (Thermodynamics, Kinetics and Properties). Part V: Group IVA Metals (1): Titanium (Ti). H. Jehn, H. Speck, E. Fromm and G. Hörz. 84 pages.
5-6 (1979):	Gases and Carbon in Metals (Thermodynamics, Kinetics and Properties). Part VI: Group IVA Metals (2): Zirconium, Hafnium (Zr, Hf). H. Jehn, H. Speck, E. Fromm and G. Hörz. 8o pages.
15 (1979):	Karlsruhe Charged Particle Reaction Data Compilation. H. Münzel, H. Klewe-Nebenius, J. Lange, G. Pfennig and K. Hemberle. Loosleaf collection, XLVI, 1652 pages.
-1	Entry 1-35. XIV, 762 pages.
-2	Entry 36-8o. XIV, 818 pages.
-Index	Index to Entries 1-35 and 36-8o. XVIII, 72 pages.

16-1 (1979): The oxygen framework in garnet and its occurrence in the structures of $Na_3Al_2Li_3F_{12}$, $Ca_3Al_2(OH)_{12}$, $RhBi_4$ and Hg_3TeO_6.
E. Hellner, R. Gerlich, E. Koch and W. Fischer. 4o pages.

17-1 (198o): in preparation.

3. Bibliography of Existing Data Compilations

As mentioned under 2 a new supplement (Physics Data 3-4 (1979)) has been issued to this worldwide survey of all existing physics data compilations.

4. The Evaluated Nuclear Structure Data Files (ENSDF)

The contribution of the Fachinformationszentrum Energie, Physik, Mathematik to the international collaboration in the evaluation of nuclear structure data (ENSDF) was reported in detail in the 1978 Progress Report. In the past year two mass chains were published, viz. A = 84 [1] and A = 87 [2]. Three further chains, viz. A = 85, 91 and 92 have passed the review procedure and are to appear shortly. Data for the mass chains A = 93, 95 and 96 are in preparation.

In order to improve the retrieval capabilities from ENSDF the data file was restructured as an ISAM file using a special 16-digit key [3]. This key was designed in such a manner, that the original sequence of data records in ENSDF is preserved in the new file, enabling the use of all analysis and display programs. However, in contrast to the old system, where retrieval was purely data set-wise, direct retrieval of individual records is now possible. This feature is particularly useful for horizontal compilations, where specific properties are selected from the file for many different nucleides. As an application a systematic study of log ft-values in beta decay was undertaken [4].

In view of the importance of radioactivity and decay data from ENSDF, which is normally computed from decay data sets via the computer code MEDLIST, a separate data file MEDGEN was constructed from the MEDLIST results. Retrieval from this new file is possible via A- and Z-values of the parent or decaying nucleides. In this manner it is not necessary to recalculate the quantities of interest for each application, but only to update the file once with results from new decay data sets entered into the ENSDF-file.

5. The Nuclear Structure References File (NSR)

The bibliographic data file associated with ENSDF, the "Nuclear Structure References" or NSR, was updated and implemented on our computer. Besides enabling us to decode references appearing in the ENSDF-file, new keywords were introduced which make retrieval of literature documents from this file possible according to the method of inverted lists.

References

[1] H.-W. Müller, J.W. Tepel, Nuclear Data Sheets 27 (1979) 339

[2] P. Luksch, J.W. Tepel, Nuclear Data Sheets 27 (1979) 389

[3] J.W. Tepel, Bull. Am. Phys. Soc. 24 (1979) 837, EC14

[4] H. Behrens, P. Luksch, H.-W. Müller, J.W. Tepel, Verhandl. DPG (VI), (1980) 15, 1119

APPENDIX I

Addresses of Contributing Laboratories

Institut für Angewandte Kernphysik II
Director: Prof.Dr. G. Schatz
Senior reporters: Dr. S.W. Cierjacks
Dr. F. Käppeler
Kernforschungszentrum Karlsruhe
Postfach 3640
7500 Karlsruhe

Institut für Kernphysik II
Director: Prof.Dr. A. Citron
Senior reporter: Dr. S.W. Cierjacks
Kernforschungszentrum Karlsruhe
Postfach 3640
7500 Karlsruhe

Institut für Neutronenphysik und Reaktortechnik
Director: Dr. G. Keßler
Senior reporter: Dr. F.H. Fröhner
Kernforschungszentrum Karlsruhe
Postfach 3640
7500 Karlsruhe

Institut für Chemie (1): Nuklearchemie
Director: Prof.Dr. G. Stöcklin
Senior reporter: Dr. S.M. Qaim
Kernforschungsanlage Jülich
Postfach 1913
5170 Jülich

Institut für Kernphysik:
Experimentelle Kernphysik II
Director: Prof.Dr. O. Schult
Senior reporter: Dr. K. Sistemich
Kernforschungsanlage Jülich
Postfach 1913
5170 Jülich

I. Institut für Experimentalphysik
Director: Prof.Dr. H. Neuert
Senior reporter: Prof.Dr. W. Scobel
Universität Hamburg
Luruper Chaussee 149
2000 Hamburg 50

Institut für Reine und Angewandte
Kernphysik
Director: Prof.Dr. K.O. Thielheim
Senior reporter: Dr. H.G. Priesmeyer
Universität Kiel, Geesthacht
Reaktorstr. 1
2054 Geesthacht/Tesperhude

Institut für Kernchemie
Director: Prof.Dr. W. Herr
Senior reporter: Dr. R. Michel
Universität zu Köln
Zülpicher Str. 47
5000 Köln

Fachbereich Anorganische Chemie
und Kernchemie
Senior reporter: Prof.Dr. H. Münzel
Technische Hochschule Darmstadt
Hochschulstr.
6100 Darmstadt

Institut für Kernchemie
Director: Prof.Dr. G. Herrmann
Senior reporter: Prof.Dr. H.O. Denschlag
Johannes Gutenberg-Universität Mainz
Friedrich von Pfeiffer Weg 14
6500 Mainz

Institut für Strahlenphysik
Director: Prof.Dr. K.-W. Hoffmann
Senior reporter: Dr. J.W. Hammer
Universität Stuttgart
Allmandring 3
7000 Stuttgart 80

Fachbereich Physik der
Technischen Universität München
Abteilung E14, Forschungsreaktor
Head and senior reporter: Prof.Dr. L. Köster
8046 Garching/München

Physikalisch-Technische Bundesanstalt
Abteilung 6, Atomphysik
Director: Prof.Dr. S. Wagner
Senior reporter: Dr. W. Mannhart
Bundesallee 100
3300 Braunschweig

Institut für Kernchemie
Senior reporter: Prof.Dr. P. Patzelt
Philipps-Universität Marburg
Lahnberge
3550 Marburg/Lahn

Fachinformationszentrum Energie, Physik und Mathematik
Director: Dr. W. Rittberger
Senior reporter: Dr. H. Behrens
Kernforschungszentrum
7514 Eggenstein-Leopoldshafen 2

APPENDIX II

CINDA Type Index

ELEMENT S	A	QUANTITY	TYPE	ENERGY MIN	MAX	DOCUMENTATION REF VOL PAGE DATE	LAB	COMMENTS
MA	NY	TOTAL	THEO-PROG	15+7		NEANDC(E)-212U 680 JUL		VOL.5.P.27.KLAPDOR+ STATMDL ANAL,NDG
MA	NY	N,2N	EXPT-PROG	+7		NEANDC(E)-212U 680 JUL		VOL.5.P.28.KHATUN+SIG VS(N-Z)/A,GRPH
MA	NY	N,ALPHA	THEO-PROG	15+7		NEANDC(E)-212U 680 JUL		VOL.5.P.27.KLAPDOR+ STATMDL ANAL,NDG
MA	NY	N,PROTON	EXPT-PROG	FAST		NEANDC(E)-212U 680 JUL		VOL.5.P.30.GAIM. ABST,NDG
MA	NY	N,PROTON	THEO-PROG	15+7		NEANDC(E)-212U 680 JUL		VOL.5.P.27.KLAPDOR+ STATMDL ANAL,NDG
MA	NY	N,PROTON	EXPT-PROG	+7		NEANDC(E)-212U 680 JUL		VOL.5.P.28.KHATUN+SIG VS(N-Z)/A,GRPH
MA	NY	N,DEUTERON	THEO-PROG	15+7		NEANDC(E)-212U 680 JUL		VOL.5.P.27.KLAPDOR+ STATMDL ANAL,NDG
MA	NY	N,N PROTON	EXPT-PROG	+7		NEANDC(E)-212U 680 JUL		VOL.5.P.28.KHATUN+SIG VS(N-Z)/A,GRPH
MA	NY	N,ALPHA	EXPT-PROG	+7		NEANDC(E)-212U 680 JUL		VOL.5.P.28.KHATUN+SIG VS(N-Z)/A,GRPH
D	002	THERMAL SCAT	EXPT-PROG	NDG		NEANDC(E)-212U 680 MUN		VOL.5.P.64.KOESTER+ COH SCAT LENGTH
H	PLE	SCATTERING	EXPT-PROG	10+7		NEANDC(E)-212U 680 PTB		VOL.5.P.70.BREDE+ TOF-SPECTRA CALC
H	PLE	SCATTERING	EXPT-PROG	10+7		NEANDC(E)-212U 680 PTB		VOL.5.P.70.BREDE+ TOF-SPECTRA CALC
C		SCATTERING	EXPT-PROG	10+7		NEANDC(E)-212U 680 PTB		VOL.5.P.70.BREDE+ TOF-SPECTRA CALC
C	012	RESON PARAMS	EXPT-PROG	30+6	11+7	NEANDC(E)-212U 680 KFK		VOL.5.P.1.CIERJACKS+RESPARS EN,WT,WN
O	016	RESON PARAMS	EXPT-PROG	11+7	15+7	NEANDC(E)-212U 680 KFK		VOL.5.P.4.HINTERBERGER+ ABST,RESPARS
O	016	RESON PARAMS	EXPT-PROG	30+6	11+7	NEANDC(E)-212U 680 KFK		VOL.5.P.1.CIERJACKS+RESPARS EN,WT,WN
NE		THERMAL SCAT	EXPT-PROG	NDG		NEANDC(E)-212U 680 MUN		VOL.5.P.64.KOESTER+ COH SCAT LENGTH
MG	024	N,PROTON	EVAL-PROG	FISS		NEANDC(E)-212U 680 PTB		VOL.5.P.66.MANNHART.CF252 SPEC SIG
AL		N,TRITON	EXPT-PROG	FAST		NEANDC(E)-212U 680 JUL		VOL.5.P.27.KHATUN+ SIG,EXCIT FN, NDG
AL		N,HELIUM3	EXPT-PROG	FAST		NEANDC(E)-212U 680 JUL		VOL.5.P.27.KHATUN+ SIG,NDG
AL	027	N,HELIUM3	THEO-PROG	15+7		NEANDC(E)-212U 680 JUL		VOL.5.P.27.KLAPDOR+ STATMDL
AL	027	N,TRITON	THEO-PROG	15+7		NEANDC(E)-212U 680 JUL		VOL.5.P.27.KLAPDOR+ STATMDL,CFD EXPT
AL	027	N,ALPHA	EVAL-PROG	FISS		NEANDC(E)-212U 680 PTB		VOL.5.P.66.MANNHART.CF252 SPEC SIG
AL	027	N,PROTON	EVAL-PROG	FISS		NEANDC(E)-212U 680 PTB		VOL.5.P.66.MANNHART.CF252 SPEC SIG
SI	028	N,HELIUM3	THEO-PROG	15+7		NEANDC(E)-212U 680 JUL		VOL.5.P.27.KLAPDOR+ STATMDL
P	031	N,TRITON	THEO-PROG	15+7		NEANDC(E)-212U 680 JUL		VOL.5.P.27.KLAPDOR+ STATMDL,CFD EXPT
P	031	N,HELIUM3	THEO-PROG	15+7		NEANDC(E)-212U 680 JUL		VOL.5.P.27.KLAPDOR+ STATMDL,CFD EXPT
S	032	N,TRITON	THEO-PROG	15+7		NEANDC(E)-212U 680 JUL		VOL.5.P.27.KLAPDOR+ STATMDL,CFD EXPT
S	032	N,PROTON	EVAL-PROG	FISS		NEANDC(E)-212U 680 PTB		VOL.5.P.66.MANNHART.CF252 SPEC SIG
S	032	N,HELIUM3	THEO-PROG	15+7		NEANDC(E)-212U 680 JUL		VOL.5.P.27.KLAPDOR+ STATMDL
AR		THERMAL SCAT	EXPT-PROG	NDG		NEANDC(E)-212U 680 MUN		VOL.5.P.64.KOESTER+ COH SCAT LENGTH
K	039	N,TRITON	THEO-PROG	15+7		NEANDC(E)-212U 680 JUL		VOL.5.P.27.KLAPDOR+ STATMDL,CFD EXPT
K	039	N,HELIUM3	THEO-PROG	15+7		NEANDC(E)-212U 680 JUL		VOL.5.P.27.KLAPDOR+ STATMDL
K	041	N,TRITON	THEO-PROG	15+7		NEANDC(E)-212U 680 JUL		VOL.5.P.27.KLAPDOR+ STATMDL,CFD EXPT
K	041	N,HELIUM3	THEO-PROG	15+7		NEANDC(E)-212U 680 JUL		VOL.5.P.27.KLAPDOR+ STATMDL
CA	040	N,TRITON	THEO-PROG	15+7		NEANDC(E)-212U 680 JUL		VOL.5.P.27.KLAPDOR+ STATMDL,CFD EXPT
CA	040	N,HELIUM3	THEO-PROG	15+7		NEANDC(E)-212U 680 JUL		VOL.5.P.27.KLAPDOR+ STATMDL
SC	045	N,TRITON	THEO-PROG	15+7		NEANDC(E)-212U 680 JUL		VOL.5.P.27.KLAPDOR+ STATMDL,CFD EXPT
SC	045	N,HELIUM3	THEO-PROG	15+7		NEANDC(E)-212U 680 JUL		VOL.5.P.27.KLAPDOR+ STATMDL,CFD EXPT
TI	046	N,TRITON	THEO-PROG	15+7		NEANDC(E)-212U 680 JUL		VOL.5.P.27.KLAPDOR+ STATMDL,CFD EXPT
TI	046	N,PROTON	EVAL-PROG	FISS		NEANDC(E)-212U 680 PTB		VOL.5.P.66.MANNHART.CF252 SPEC SIG
TI	046	N,HELIUM3	THEO-PROG	15+7		NEANDC(E)-212U 680 JUL		VOL.5.P.27.KLAPDOR+ STATMDL
TI	047	N,PROTON	EVAL-PROG	FISS		NEANDC(E)-212U 680 PTB		VOL.5.P.66.MANNHART.CF252 SPEC SIG
TI	048	N,PROTON	EVAL-PROG	FISS		NEANDC(E)-212U 680 PTB		VOL.5.P.66.MANNHART.CF252 SPEC SIG
V		N,TRITON	EXPT-PROG	FAST		NEANDC(E)-212U 680 JUL		VOL.5.P.27.KHATUN+ SIG,NDG
V		N,HELIUM3	EXPT-PROG	FAST		NEANDC(E)-212U 680 JUL		VOL.5.P.27.KHATUN+ SIG,NDG
V	051	N,PROTON	EVAL-PROG	FISS		NEANDC(E)-212U 680 PTB		VOL.5.P.66.MANNHART.CF252 SPEC SIG
CR		N,TRITON	EXPT-PROG	FAST		NEANDC(E)-212U 680 JUL		VOL.5.P.27.KHATUN+ SIG,NDG
CR		N,HELIUM3	EXPT-PROG	FAST		NEANDC(E)-212U 680 JUL		VOL.5.P.27.KHATUN+ SIG,NDG
CR	050	N,N PROTON	EXPT-PROG	FISS		NEANDC(E)-212U 680 JUL		VOL.5.P.28.KHATUN+ SIG, NDG
CR	050	N,TRITON	THEO-PROG	15+7		NEANDC(E)-212U 680 JUL		VOL.5.P.27.KLAPDOR+ STATMDL,CFD EXPT
CR	050	N,HELIUM3	THEO-PROG	15+7		NEANDC(E)-212U 680 JUL		VOL.5.P.27.KLAPDOR+ STATMDL
CR	050	N,DEUTERON	EXPT-PROG	FISS		NEANDC(E)-212U 680 JUL		VOL.5.P.28.KHATUN+ SIG, NDG
MN		N,TRITON	EXPT-PROG	FAST		NEANDC(E)-212U 680 JUL		VOL.5.P.27.KHATUN+ SIG,NDG
MN		N,HELIUM3	EXPT-PROG	FAST		NEANDC(E)-212U 680 JUL		VOL.5.P.27.KHATUN+ SIG,NDG
FE		N,TRITON	EXPT-PROG	FAST		NEANDC(E)-212U 680 JUL		VOL.5.P.27.KHATUN+ SIG,NDG
FE		N,HELIUM3	EXPT-PROG	FAST		NEANDC(E)-212U 680 JUL		VOL.5.P.27.KHATUN+ SIG,NDG
FE	054	N,PROTON	EVAL-PROG	FISS		NEANDC(E)-212U 680 PTB		VOL.5.P.66.MANNHART.CF252 SPEC SIG

ELEMENT S A	QUANTITY	TYPE	ENERGY MIN MAX	DOCUMENTATION REF VOL PAGE DATE	LAB	COMMENTS
FE 054	N,TRITON	THEO-PROG	15+7	NEANDC(E)-212U 680 JUL		VOL.5.P.27.KLAPDOR+ STATMDL,CFD EXPT
FE 054	N,HELIUM3	THEO-PROG	15+7	NEANDC(E)-212U 680 JUL		VOL.5.P.27.KLAPDOR+ STATMDL
FE 056	RESON PARAMS	EXPT-PROG	27+4	NEANDC(E)-212U 680 KFK		VOL.5.P.5.WISSHAK+ WG,S-WAVE
CO	N,TRITON	EXPT-PROG	FAST	NEANDC(E)-212U 680 JUL		VOL.5.P.27.KHATUN+ SIG,NDG
CO	N,HELIUM3	EXPT-PROG	FAST	NEANDC(E)-212U 680 JUL		VOL.5.P.27.KHATUN+ SIG,NDG
CO 059	N,ALPHA	EVAL-PROG	FISS	NEANDC(E)-212U 680 PTB		VOL.5.P.66.MANNHART.CF252 SPEC SIG
CO 059	N,TRITON	THEO-PROG	15+7	NEANDC(E)-212U 680 JUL		VOL.5.P.27.KLAPDOR+ STATMDL,CFD EXPT
CO 059	N,HELIUM3	THEO-PROG	15+7	NEANDC(E)-212U 680 JUL		VOL.5.P.27.KLAPDOR+ STATMDL,CFD EXPT
NI	N,TRITON	EXPT-PROG	FAST	NEANDC(E)-212U 680 JUL		VOL.5.P.27.KHATUN+ SIG,NDG
NI	N,HELIUM3	EXPT-PROG	FAST	NEANDC(E)-212U 680 JUL		VOL.5.P.27.KHATUN+ SIG,NDG
NI 058	N,PROTON	EVAL-PROG	FISS	NEANDC(E)-212U 680 PTB		VOL.5.P.66.MANNHART.CF252 SPEC SIG
NI 058	N,DEUTERON	EXPT-PROG	FISS	NEANDC(E)-212U 680 JUL		VOL.5.P.28.KHATUN+ SIG, NDG
NI 058	N,ALPHA	EXPT-PROG	FISS	NEANDC(E)-212U 680 JUL		VOL.5.P.28.KHATUN+ SIG, NDG
NI 058	N,N PROTON	EXPT-PROG	FISS	NEANDC(E)-212U 680 JUL		VOL.5.P.28.KHATUN+ SIG, NDG
NI 060	N,PROTON	EXPT-PROG	FISS	NEANDC(E)-212U 680 JUL		VOL.5.P.28 KHATUN+ SIG, NDG
NI 061	N,PROTON	EXPT-PROG	FISS	NEANDC(E)-212U 680 JUL		VOL.5.P.28.KHATUN+ SIG, NDG
NI 062	N,ALPHA	EXPT-PROG	FISS	NEANDC(E)-212U 680 JUL		VOL.5.P.28.KHATUN+ SIG, NDG
AS	THERMAL SCAT	EXPT-PROG	00+0	NEANDC(E)-212U 680 MUN		VOL.5.P.65.KOESTER+ SCAT SIG
AS	THERMAL SCAT	EXPT-PROG	NDG	NEANDC(E)-212U 680 MUN		VOL.5.P.64.KOESTER+ COH SCAT LENGTH
SE	THERMAL SCAT	EXPT-PROG	00+0	NEANDC(E)-212U 680 MUN		VOL.5.P.65.KOESTER+ SCAT SIG
SE	THERMAL SCAT	EXPT-PROG	NDG	NEANDC(E)-212U 680 MUN		VOL.5.P.64.KOESTER+ COH SCAT LENGTH
KR	N,GAMMA	EXPT-PROG	25+3 20+5	NEANDC(E)-212U 680 KFK		VOL.5.P.9.LEUGERS+ GRPHS,TBL
KR	THERMAL SCAT	EXPT-PROG	NDG	NEANDC(E)-212U 680 MUN		VOL.5.P.64.KOESTER+ COH SCAT LENGTH
KR	TOTAL	EXPT-PROG	70+3 20+5	NEANDC(E)-212U 680 KFK		VOL.5.P.9.LEUGERS+ GRPHS
KR 084	TOTAL	EXPT-PROG	70+3 20+5	NEANDC(E)-212U 680 KFK		VOL.5.P.9.LEUGERS+ GRPHS
KR 084	N,GAMMA	EXPT-PROG	70+3 20+5	NEANDC(E)-212U 680 KFK		VOL.5.P.9.LEUGERS+ GRPHS
NB	N,HELIUM3	EXPT-PROG	FAST	NEANDC(E)-212U 680 JUL		VOL.5.P.27.KHATUN+ SIG,NDG
NB	N,TRITON	EXPT-PROG	FAST	NEANDC(E)-212U 680 JUL		VOL.5.P.27.KHATUN+ SIG,NDG
TC 099	RESON PARAMS	EXPT-PROG	+1	NEANDC(E)-212U 680 KIG		VOL.5.P.41.PRIESMEYER+ WT,WN,EN
AG	THERMAL SCAT	EXPT-PROG	NDG	NEANDC(E)-212U 680 MUN		VOL.5.P.64.KOESTER+ COH SCAT LENGTH
IN	THERMAL SCAT	EXPT-PROG	NDG	NEANDC(E)-212U 680 MUN		VOL.5.P.64.KOESTER+ COH SCAT LENGTH
IN 113	TOTAL	EVAL-PROG	FISS	NEANDC(E)-212U 680 PTB		VOL.5.P.66.MANNHART.CF252 SPEC SIG
IN 115	N,GAMMA	EVAL-PROG	FISS	NEANDC(E)-212U 680 PTB		VOL.5.P.66.MANNHART.CF252 SPEC SIG
IN 115	TOTAL	EVAL-PROG	FISS	NEANDC(E)-212U 680 PTB		VOL.5.P.66.MANNHART.CF252 SPEC SIG
I 129	RESON PARAMS	EXPT-PROG	+2	NEANDC(E)-212U 680 KIG		VOL.5.P.41.PRIESMEYER+TRANSMISS,SRES
XE	N,GAMMA	EXPT-PROG	25+3 20+5	NEANDC(E)-212U 680 KFK		VOL.5.P.9.LEUGERS+ GRPHS,TBL
CS	RESON PARAMS	EXPT-PROG	30+1 12+3	NEANDC(E)-212U 680 KIG		VOL.5.P.41.PRIESMEYER+TRANSSPEC GRPH
CS 135	RESON PARAMS	EXPT-PROG	42+1	NEANDC(E)-212U 680 KIG		VOL.5.P.41.PRIESMEYER+ RESPARS
CS 135	RESON PARAMS	EXPT-PROG	42+1	NEANDC(E)-212U 680 KIG		VOL.5.P.41.PRIESMEYER+ CAPTURE
BA 138	N,GAMMA	EXPT-PROG	30+4	NEANDC(E)-212U 680 KFK		VOL.5.P.9.BEER+ ABST
LA	SCATTERING	EXPT-PROG	76+6	NEANDC(E)-212U 680 IFS		VOL.5.P.60.HAMMER+ POLARIZED BEAMS
CE 140	N,GAMMA	EXPT-PROG	30+4	NEANDC(E)-212U 680 KFK		VOL.5.P.9.BEER+ ABST
CE 142	N,GAMMA	EXPT-PROG	30+4	NEANDC(E)-212U 680 KFK		VOL.5.P.9.BEER+ ABST
YB	N,GAMMA	EXPT-PROG	50+3 20+5	NEANDC(E)-212U 680 KFK		VOL.5.P.5.BEER+ GRPHS, TOF,VDG
YB 170	N,GAMMA	EXPT-PROG	50+3 20+5	NEANDC(E)-212U 680 KFK		VOL.5.P.5.BEER+ GRPHS, TOF,VDG
LU	N,GAMMA	EXPT-PROG	50+3 20+5	NEANDC(E)-212U 680 KFK		VOL.5.P.5.BEER+ GRPHS, TOF,VDG
LU 175	N,GAMMA	EXPT-PROG	30+4	NEANDC(E)-212U 680 KFK		VOL.5.P.9.BEER+ ABST
LU 175	N,GAMMA	EXPT-PROG	50+3 20+5	NEANDC(E)-212U 680 KFK		VOL.5.P.5.BEER+ GRPHS, TOF,VDG
LU 176	N,GAMMA	EXPT-PROG	30+4	NEANDC(E)-212U 680 KFK		VOL.5.P.9.BEER+ ABST
TA 181	N,GAMMA	EXPT-PROG	30+4	NEANDC(E)-212U 680 KFK		VOL.5.P.9.BEER+ ABST
W 184	N,GAMMA	EXPT-PROG	50+3 20+5	NEANDC(E)-212U 680 KFK		VOL.5.P.5.BEER+ GRPHS, TOF,VDG
AU 197	N,GAMMA	EVAL-PROG	FISS	NEANDC(E)-212U 680 PTB		VOL.5.P.66.MANNHART.CF252 SPEC SIG
AU 197	N,2N	EVAL-PROG	FISS	NEANDC(E)-212U 680 PTB		VOL.5.P.66.MANNHART.CF252 SPEC SIG
U 235	EVALUATION	EVAL-PROG	10-3 10+2	NEANDC(E)-212U 680 KFK		VOL.5.P.25.FROEHNER+ SIG+RESPARS,NDG
U 235	FISS YIELD	EXPT-PROG	PILE	NEANDC(E)-212U 680 MNZ		VOL.5.P.57.DENSCHLAG+ ABST
U 235	N,FISSION	EVAL-PROG	FISS	NEANDC(E)-212U 680 PTB		VOL.5.P.66.MANNHART.CF252 SPEC SIG
U 235	FISS PROD G	EXPT-PROG	PILE	NEANDC(E)-212U 680 JUL		VOL.5.P.35.BATTISTUZZI+ MO-104 LVLS
U 238	EVALUATION	EVAL-PROG	10-3 40+3	NEANDC(E)-212U 680 KFK		VOL.5.P.25.FROEHNER+ SIG+RESPARS,NDG

ELEMENT S	A	QUANTITY	TYPE	ENERGY MIN	MAX	DOCUMENTATION REF VOL PAGE DATE	LAB	COMMENTS
U	238	SCATTERING	EXPT-PROG	76+6		NEANDC(E)-212U 680	IFS	VOL.5.P.60.HAMMER+ POLARIZED BEAMS
U	238	N,FISSION	EVAL-PROG	FISS		NEANDC(E)-212U 680	PTB	VOL.5.P.66.MANNHART.CF252 SPEC SIG
NP	237	FISS YIELD	EXPT-PROG	80+5	55+6	NEANDC(E)-212U 680	KFK	VOL.5.P.17.NAQVI+ GRPH
NP	237	N,FISSION	EVAL-PROG	FISS		NEANDC(E)-212U 680	PTB	VOL.5.P.66.MANNHART.CF252 SPEC SIG
NP	237	NUBAR (NU)	EXPT-PROG	80+5	55+6	NEANDC(E)-212U 680	KFK	VOL.5.P.17.NAQVI+ GRPH
NP	237	FRAG SPECTRA	EXPT-PROG	80+5	55+6	NEANDC(E)-212U 680	KFK	VOL.5.P.17.NAQVI+ GRPH,TOT KIN EN
PU	239	N,FISSION	EVAL-PROG	FISS		NEANDC(E)-212U 680	PTB	VOL.5.P.66.MANNHART.CF252 SPEC SIG
AM	241	N,GAMMA	EXPT-PROG	10+4	25+5	NEANDC(E)-212U 680	KFK	VOL.5.P.14.WISSHAK+ ABST
AM	241	EVALUATION	EVAL-PROG	10-3	15+2	NEANDC(E)-212U 680	KFK	VOL.5.P.25.FROEHNER+ SIG+RESPARS,NDG
AM	241	N,FISSION	EXPT-PROG	10+4	10+6	NEANDC(E)-212U 680	KFK	VOL.5.P.14.HAGE+ ABST
AM	241	N,FISSION	EXPT-PROG	10+4	25+5	NEANDC(E)-212U 680	KFK	VOL.5.P.14.WISSHAK+ ABST
AM	241	SPECT N,GAMT	EXPT-PROG	14-3	30+4	NEANDC(E)-212U 680	KFK	VOL.5.P.15.WISSHAK+ BRANCHING RATIO
AM	242	EVALUATION	EVAL-PROG	10-3	40+0	NEANDC(E)-212U 680	KFK	VOL.5.P.25.FROEHNER+ SIG+RESPARS,NDG
AM	243	EVALUATION	EVAL-PROG	10-3	25+2	NEANDC(E)-212U 680	KFK	VOL.5.P.25.FROEHNER+ SIG+RESPARS,NDG
CM	244	EVALUATION	EVAL-PROG	10-3	10+3	NEANDC(E)-212U 680	KFK	VOL.5.P.25.FROEHNER+ SIG+RESPARS,NDG